UNITED NATIONS EDUCATIONAL, SCIENTIFIC AND CULTURAL ORGANIZATION
INTERNATIONAL ATOMIC ENERGY AGENCY
INTERNATIONAL CENTRE FOR THEORETICAL PHYSICS
I.C.T.P., P.O. BOX 586, 34100 TRIESTE, ITALY, CABLE: **CENTRATOM TRIESTE**

H4.SMR/916 - 9

SEVENTH COLLEGE ON BIOPHYSICS:

Structure and Function of Biopolymers: Experimental and Theoretical Techniques.

4 - 29 March 1996

Biological Microcalorimetry

P. L. MATEO
Dept. of Physical Chemistry
Faculty of Science &
Institute of Biotechnology
Biological Research Centre
University of Granada
Granada, SPAIN

SEVENTH COLLEGE ON BIOPHYSICS

Trieste, March 1996

Lectures on Biological Microcalorimetry

Pedro L. Mateo, Department of Physical Chemistry, Faculty of Sciences, and Institute of Biotechnology, University of Granada, 18071 Granada, Spain.

It is now understood that it is essential to include both energetics and dynamics into the traditional structure-function correlation. Calorimetry, or microcalorimetry when dealing with macromolecules, is the ideal technique available for characterizing the energetics of biological processes and systems. One important reason for this is that calorimetry measures the heat of a given process or the heat capacity of a certain system directly without having to make any assumptions or further calculations; it also provides thermodynamic information unobtaniable by other techniques.

Calorimetric methods can be broadly divided into two groups: isothermal calorimetry (IC) and differential scanning calorimetry (DSC). The former measures the heat (enthalpy) evolution associated to a certain macromolecule-ligand interaction, whereas the latter determines the heat capacity of the macromolecule as a function of temperature.

There are three fundamental types of IC instruments with different operating characteristics; these are known as batch, flow, or titration calorimeters. Althought each one has its own advantage and limitations, titration calorimeters are now the most widely used IC instruments. IC is, in principle, a self-sufficient technique, providing as it does the meaningful thermodynamic functions for a given binding process, i.e. the number of binding sites, binding constants and the ΔH, ΔS, ΔG and ΔCp values associated with the interaction. Nevertheless, when dealing with somewhat complex binding processes, such as cooperative sites, additional non-calorimetric techniques are required for a complete thermodynamic description of the process.

The more important reasons for thermodynamic changes in ligand binding include: 1) a change in solvation; 2) specific interactions at the binding site; 3) the release or absorption of protons by the macromolecule, ligand and buffer; 4) conformational changes; 5) changes in the association state of the system. Complementary techniques are again often necessary to differentiate among these possible contributions. The knowledge of the binding-site structure may also allow us to find out the relative importance of hydrogen bonding, hydrophobic, electrostatic and van der Waals forces in the specificity of the interaction.

The interaction of AMP with both glycogen phosphorylase a and b provides a good illustration of the use of IC to analyze ligand binding to both equal-and-independent sites and to cooperative sites.

High-sensitivity DSC is a most appropriate technique to study the energetics of temperature-induced conformational changes in macromolecules, e.g. protein thermal unfolding. Under the assumption that the thermal unfolding process occurs under

equilibrium conditions, DSC allows us to obtain the heat capacity of the protein in the experimental temperature range, the overall thermodynamic parameters (ΔH, ΔS, ΔCp) associated with the transition, and the partition function, and hence the population of possible intermediate states and their thermodynamic characterization.

DSC provides directly the ΔH of the process by integration of the experimental Cp function; in addition we can obtain the enthalpy change, ΔH^{vH}, from the shape of the transition using the van't Hoff equation and assuming a two-state mechanism. When both ΔH values are equal it is a good indicator that the transition, follows the two-state model. When $\Delta H > \Delta H^{vH}$, sufficiently populated intermediate states are present during the transition, whereas $\Delta H < \Delta H^{vH}$ points to the possible existence of intermolecular interactions (associations) in the initial, native state of the protein. In addition, a knowledge of ΔH, ΔS and ΔCp leads to the $\Delta G(T)$, the stability function, the shape of which predicts the "cold-denaturation" of proteins.

Some DSC protein studies are briefly described to show the application of this technique to the two-state situation and to multi-step transitions, where the individual transitions can in principle be correlated with the unfolding of specific regions, coperative domains of the macromolecule. The complementary use of both IC and DSC is also commented upon.

Thermodynamic analysis of DSC calorimetric traces due to protein unfolding relies on the assumption that chemical equilibrium exists throughout the process. It is not clear, however, whether or not equilibrium thermodynamics can be applied to calorimetrically irreversible transitions (no heat effect in the reheating of the sample). I show here that the scan-rate effect on the calorimetric traces may be used to ascertain their equilibrium character. Several examples illustrate how the shape of the traces, as well as the effects of the scan rate on them, can be explained on the basis of a two-state kinetic model. According to this model the conversion of the native state to an irreversibly denatured one (aggregated, for instance) is determined by a first-order kinetic constant, which changes with temperature according to the Arrhenius equation. In these cases no thermodynamic information, other than enthalpy changes, can be derived from the traces. This two-state kinetic model is one particular case within the wider Lumry-Eyring scheme, $N \rightleftarrows U \rightarrow F$, where N, U and F respectively are the native, unfolded and irreversible arrived at final states of the protein.

Therefore, efforts to improve the thermal stability of proteins should take into account the increase in ΔG and also, whenever it applies, the kinetics and nature of the step(s) responsible for the irreversibility of the overall denaturation process.

REFERENCES

General

- J.M. Sturtevant. Proc. Natl. Acad. Sci.USA., 74, 2236-2240, (1977).
- Biochemical Thermodynamics. N.M. Jones Ed. Elsevier. Amsterdam (1979).
- Biological Microcalorimetry. A.E. Beezer Ed. Academic Press. London (1980).
- Biothermodynamics. J.T. Edsall and H. Gutfreund. John Wiley & Sons. New York (1983).
- Thermodynamic Data for Biochemistry and Biotechnology. H.J. Hinz. Ed. Springer-Verlag. Heidelberg (1986).
- Binding and Linkage. J. Wyman and S.J. Gill. University Science Books. Hill Valley, California (1990).

Isothermal Calorimetry

- R.L. Biltonen and N. Langerman. Methods Enzymol. 61, 261-317 (1979).
- I.R. McKinnon et al. Anal. Biochem. 139, 134-139 (1984).
- P.L. Mateo et al. J. Biol. Chem. 261, 17067-17072 (1986).
- C. Barón et al. J. Biol. Chem. 264, 12872-12878 (1989).
- T. Wiseman et al. Anal. Biochem. 179, 131-137 (1989).
- E. Freire et al. Anal. Biochem. 62, 950 A - 959 A (1990).

Differential Scanning Calorimetry

- P.L. Privalov. Adv. Protein Chem. 35, 1-104 (1982) and 33, 167-241 (1979).
- P.L. Mateo in Thermochemistry and its applications to chemical and biochemical systems. M.A.V.R. da Silva Ed. pp 541-568. Reidel. Dordrecht (1984).
- S.A. Potekhin and P.L. Privalov. Methods Enzymol. 131, 4-50 (1986).
- J.M. Sturtevant et al. Annu. Rev. Phys. Chem. 38, 463-488 (1987).
- P.L. Privalov. Annu. Rev. Biophys. Biophys. Chem. 18, 47-69 (1989).
- J.M. Sanchez-Ruiz et al. Biochemistry 27, 1648-1652 (1988).
- P.L. Privalov. Crit. Rev. Biochem. Mol. Biol. 25,281-306 (1990).
- F. Conejero-Lara et al. Eur. J. Biochem. 200, 663-670 (1991).
- J.M. Sánchez-Ruiz. Biophys. J. 61, 921-935 (1992).
- A.R. Viguera et al. Biochemistry 33, 2142-2150 (1994).
- J.C. Martínez et al. Biochemistry 33, 3919-3926 (1994).
- J.C. Martínez et al. Biochemistry 34, 5224-5233 (1995).
- J.M. Sánchez-Ruiz. Subcell. Biochem. 24, 133-176 (1995).
- E. Freire. Methods Mol. Biol. 40, 191-218 (1995).
- J.F. Brandts and Lin. Biochemistry 29, 6927-6940 (1990).
- E. Freire and R. Biltonen. Biopolymers 17, 463-479 (1978).

CALORIMETRIA DIFERENCIAL DE BARRIDO

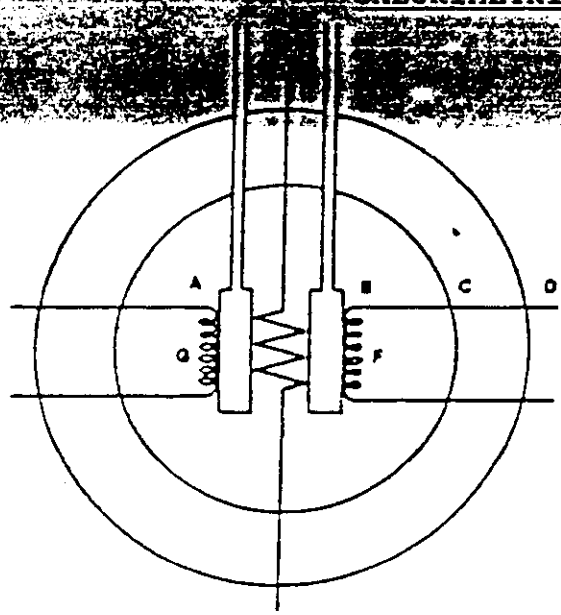

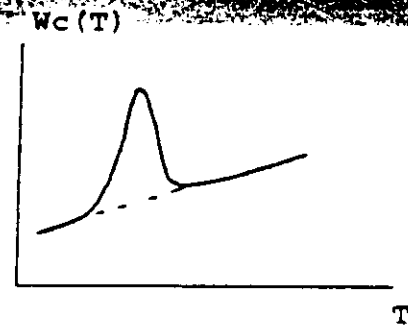

$$\Delta Cp(T) = \frac{Wc(T)}{\alpha}$$

CALORIMETRIA ISOTERMICA DE REACCION

FLUJO

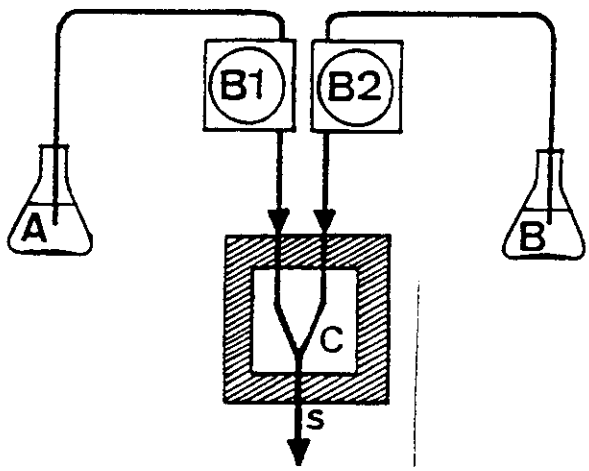

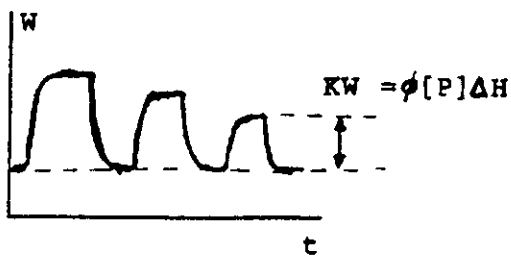

TITULACION

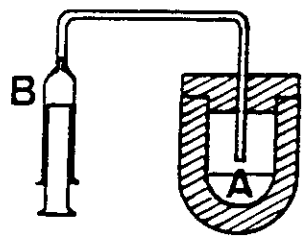

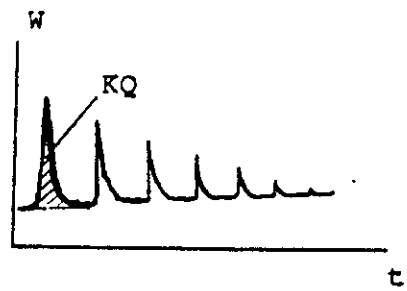

BATCH

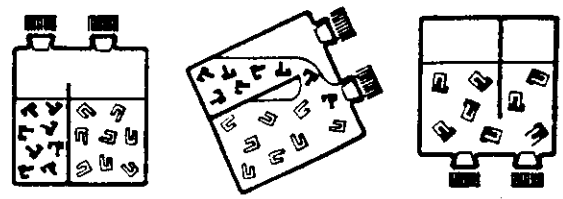

$$P + L \rightleftharpoons PL \qquad K_1$$

$$PL + L \rightleftharpoons PL_2 \qquad K_2$$

$$\vdots \qquad\qquad \vdots$$

$$PL_{n-1} + L \rightleftharpoons PL_n \qquad K_n$$

$$K_i = \frac{[PL_i]}{[PL_{i-1}][L]} \quad ; \; i = 1, 2, \ldots n$$

$$\nu = \frac{[L]_b}{[P]_T} = \frac{[PL] + 2[PL_2] + \cdots + n[PL_n]}{[P] + [PL] + \cdots + [PL_n]}$$

$$0 \le \nu \le n$$

$$\nu = \frac{K_1[L] + 2K_1K_2[L]^2 + \cdots + nK_1K_2\cdots K_n[L]^n}{1 + K_1[L] + K_1K_2[L]^2 + \cdots + K_1K_2\cdots K_n[L]^n}$$

AD41R

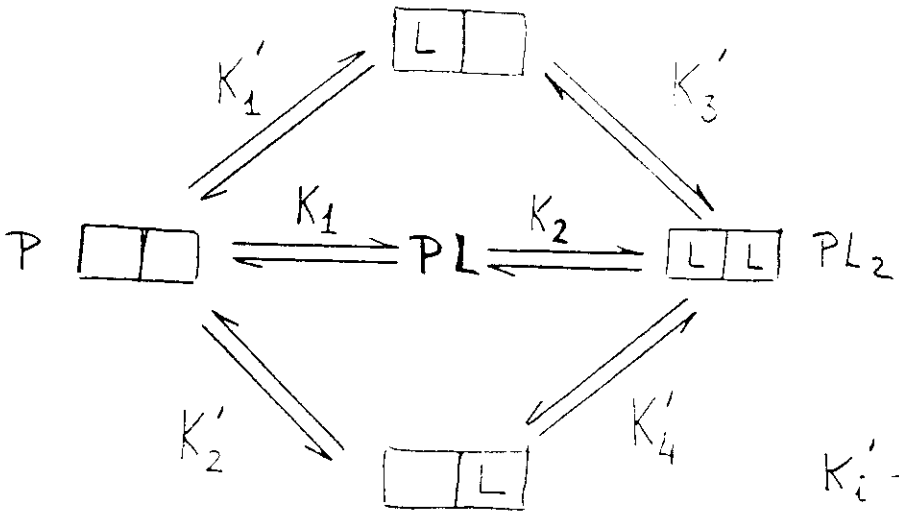

$$K_1 = \frac{[PL]}{[P][L]}$$

$$K_2 = \frac{[PL_2]}{[PL][L]}$$

K_1 and K_2 → macro. consts.

K_i' → microscopic consts.

$$K_1 = K_1' + K_2' \quad ; \quad K_2 = \frac{K_1' K_2'}{K_1' + K_2'}$$

If the two sites are equal and independent

$$\text{all } K_i' = K \Rightarrow \left\{ \begin{array}{l} K_1 = 2K \\ K_2 = \dfrac{K}{2} \end{array} \right\} \Rightarrow \nu = \frac{2K[L]}{1 + K[L]}$$

$$K_i = \frac{n - i + 1}{i} K \Longrightarrow \begin{cases} \nu = \dfrac{n K [L]}{1 + K [L]} & \text{or} \\ Y = \dfrac{\nu}{n} = \dfrac{K [L]}{1 + K [L]}, & 0 \le Y \le 1 \end{cases}$$

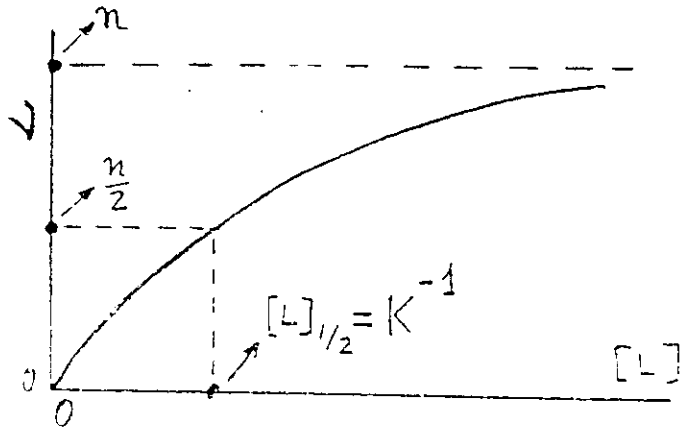

Scatchard Plot

$$\frac{\nu}{[L]} = nK - \nu K$$

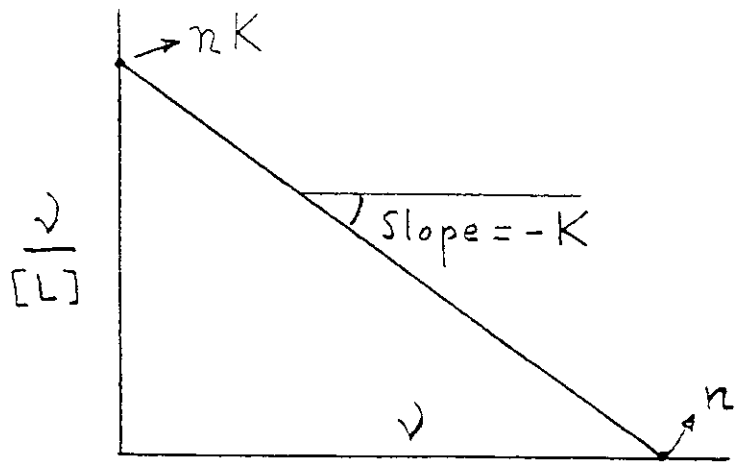

Hill Plot

$$\log \frac{\nu}{n - \nu} = \log \frac{Y}{1 - Y} = \log K + \log [L]$$

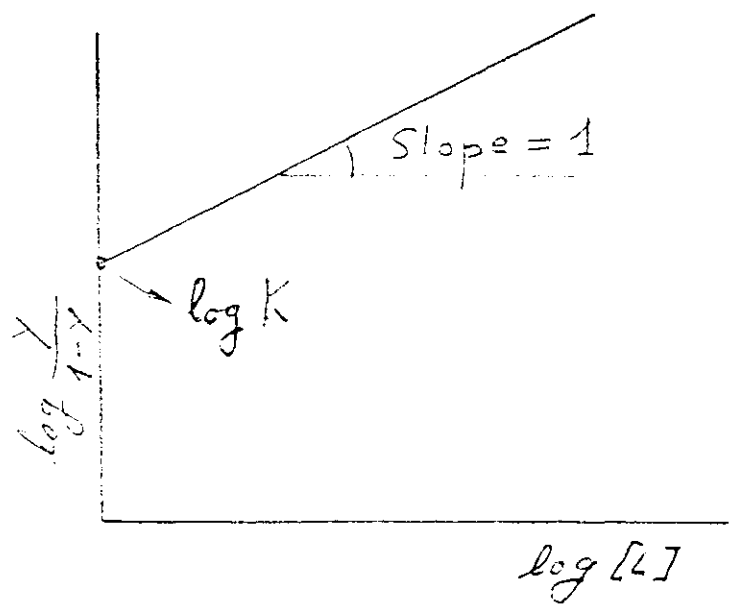

Different sets of independent sites

$$\nu = \sum^{N} \nu_i \;;\; \nu_i = \frac{n_i K_i [L]}{1 + K_i [L]} \;;\; \nu = \sum^{N} \frac{n_i K_i [L]}{1 + K_i [L]} \;;\; \frac{\nu}{[L]} = \sum^{N} \frac{n_i K_i}{1 + K_i [L]}$$

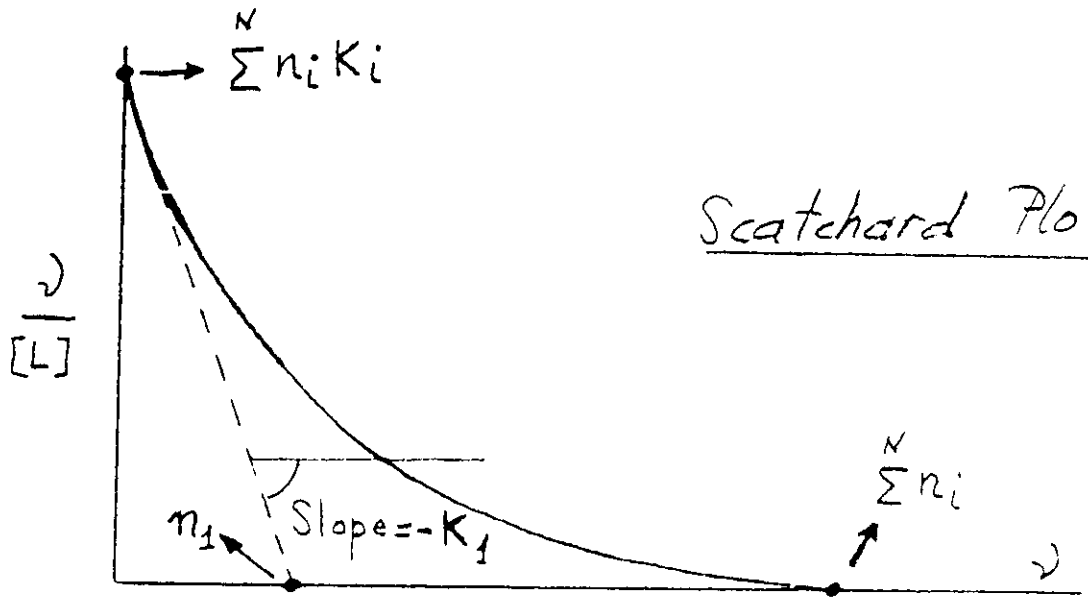

Dependent sites (co-operativity)

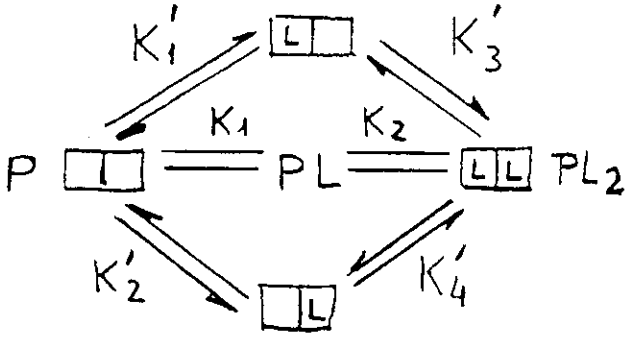

Here $K_1' = K_2'$ and $K_3' = K_4'$

$$\begin{cases} K_1' = K_3' \Rightarrow \text{no co-op.} \\ K_1' < K_3' \Rightarrow (+) \text{ co-op.} \\ K_1' > K_3' \Rightarrow (-) \text{ co-op.} \end{cases}$$

For n sites

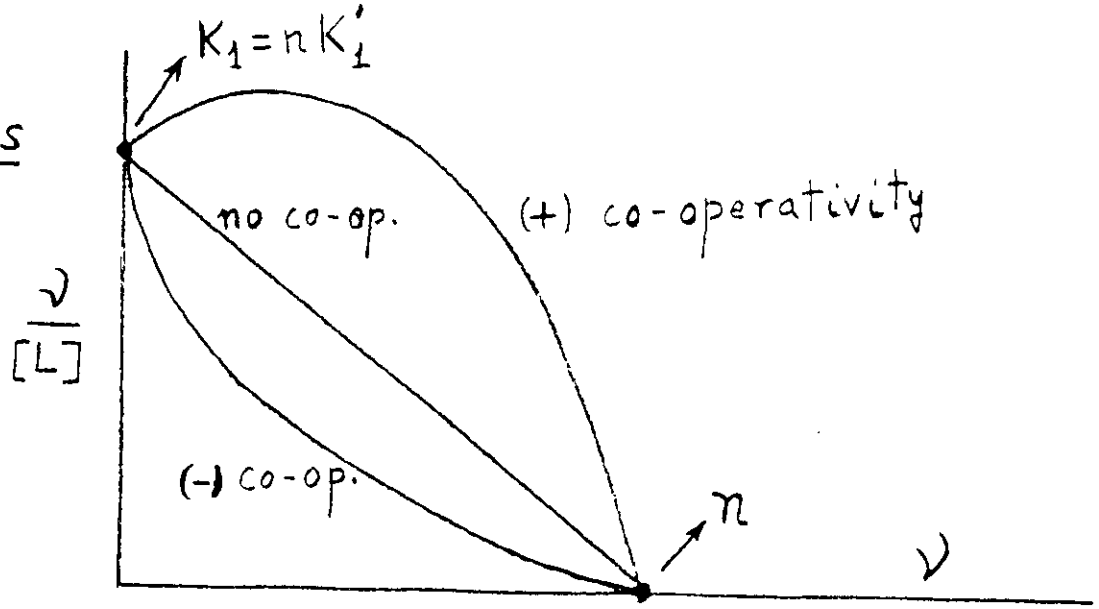

$[P][L]^n$

$$\nu = \frac{n[PLn]}{[P]+[PLn]} = \frac{n K [L]^n}{1+K[L]^n} \Rightarrow \log \frac{\nu}{n-\nu} = \log \frac{Y}{1-Y} = \log K + n \log [L]$$

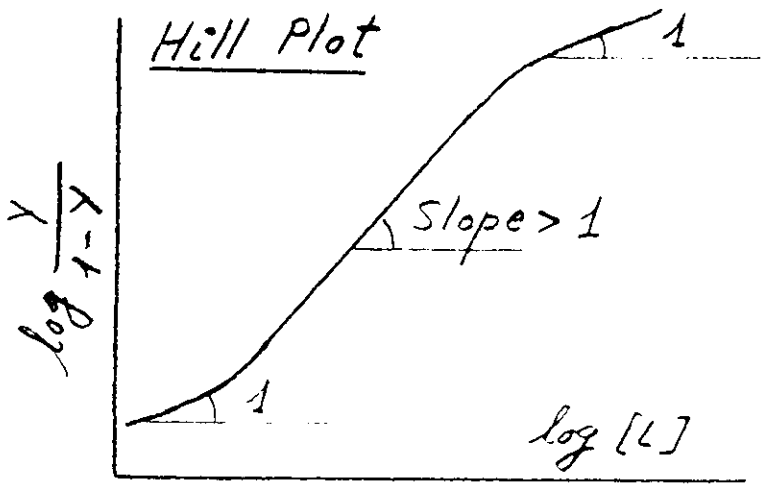

$1 < \text{slope} < n \Rightarrow (+)$ co-op.

$0 < \text{slope} < 1 \Rightarrow (-)$ co-op.

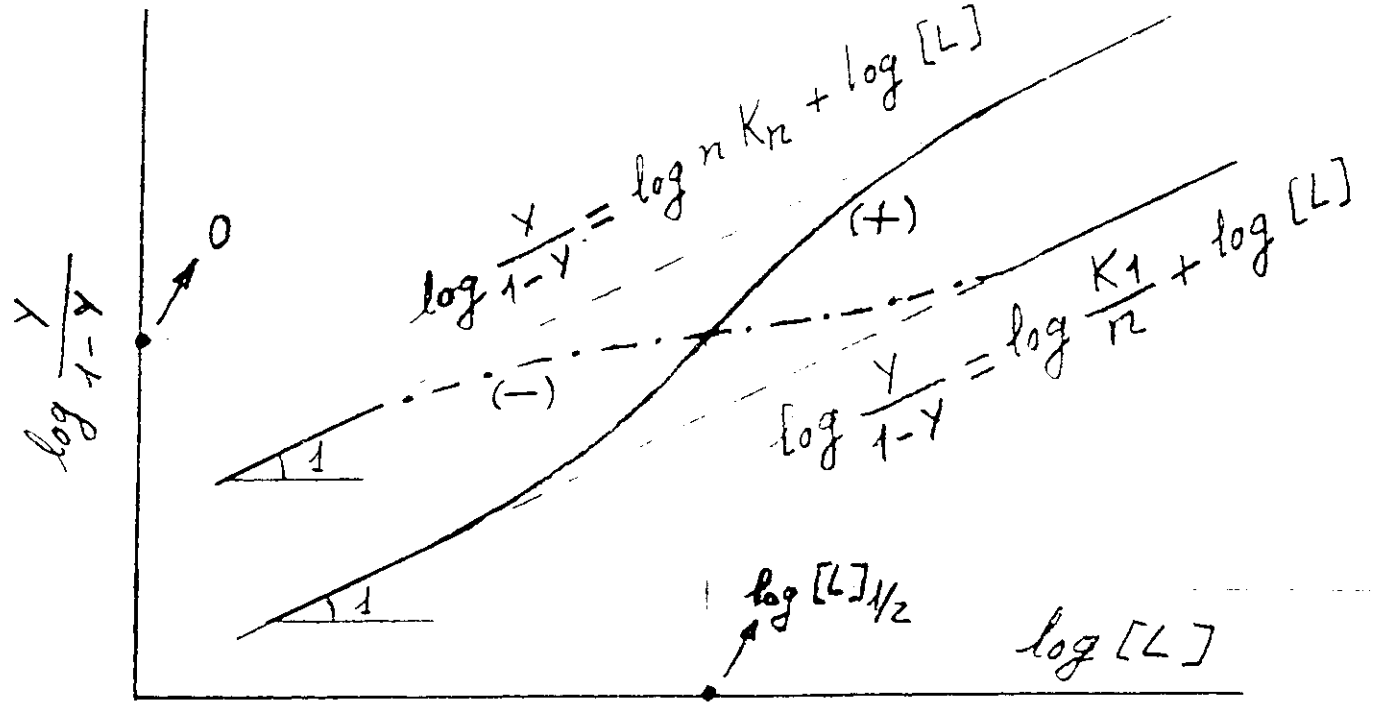

Two sites

$$\left.\begin{aligned} \text{Hill slope} &= \frac{4}{(K_1/K_2)^{1/2}+2} \\ [L]_{1/2} &= \frac{1}{(K_1 K_2)^{1/2}} \end{aligned}\right\} \Rightarrow \begin{cases} K_1 \\ K_2 \end{cases}$$

$$\nu = \frac{[L]_b}{[P]_T} = \frac{n K [L]}{1 + K[L]}$$

$$\frac{1}{\nu} = \frac{1}{n} + \frac{1}{nK[L]}$$

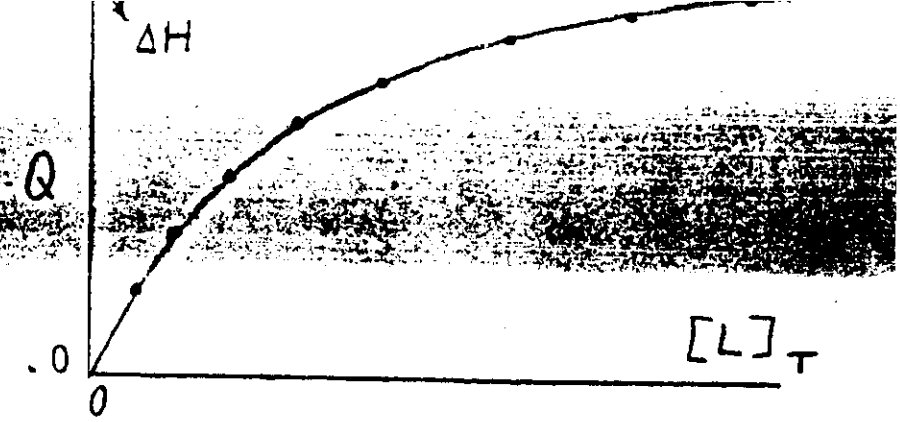

$$\frac{\nu}{n} = Y = \frac{Q}{\Delta H} \; ; \quad \nu = n\frac{Q}{\Delta H} \; ; \quad [L] = [L]_T - n\frac{Q}{\Delta H}[P]_T$$

$$\frac{1}{Q} = \frac{1}{\Delta H} + \frac{1}{\Delta H\, K\, [L]}$$

Fitting of $1/Q$ vs $1/[L]$ → $\begin{cases} K \\ \Delta H \end{cases}$ → new fitting (iteration) → values of K and ΔH → $\Delta G°$ and $\Delta S°$

ΔH	-	-	-
T	-	-	-

$$\Delta C_p = \left(\frac{\partial \Delta H}{\partial T}\right)_p$$

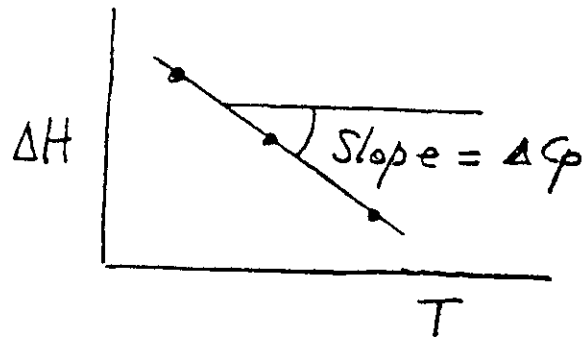

Experimental signal

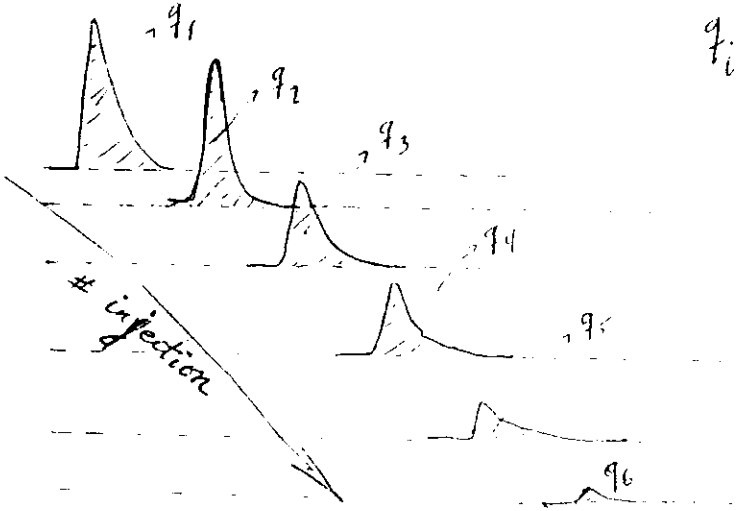

Experimental heat

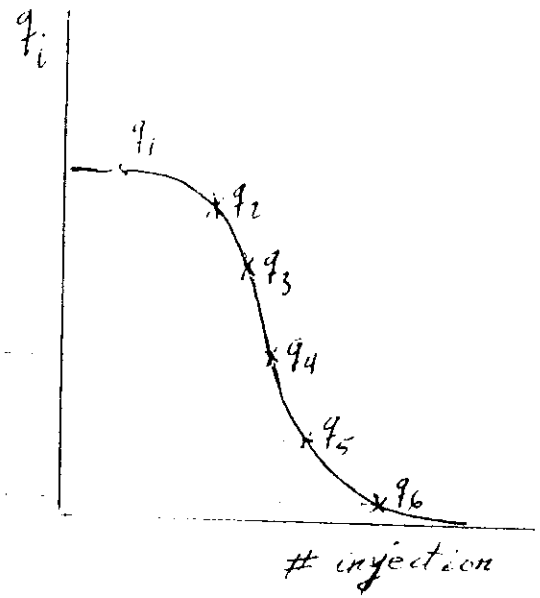

Titration curve of cumulative amount of heat vs total ligand concentration

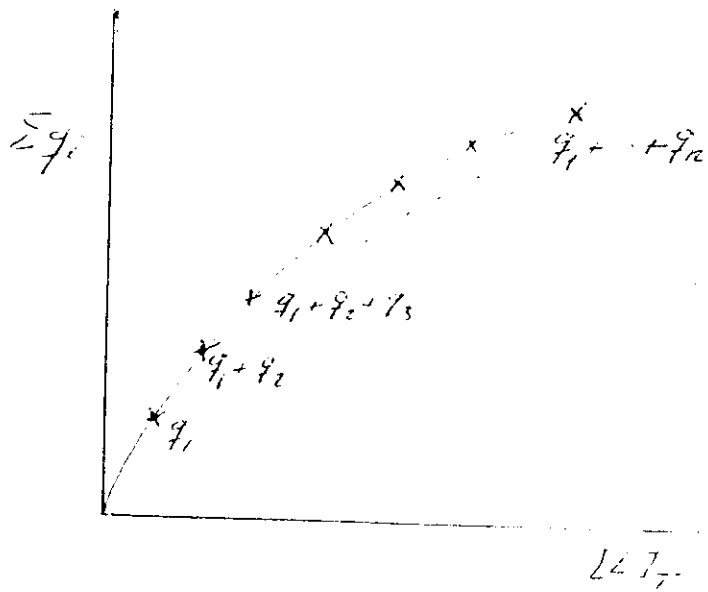

Heat evolution in each injection

$$q_i = V \cdot \Delta H \cdot \Delta[L_{13}] \quad \frac{\text{after } N \text{ injections of}}{\text{identical volume}} \quad > \quad Q = V \cdot \Delta H \sum_{i=1}^{N} \Delta[L_{13}]_i = V \Delta H \cdot [L_{13}]$$

Total cumulative heat

V - calorimetric cell volume

ΔH - binding enthalpy per mol of ligand

$\Delta[L_{13}]$ - change in the bound ligand concentration

Binding to One Set of Independent Binding Sites

$$\nu = \frac{[L_B]}{[M]} = \frac{nK[L]}{1+K[L]}$$

$$[L] = [L_T] - [L_B] = [L_T] - \frac{Q}{V \cdot \Delta H}$$

$$Q = V \cdot \Delta H \cdot [L_B] = V \cdot \Delta H \cdot [M] \frac{nK[L]}{1+K[L]}$$

$$Q^2\left(\frac{K}{V \cdot \Delta H}\right) + Q(-1 - [M] \cdot n \cdot K - K \cdot [L_T]) + ([M] \cdot V \cdot \Delta H \cdot n \cdot K \cdot [L_T]) = 0$$

$$Q = \frac{(1 + [M] \cdot n \cdot K + K \cdot [L_T]) - [(1 + [M] \cdot n \cdot K + K[L_T])^2 - 4[M] \cdot n \cdot K^2 \cdot [L_T]]^{1/2}}{\frac{2K}{V \cdot \Delta H}}$$

Sources of thermodynamic changes for ligand binding

1.- Change in solvation

2.- Specific interactions at the binding site

3.- Release or absorption of protons

4.- Change in the state of agregation

5.- Conformational change

Supported by NIH grants RR-04328, GM-37911, and NS-24520

Isothermal Titration

Ernesto Freire, Obdulio L. Mayorga[1], and Martin Straume
Biocalorimetry Center
Department of Biology
The Johns Hopkins University
Baltimore, MD 21218

Calorimetric techniques have contributed a great deal to our current understanding of the mechanisms of regulation and control of biological structures and processes at the molecular level. Over the past decade and a half, advances have been made in both the development of highly sensitive microcalorimetric instrumentation and the development of analytical procedures to extract thermodynamic information about biological systems (see References 1–4 for reviews).

The principal calorimetric techniques that have contributed this information are differential scanning calorimetry (DSC) and isothermal titration calorimetry (ITC). By applying DSC, researchers have learned about the nature and magnitude of the forces that stabilize biological macromolecules (such as proteins and nucleic acids) and macromolecular assemblies (lipid bilayers, protein–lipid complexes, and protein–nucleic acid complexes). Accurate determination of the energy of stabilization of these biological structures by DSC has made possible elucidation of mechanistic details regarding interactions between regions within macromolecules and among components in multimolecular assemblies. DSC experiments involve perturbing the system under study by varying the thermal energy content of the sample (i.e., by scanning temperature as the independent variable under experimental control). The heat capacity of the system is then measured against temperature as the direct thermodynamic observable (recall that the heat capacity is the temperature derivative of enthalpy).

In contrast, ITC measures the energetics of biochemical reactions or molecular interactions (ligand-binding phenomena, enzyme–substrate interactions, and interactions among components of multimolecular complexes) at constant temperature. In this case, reaction is triggered by changing the chemical composition of the sample by titration of a required reactant. The heat associated with the reaction is the direct thermodynamic observable (related to both the enthalpy and extent of reaction). In an ITC experiment, the total concentration of reactant is therefore the independent variable under experimental control.

Because the majority of biological reactions can be induced isothermally, the potential range of applications of ITC far exceeds that of DSC. However, until recently, the use of ITC has been limited because of a lack of sufficient sensitivity. The situation has changed with the recent development of instruments capable of measuring heat effects arising from reactions involving as little as nanomole amounts of reactants (*5–11*). This new generation of titration calorimeters makes possible direct thermodynamic characterization of association processes exhibiting very high affinity binding constants (10^8–10^9 M^{-1}) that are frequently found in biological reactions (*5–11*).

In this article we will present an overview of ITC and recent advances in ITC technology, discuss future directions for further evolution and application of ITC to biomedical research, outline the mathematical treatment of data for some simple binding models, and describe some recent applications of ITC to systems of biological interest.

Binding equilibrium

The association of biological macromolecules with one another as well as their association with small ligand molecules plays a central role in the structural assembly and functional regulation of biological systems and thus has attracted the attention of many investigators in recent decades. Throughout the years, biologists have studied these processes using a variety of experimental techniques and analytical methods to obtain accurate descriptions of their equilibrium behavior.

Several parameters must be included in the description of binding or association equilibria. First is the number of binding sites or stoichiometry of the reaction. Second is the strength of the association, usually expressed in terms of the association constant, K_a, or the Gibbs free energy of association, $\Delta G = -RT \ln K_a$. Third is the characterization of multiple sites and positive or negative cooperative interactions for those cases in which more than one binding site is present. Fourth is the characterization of the enthalpic and entropic contributions to the Gibbs free energy of association ($\Delta G = \Delta H - T\Delta S$). Fifth is the characterization of the dependence of the binding equilibrium on other environmental variables such as pH, ionic strength, and so forth. Most experimental techniques and analytical methods for binding studies are designed to evaluate these different parameters.

Two different approaches are normally used to study the binding equilibrium between two molecules. One approach relies on the direct measurement of the concentrations of free and bound ligand molecules using a technique such as equilibrium dialysis. The other approach takes advantage of the existence of changes in physical observables that are proportional to the extent of binding saturation. The binding of oxygen to hemoglobin, for example, causes changes in the optical absorbance in the Soret region (~420 nm) of he noglobin (*12–14*). The magnitude of these changes is proportional to the degree of saturation and has been used extensively in the analysis of this binding process (*12–14*).

Calorimetric titration, which belongs to this second type of approach, measures the heat released or absorbed by

[1] Permanent address: Department of Physical Chemistry, University of Granada, Granada, Spain

0003-2700/90/0362-950A/$02.50/0.

Calorimetry

Direct Thermodynamic Characterization of Biological Molecular Interactions

INSTRUMENTATION

the stepwise addition of a ligand molecule to a solution containing the macromolecule under study. In general, whatever the approach used to examine binding, the goal is to generate a binding isotherm, a curve that represents the degree of saturation in terms of the ligand concentration. In ITC, the degree of saturation is defined in terms of the heat associated with the reaction.

Throughout the years, different mathematical procedures have been devised to estimate association constants, numbers of binding sites, and cooperative interactions from ligand-binding isotherms. In this respect, the analysis of calorimetrically determined binding isotherms follows the same principles. Among biologists, linearized representations of the data have been widely used in the past. A particularly popular transformation has been the Scatchard plot, in which the ratio of the concentrations of bound and free ligand is plotted against the concentration of bound ligand. These transformations, however, usually introduce statistical biases in the analysis because they obscure the distinction between dependent and independent variables.

In general, a more robust and statistically significant parameter estimation can be achieved by direct nonlinear least-squares analysis of the dependent versus independent variable. With the widespread availability of computers, the trend toward this type of analysis has gained popularity in recent years (*15*, *16*) and this is the type we will discuss here.

The major advantage of titration calorimetry derives from the fact that the binding isotherms are defined in terms of the heats of reaction and as such they allow a direct estimation of enthalpy changes in addition to the association constant. Use of the relation $\Delta G = -RT \ln K = \Delta H - T\Delta S$ allows further calculation of the entropy change. Thus a single calorimetric titration provides a complete characterization of the energetics of binding. In contrast, estimation of enthalpy and entropy changes using noncalorimetric techniques requires several binding experiments at multiple temperatures and subsequent analysis of the temperature dependence of the association constant. Calorimetry is unique because it provides direct measurement of the thermodynamic quantities of interest.

What is ITC?

With ITC, one measures directly the energetics (via heat effects) associated with reactions or processes occurring at constant temperature. Experiments are performed by titration of a reactant into a sample solution containing the other reactant(s) necessary for reaction. After each addition, the heat released or absorbed as a result of the reaction is monitored by the isothermal titration calorimeter. Thermodynamic analysis of the observed heat effects then permits quantitative characterization of the energetic processes associated with the binding reaction.

Applications of ITC in the 1970s were directed toward characterization of the thermodynamics of enzyme-catalyzed reactions (*17–19*), ligand binding to macromolecules (*20–23*), and ligand- or pH-induced macromolecular conformational changes (*24*). However, reliable measurement of heat effects could be performed only at levels of 10^{-3} cal or greater (see References 25–27 for reviews). Because of these limits in sensitivity, only those biological reactions exhibiting relatively strong heat effects could be studied. Entire binding isotherms for ligand-binding reactions could be obtained only for reactions exhibiting ligand association constants of 10^4 M^{-1} or less because sufficiently low reactant concentrations could not be examined to determine higher affinity binding constants. For those binding reactions with $K_a > 10^4$ M^{-1}, only overall binding enthalpies, but not binding constants, could be determined directly from calorimetric titrations (some other method was required to determine K_a).

Over the years, technologies and instrument designs have evolved to produce isothermal titration calorimeters with much improved capabilities for detection of ever smaller heat effects. Such efforts during the 1980s led to the design and construction of titration microcalorimeters capable of measuring heat effects down to levels of 10^{-6} cal (*5–11*). The most significant of these developments have been those related to increasing the specific sensitivity and improving the time response of titration microcalorimeters. Because biomolecular association reactions are frequently characterized by very high binding constants (in the range of 10^8 M^{-1} or greater), experiments must be conducted under conditions of very dilute reactants (10^{-6} M or less) to accurately determine equilibrium constants as well as binding enthalpies. As such, a major goal in calorimetric design is optimization of the specific instrument sensitivity (heat per unit volume) rather than the absolute sensitivity.

Fundamental principles of isothermal titration calorimeter operation

Figure 1 is a schematic showing a differential, power compensation isothermal titration calorimeter (ITC-2) developed at the Biocalorimetry Center at The Johns Hopkins University. Detection of heat effects in this isothermal calorimeter is accomplished by use of semiconductor thermopiles interposed between the titration cells and a heat sink (a large metal mass in thermal equilibrium with a thermostatted water bath). Two titration cells reside in the calorimeter assembly; one acts as the reference and the other as the sample titration cell. When an ITC experiment is being performed, the reference cell contains buffer only and the sample cell contains buffer plus the reactant to which the injected material will be titrated.

Prior to beginning the experiment, the instrument's injection mechanism is filled with titrant, the titration cells are filled with the material to be titrated, and the calorimeter is equilibrated

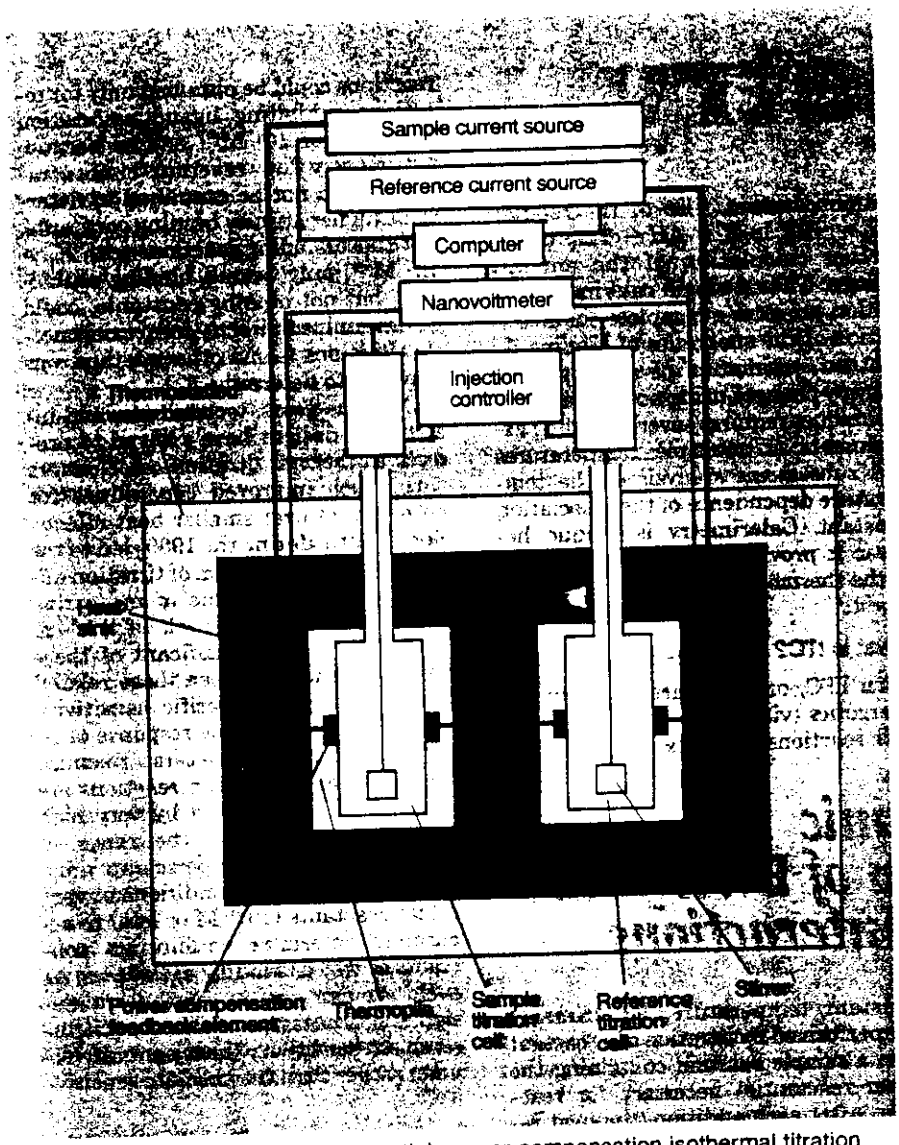

Figure 1. Schematic of the differential, power compensation isothermal titration calorimeter.
See text for operational details.

to the desired temperature such that all components of the instrument (i.e., titration cells, heat sink, and thermostatted water bath) have come to thermal equilibrium relative to each other. Identical injections of reactant are then introduced into both mechanically stirred titration cells by a dual-injection mechanism. The contents of the reference cell exhibit heat effects arising from injection and dilution of the reactant being titrated. The contents of the sample cell exhibit these same heat effects in addition to that associated with the reaction under study. Dual-injection isothermal tiration calorimeters compensate in real time for both the heat effects arising from dilution of the injected reactant into the sample and for any mechanical heat effects arising from injection, yielding the heat of reaction of interest directly.

The titration cell compartments are constructed to permit heat flow between the titration cells and the heat sink only through the thermopile thermal detectors. The output of the thermopiles, an electrical potential (voltage), is directly proportional to the temperature difference across the faces of the thermopiles. This temperature difference, in turn, is proportional to the thermal power (rate of heat transfer [cal s^{-1}]) being exchanged between the titration cells and the heat sink. In the absence of power compensation, the time integral of this rate of heat transfer is the total heat of reaction induced in the respective titration cells as a result of injection.

Because the thermopiles of the sample and reference titration cells are connected in opposition electrically, the experimental quantity actually monitored by this differential isothermal titration calorimeter is the difference in the rates of heat production or absorption between the sample cell and the reference cell. A nanovoltmeter measures the differential voltage output produced by the thermopiles and transmits this information to a computer interfaced for data acquisition and dynamic control of a power compensation mechanism. Power compensation is accomplished by continuously regulating the amount of heat applied to the titration cells so as to drive the temperature difference between the two cells toward the baseline, steady-state value.

The computer monitors the nanovoltmeter output (which is proportional to the temperature difference between the two titration cells) and adjusts the current applied to the cell feedback elements to compensate for the detected change in differential temperature between the cells. The applied thermal power as a function of time required to return the isothermal titration calorimeter to its steady-state temperature differential following an injection then becomes the experimentally determined quantity and is directly proportional to the heat of reaction of interest.

Increased intrinsic sensitivity

Very precise determination of temperature changes is necessary for reliable detection of heat effects on the order of 10^{-6} cal or less. The output of thermopile temperature detectors, as employed in the isothermal titration calorimeter developed in our laboratory and discussed here, is an electrical potential proportional to the temperature difference across the thermopiles. The magnitude of the voltage change per change in temperature is therefore an important consideration in instrument design so as to produce the maximum measurable response. During the past decade, semiconductor bismuth–telluride thermopiles have been introduced possessing 70 thermocouples (the individual temperature-sensing elements of thermopiles) per square centimeter. The use of thermopiles with a high density of thermocouple junctions per unit area provides enhanced voltage per degree response. The ITC-2 is equipped with 1056 of these junctions and is able to detect changes on the order of 10^{-8} cal s^{-1} (i.e., 40–50 nW) in thermal power.

Minimization of baseline noise is another factor important for improving isothermal titration calorimeter sensitivity levels. In the ITC-2 we have housed the titration calorimeter assembly in an ultrastable thermostat-

ted water bath to regulate temperature. Any fluctuations in bath temperature will transmit the temperature change via the heat sink to the titration cells and contribute to baseline noise, compromising instrument performance. The thermal damping effect provided by the mass of the metal heat sink in ITC-2 coupled with a stable thermostat capable of maintaining temperatures to within 10^{-6}–10^{-5} °C over periods of minutes (and within 10^{-4} °C over 8 h) (*28*) has reduced the magnitude of baseline noise to a level on the order of 10^{-8} cal s^{-1} (i.e., tens of nanowatts), thereby facilitating detection of small heat effects.

The ability to perform differential measurements of reference and sample responses in dual-injection instruments facilitates more accurate determination of heats of reaction. Because reaction is initiated in an ITC experiment by injection of a reactant, heat effects resulting from the mechanical disturbance of the injection event itself and dilution of the titrant are present in addition to the heat of reaction, which is the quantity of interest. A differential, dual-injection isothermal titration calorimeter compensates for these heat effects in real time. This eliminates the need for two separate experiments (a reference experiment to yield heats of injection and dilution and a sample experiment to exhibit these effects and that of the reaction of interest) as required in a single-injection ITC (*11*).

Treatment of data obtained from single-injection ITC experiments involves subtracting these two individually observed responses to yield estimates of the heat of reaction of interest (*11*). Because they compensate in real time for any mechanical and dilution heat effects, dual-injection titration microcalorimeters capable of differential measurements do not introduce the additional error arising from consideration of two separate measurements.

Improved time response

The implementation of power compensation mechanisms some years ago has been a major factor in improving the time response of isothermal titration and differential scanning calorimeters and therefore in providing more accurate measurement of small heats of reaction (*7*). Because the total heat associated with a reaction is the time integral of the differential thermal power released or absorbed as a result of the reaction, reducing the time response is a means to more sensitive detection of total heat effects per injection. Heat conduction isothermal titration calorimeters passively transfer heat between the titration cell(s) and heat sink, giving rise to instrument time responses with lifetimes on the order of 100–300 s (*8–10*). The instrument discussed here uses continuous power compensation for active heat transfer and exhibits both considerably reduced instrument response times and improved signal-to-noise (S/N) characteristics. Active power compensation mechanisms, as introduced by McKinnon et al. (*7*), lead to reduced instrument response times and produce greater thermal power amplitude (the experimental observable) for equivalent heat effects. In other words, the S/N is increased as a result of the enhanced thermal power amplitude necessary to generate the same total observed heat signal (area under the thermal power versus time curve) in a shorter period of time before return to baseline.

This effect is demonstrated in Figure 2 in which the response signal of the instrument to identical 25 μcal pulses is recorded for both the case in which power compensation is active and in which it is not (heat conduction mode). In both cases, the areas under the curves are identical but the signal deflection is approximately four times larger when power compensation is active. In the absence of power compensation, the instrument time response is 100 s whereas under power compensation conditions it is only 15 s. The recorded quantity in a power compensation titration calorimeter is the amount

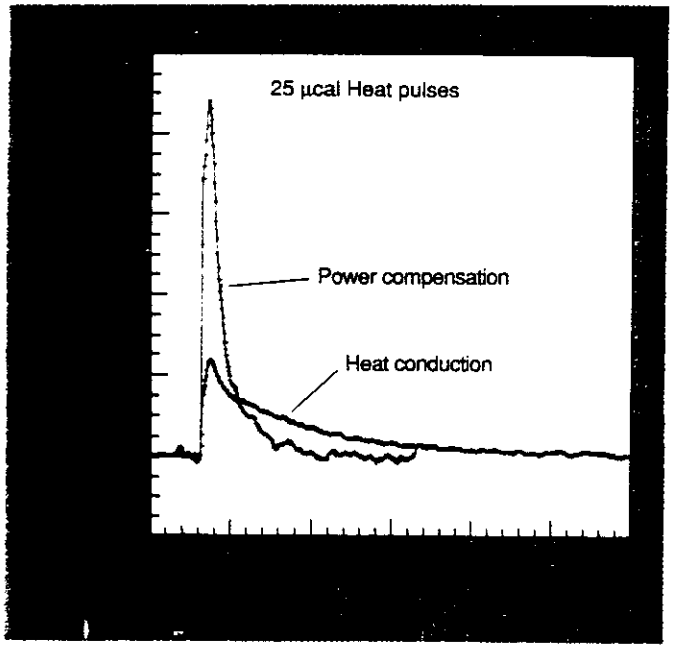

Figure 2. Power compensation vs. heat conduction modes of ITC-2 operation.

The observed differential thermal power vs. time response in the power compensation mode is distributed over a shorter period of time than that measured in the heat conduction mode. The amplitude of the thermal power response in the power compensation mode is greater than that detected in the heat conduction mode because of the more rapid instrument response.

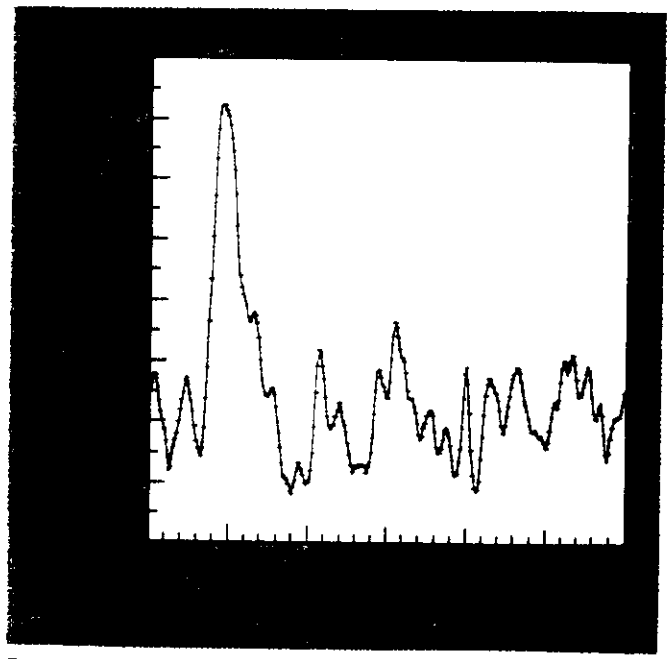

Figure 3. Differential thermal power vs. time response obtained from introduction of a 0.5 μcal mL^{-1} electrical calibration pulse into the sample titration cell of ITC-2 (sample contains 5 mL of water).

The maximum peak amplitude is 105 ncal s^{-1} (21 ncal s^{-1} mL^{-1}) with S/N sufficiently high to permit reliable measurements to considerably less than 1 μcal mL^{-1} $event^{-1}$.

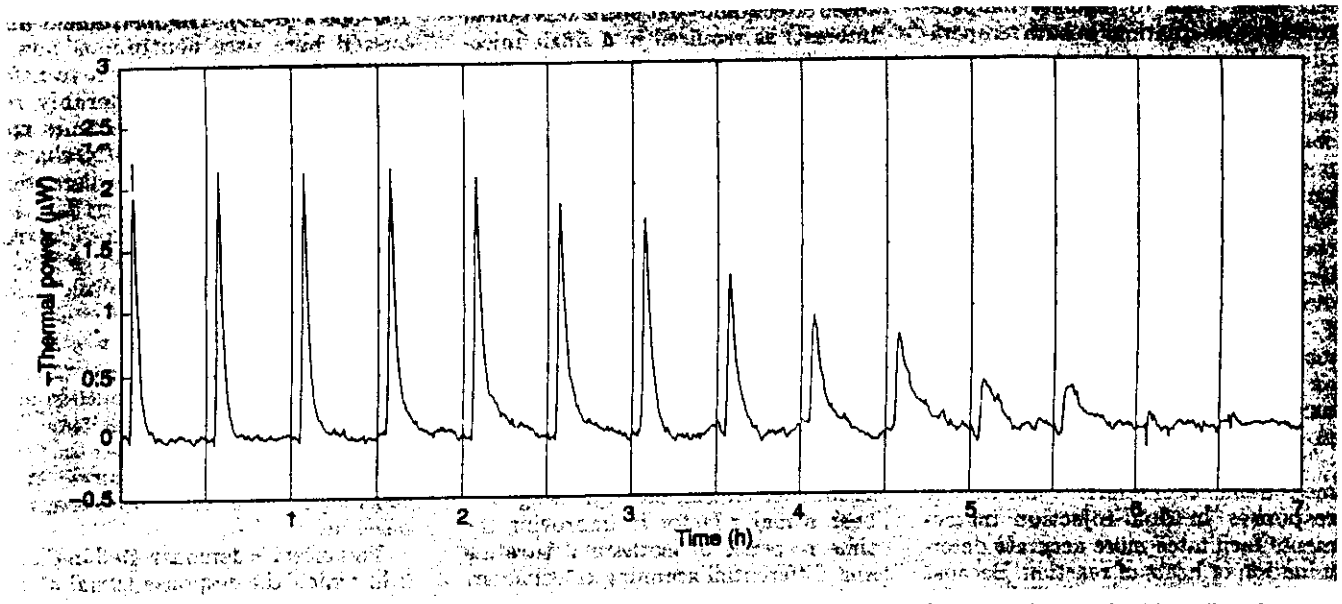

Figure 4. Isothermal calorimetric titration of cholera toxin B-subunit pentamer with oligo-G_{M1}, the oligosaccharide cell surface receptor for cholera toxin.

The differential power output in microwatts (4.184 μW = 1 μcal s^{-1}) is shown as a function of time and was obtained from successive injections of 3 nmol of oligo-G_{M1} (30-μL injections of 0.1 mM oligo-G_{M1}) into a solution of 4.9 nmol of B-subunit pentamer in 1.4 mL. (Reprinted from Reference 10.)

of thermal power that must be applied to compensate for the heat of reaction induced by injection. Because the intrument is both continuously monitoring the temperature differential (thermopile output) and continuously regulating the amount of applied thermal power (through the feedback elements) to actively return the system to the preinjection, steady-state temperature differential, the time required to obtain the total heat associated with the induced reaction is reduced.

In order to have the capability to compensate for exothermic and endothermic effects, a constant amount of thermal power is applied to both titration cells and a steady-state flux of thermal throughput from the cells to the heat sink is established. The amount of steady-state power applied to the cells is sufficiently small (0.5 mA of current through ~230 Ω of resistance, producing 14–15 × 10^{-6} cal s^{-1} of thermal power in 5 mL of cell volume) so that the overall temperature is not perturbed beyond the fluctuation regime of the thermostat. Compensation is accomplished by regulating the power introduced through the feedback elements (by changing the amount of applied current) in proportion to the change in thermopile output (detected change in temperature).

In addition to power compensation, the thin, disk-shaped gold titration cells used in the ITC-2 contribute to optimizing the response time. Positioning the walls of the titration cells in close opposition to each other minimizes the distance heat must travel through the medium prior to encountering the thermopiles (which are in direct contact with the cell faces between the titration cells and heat sink). This design facilitates rapid detection of heat effects induced in the titration cell contents by injection of titrant.

Definitions used for reporting response times and noise levels vary in the literature and commercial documentation. Our definition of response time is the time required for decay of the thermal power amplitude to $1/e$ of its maximum value. Response times are frequently referred to, however, in the context of rise times to half maximal amplitude. By that definition, the ITC-2 has a response time of 3–4 s. In considering baseline noise levels, we report baseline noise as the standard deviation of the noise amplitude in individual baselines, in contrast to the standard error of reproducibility obtained from a large number of multiple, identical injections.

The differential, power compensation isothermal titration calorimeter described here currently has a limit of resolution of 10^{-6} cal of total heat. This represents a substantial improvement of approximately 3 orders of magnitude in sensitivity from the ~10^{-3} cal resolution in earlier reaction calorimeters. The titration cell volume is 5 mL, making the limit of specific sensitivity ~0.2 × 10^{-6} cal mL^{-1}.

An example of the limiting resolution of the instrument is presented in Figure 3, which shows its response to a pulse of 0.5 × 10^{-6} cal mL^{-1} (2.5 × 10^{-6} cal total heat) introduced into the sample titration cell. The baseline noise level is ±4–8 × 10^{-9} cal s^{-1} (standard deviation) or a peak-to-peak noise of 40 × 10^{-9} cal s^{-1} corresponding to a specific noise level of ±0.8–1.6 × 10^{-9} cal s^{-1} mL^{-1} (standard deviation) or a peak-to-peak specific noise of 8 × 10^{-9} cal s^{-1} mL^{-1}.

Analysis of ITC data

The function of many biological systems is modulated by ligand binding (e.g., binding of hormones or toxins to their target receptors, allosteric or feedback control of enzymes or other functional proteins, signal peptide–membrane interactions, and protein–nucleic acid interactions). Characterization of the energetics of such processes may be accomplished by ITC experiments. Upon binding of a ligand to a macromolecule (e.g., protein) or macromolecular assembly (e.g., multisubunit protein or membrane systems), heat will be released or absorbed accompanying the binding event (i.e., the enthalpy of ligand binding). The heat effects associated with each addition of ligand represent the experimentally observed response in an ITC experiment. For each injection, the heat released or absorbed is given by

$$q = V\Delta H\Delta[L_B] \qquad (1)$$

where q is the heat associated with the change in bound ligand concentration, $\Delta[L_B]$ is the change in bound ligand concentration, ΔH is the enthalpy of binding (mol ligand)$^{-1}$, and V is the reaction volume.

Because q is directly proportional to

the increase in ligand bound resulting from each injection, its magnitude decreases as the fractional saturation of the system is titrated stepwise to completion. This is illustated in Figure 4 in which the B-subunit pentamer of cholera toxin is calorimetrically titrated with oligo-G_{M1}, the oligosaccharide binding region of its glycolipid cell surface receptor (see the section "Cholera toxin binding to oligo-G_{M1}" later in this article for more detail). The total cumulative heat released or absorbed is directly proportional to the total amount of bound ligand as

$$Q = V\Delta H \sum \Delta[L_B] = V\Delta H[L_B] \quad (2)$$

where Q is the cumulative heat and $[L_B]$ is the concentration of bound ligand.

Evaluation of calorimetric titration data as either individual or cumulative heat requires consideration of the heat evolved or absorbed as a function of total ligand added, or the total ligand concentration (the independent variable). Therefore, in the analysis of experimental data, the binding equations must be expressed in terms of the individual or cumulative heat released or absorbed as a function of total ligand concentration because these are the quantities experimentally known.

Multiple sets of independent binding sites

The most widely used theoretical framework for the analysis of binding data in biology is the so-called Multiple Sets of Independent Binding Sites model (for a complete review, see References 29 and 30). Within this framework, a macromolecule possesses an arbitrary number of sets of noninteracting binding sites. All of the sites in the same set possess the same intrinsic affinity for the ligand molecule. The great popularity of this model is due in part to its flexibility, which allows characterization of a large number of situations (See References 29 and 30 for some representative examples).

As expressed in Equation 1, the heat associated with the binding reaction is directly proportional to the concentration of bound ligand, $[L_B]$. For a system exhibiting multiple sets of independent binding sites, the concentration of ligand bound to each set is given by

$$[L_{B,i}] = [M]\frac{n_iK_i[L]}{1 + K_i[L]} \quad (3)$$

where $[L_{B,i}]$ is the concentration of ligand bound to binding sites of set i, $[M]$ is the total concentration of macromolecule available for binding ligand, K_i is the intrinsic site association constant for binding sites of set i, n_i is the number of binding sites of set i on each macromolecule M, and $[L]$ is the concentration of free ligand.

The cumulative amount of heat released or absorbed as a result of ligand binding is given by the sum of the heats corresponding to each set as

$$Q = V\sum_i \Delta H_i[L_{B,i}]$$

$$= V[M]\sum_i \frac{n_i\Delta H_iK_i[L]}{1 + K_i[L]} \quad (4)$$

where ΔH_i is the enthalpy of binding (mol ligand)$^{-1}$ to binding sites of set i. This equation can be expressed in terms of the total ligand concentration by way of the mass conservation expression $[L_T] = [L_B] + [L]$ (where $[L_T]$, $[L_B]$, and $[L]$ represent the total, bound, and free ligand concentrations, respectively). Analysis of calorimetric titration data is then performed by estimating the variable model parameters (n_i, K_i, and ΔH_i) by fitting either to the cumulative heat, Q, or to the individual heat, q (where the individual heat associated with the j-th injection event is q_j such that $q_j = Q_j - Q_{j-1}$). Analysis of data directly in terms of individual heats, q, is preferable because it eliminates propagation of the uncertainties associated with each successive injection that are necessarily present in cumulative heat data.

The two simplest cases are for one and two independent sets of ligand-binding sites. These cases allow explicit, closed-form expressions for Q as a function of total ligand concentration as illustrated in Figures 5 and 6.

Figure 5 presents a schematic depiction and the closed-form equations characteristic of ligand binding to a macromolecule possessing one set of independent ligand-binding sites, the simplest special case of the general expression given by Equation 4. In the example depicted in this figure, the ligand-binding macromolecule possesses four independent and equivalent ligand-binding sites. Although $n = 4$ in this example, the expressions presented here are valid for any value of n. The open circles in the figure correspond to binding sites without bound ligand whereas the shaded squares represent binding sites with ligand bound. The binding constant, K, characterizes the affinity of each ligand-binding site for ligand L. The factors of 4, $\frac{3}{2}$, $\frac{2}{3}$, and $\frac{1}{4}$ are the particular statistical factors necessary to define the respective macroscopic equilibria for this case (i.e., $n = 4$) in terms of the site affinity constant, K.

The total cumulative heat, Q, is most conveniently expressed in terms of the free ligand concentration, $[L]$. However, the independent variable in ITC experiments is the total ligand concentration, $[L_T]$ (where $[L_T] = [L_B] + [L]$ and $[L_B]$ is the concentration of bound ligand). By recognizing that $[L_B] = Q/V\Delta H$ (where V is the reaction volume and ΔH is the binding enthalpy per mole of ligand), a closed-form expression is obtained for the cumulative heat, Q, in terms of the total ligand concentration, $[L_T]$. The energetics of a system obeying this model for ligand

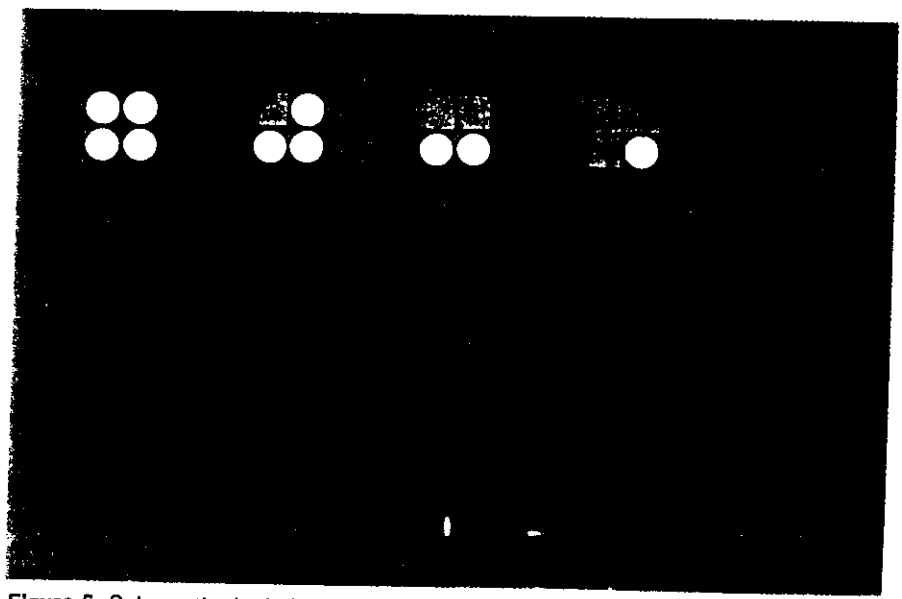

Figure 5. Schematic depiction and closed-form equations characteristic of ligand binding to a macromolecule possessing one set of independent ligand-binding sites.
Shaded regions represent subunits to which ligand is bound. See text for a detailed description of relevant concepts.

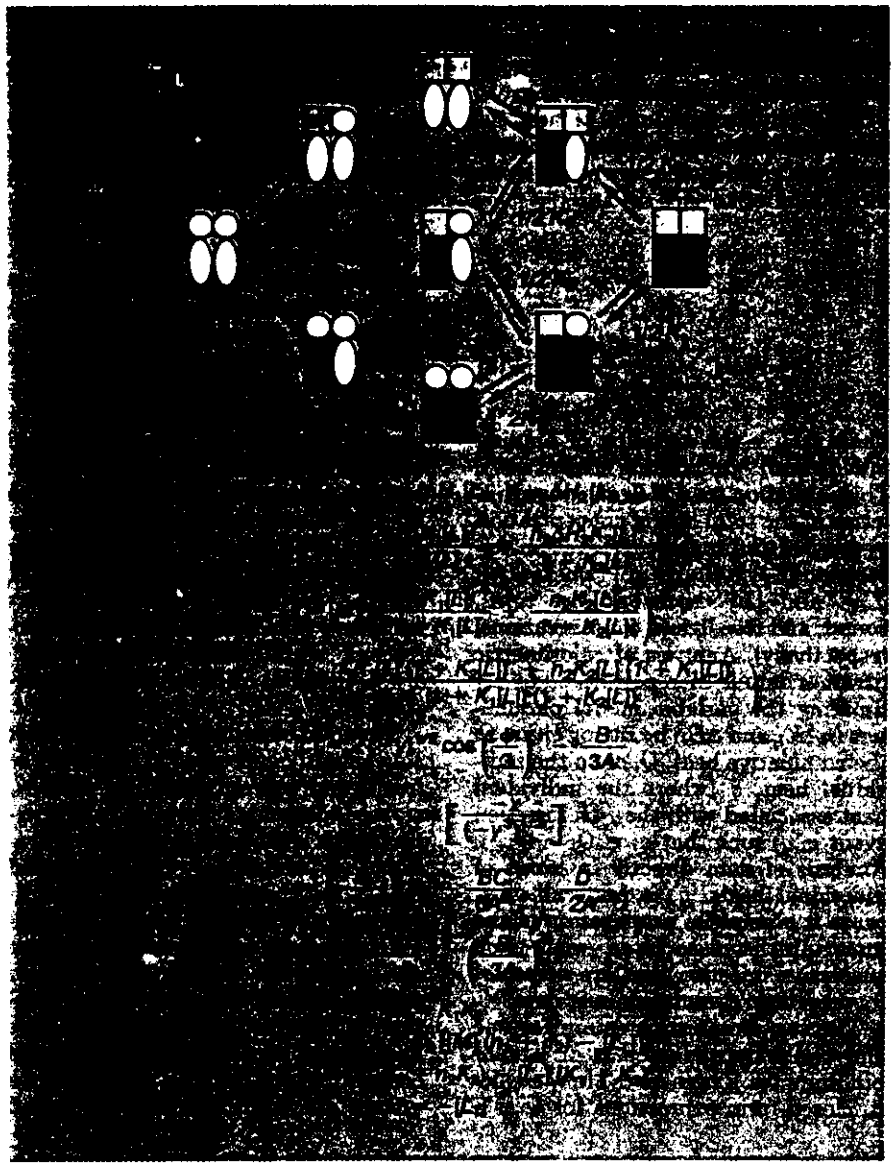

Figure 6. Closed-form equations for ligand binding to a macromolecule possessing two sets of independent binding sets.

Shaded regions represent subunits to which ligand is bound. See text for a detailed description of relevant concepts.

binding may therefore be considered in terms of $[L_T]$, $[M]$ (the total concentration of ligand-binding macromolecule), n, K, and ΔH for a known V.

This simple case is one of the few permitting such an explicit analytical solution. In general, a numerical approach is needed to express Q in terms of $[L_T]$. Estimation of the model parameters characteristic of this binding model (n, K, and ΔH) then requires fitting to either the cumulative heat, Q, or to the individual heat, q.

Figure 6 shows the closed-form equations for ligand binding to a macromolecule possessing two sets of independent binding sites. This case is an extension of the model presented in Figure 5 according to the general expression of Equation 4 and permits derivation of convenient closed-form expressions for the cumulative heat versus total ligand concentration. For illustrative purposes, this figure shows an example of a macromolecule possessing a total of four binding sites for ligand L, two of which have a site binding constant K_1 and the other two characterized by site binding constant K_2 (i.e., $n_1 = 2$ and $n_2 = 2$).

Even though the example in the figure uses $n_1 = n_2 = 2$, the equations in the figure are valid for any values of n_1 and n_2. The open circles and ovals represent the two respective types of binding sites without ligands whereas the shaded squares and rectangles correspond to the respective types of sites with ligands. The factors 2 and $\frac{1}{2}$ are the statistical factors necessary to define the indicated macroscopic equilibria in this example in terms of the site binding constants, K_1 and K_2 (i.e., for the case where both n_1 and $n_2 = 2$).

The total cumulative heat, Q, will be composed of contributions from binding to each of the two sets of ligand-binding sites on the macromolecule, Q_1 and Q_2. These, in turn, are related to the reaction volume, V, the respective site-binding enthalpies, ΔH_1 and ΔH_2 (per mole of bound ligand), and the concentrations of ligand L bound to the respective types of sites on the macromolecule, $[L_{B,1}]$ and $[L_{B,2}]$. Although the solution for this case is considerably more involved than that for the single-set-of-sites case (see Figure 5), expressions in terms of the total ligand concentration, $[L_T]$ (the independent variable in a titration experiment), may be obtained explicitly.

Cases in which more than two sets of binding sites are present cannot be solved in closed form and iterative numerical procedures must be used to solve Equation 4. In general, other situations like those in which cooperative interactions are present can be approached following the same philosophy, that is, development of the binding equations in terms of the total ligand concentration. For example, this approach has been used for the cooperative binding of cholera toxin to oligo-G_{M1}, the oligosaccharide binding region of its glycolipid cell surface receptor (*10*).

ITC applied to biological systems

We conclude this article by surveying some representative biological systems that have been studied by ITC.

Nucleotide binding to ribonuclease A. The detailed thermodynamic properties of 3′-cytidine monophosphate (3′CMP) binding to ribonuclease A (RNaseA) were studied in a comprehensive calorimetric titration study undertaken by Biltonen and co-workers in the 1970s (*20*, *21*, *31*, *32*). Initial experiments were directed toward characterizing the fundamental thermodynamic binding properties of this system (Gibbs free energy, enthalpy, and entropy of interaction) in addition to binding stoichiometry and how these properties are influenced by salt concentration (*20*). In low-ionic-strength solution ($\mu = 0.05$ in either NaCl or KCl, pH 5.5), a binding stoichiometry of one 3′CMP bound per RNaseA molecule was found exhibiting $\Delta G = \sim -6.2$ kcal mol^{-1} (corresponding to an association constant of 3.7×10^4 M^{-1}), $\Delta H = \sim -15.5$ kcal mol^{-1}, and $\Delta S = \sim -30$ cal K^{-1} mol^{-1} for the binding process.

The thermodynamic binding param-

eters varied in a continuous manner with increasing ionic strength until at $\mu = 3$ (in sodium acetate, pH 5.5), the ΔG for binding became less favorable to ~ -4.5 kcal mol^{-1} (corresponding to an association constant of 2.1×10^3 M^{-1}) as a result of a considerably less favorable ΔH for binding (which became ~ -6 kcal mol^{-1}) and despite a somewhat more favorable ΔS for binding (~ -5 cal K^{-1} mol^{-1}).

Analysis of the enthalpic and entropic contributions to the free energy of protonation of the four histidine residues of RNaseA suggested that binding of 3′CMP is coupled to ionization of three of these residues. It has been suggested that the negative phosphate moiety of 3′CMP interacts electrostatically with two positively charged histidines and that interaction with the third (which shows an anomolously large enthalpy of protonation) involves a conformational rearrangement of the structure of RNaseA (*21*). The dependence on pH of the enthalpic and entropic contributions to the overall free energy of 3′CMP binding, when considered in conjunction with structural information, led to the conclusion that both van der Waals and electrostatic interactions contribute to binding but that the binding process is only weakly coupled to the conformational change associated with protonation of the histidine residues (*31*, *32*).

Ligand binding and conformational transitions in human hemoglobin. The energetics associated with the binding of a variety of ligands to native and mutant human hemoglobins have been examined by application of titration calorimetric methods (*33–36*). By performing calorimetric titrations in buffers differing in their heats of protonation, the enthalpies of protonation of ionizable groups (histidines and/or α-amino groups) in response to oxygen, carbon monoxide, and inositol hexaphosphate (IHP) binding have been determined at different pHs. Enthalpies of carbon monoxide binding have been reported to be ~ -23 kcal (mol CO)$^{-1}$ in the pH range from 6 to 9 (after correction for enthalpies of ionization of protein groups) (*33*).

These results were shown to be consistent with a model in which two ionizable histidines explain the origin of the Bohr proton effect. Interpretation of the relative enthalpic contributions of carbon monoxide binding and protein group ionization in a mutant and native human hemoglobin suggests that the enthalpy of protonation of ionizable protein groups is an important driving force for regulating heme site ligation as well as subunit association and hemoglobin tetramer conformational transitions.

The regulation of hemoglobin's functional properties is related to its ability to bind oxygen cooperatively. Calorimetric information from carbon monoxide-binding results obtained from a mutant hemoglobin (Hb M Iwate) and native hemoglobin, in conjunction with independent determinations of T-to-R transition free energies, suggests that the structural transition responsible for modifying the affinity of human hemoglobin for oxygen (the T-to-R transition, which gives rise to its cooperative oxygen-binding properties) is enthalpically controlled at pH 7.4 (with $\Delta H = 9 \pm 2.5$ kcal mol^{-1}) but entropically controlled at pH 9 (with $\Delta H = -12 \pm 2.5$ kcal mol^{-1}) (*34*).

The interaction of the regulatory ligand inositol hexaphosphate exhibits binding enthalpies of up to ~ -25 kcal mol^{-1} at pH 7.4 (after correction for buffer ionization effects). This binding corresponds to ~ -11 kcal (mol H$^+$ absorbed)$^{-1}$ associated with IHP binding. The binding of this regulatory ligand has therefore been concluded to be driven primarily by the exothermic protonation of histidine and/or α-amino groups as induced by the proximity of the negative phosphate charges on IHP (*35*, *36*).

Signal peptide–lipid association. The interactions of the signal peptide of ornithine transcarbamylase with phospholipid vesicles of varying composition have recently been studied by isothermal titration calorimetry (*9*). It is the signal peptide sequences of newly translated mitochondrial proteins that have been recognized as being responsible for targeting and facilitating transport of these proteins into mitochondria. Because these sequences contain a large proportion of basic amino acids, they are expected to exhibit a strong interaction with the highly negative charged inner mitochondrial membrane. Titration of the signal peptide into phospholipid bilayers of surface charge density similar to that of the inner mitochondrial membrane reveals a strong binding characterized by an association constant on the order of 10^6 M^{-1} and an enthalpy change of -60 kcal mol^{-1}.

The experiments were consistent with a binding stoichiometry of 1 peptide bound per 20 negatively charged phospholipid molecules. The magnitude of the binding constant indicates a strong membrane association, similar to that required for mitochondrial protein import and similar to that obtained from inhibition studies of the precursor protein (pre-ornithine transcarbamylase) by the synthetic signal sequence (*37*).

Cholera toxin binding to oligo-G_{M1}. Cholera toxin is a multisubunit protein consisting of a five-subunit ring, the B-subunit pentamer (M_r = 58 000), which surrounds the dimeric A-subunit (M_r = 27 000). The B-subunit pentamer binds to five ganglioside G_{M1} molecules on the outer surface of the cell membrane, and subsequently the A-dimer penetrates the cell membrane where it activates adenylate cyclase. The association of the B-subunit pentamer with the oligosaccharide region (oligo-G_{M1}) of the ganglioside triggers the sequence of events that leads to the release of the A-subunit from the B-subunit pentameric ring and its insertion into the interior of the membrane.

For many years it was known that the association of oligo-G_{M1} with the toxin exhibited positive cooperativity (*38*) even though the actual energetics and mechanism of this behavior remained difficult to elucidate by conventional techniques. These cooperative effects have their origin at the oligosaccharide–protein interface and result in the modification of the behavior of the pentameric ring (*39*) during membrane association, presumably facilitating the release of the A-subunit into the membrane interior.

Recently, the binding of oligo-G_{M1} was measured by isothermal titration calorimetry (*10*). These experiments also indicated positive cooperativity and allowed a complete mapping of intrinsic as well as cooperative interactions. The data were consistent with a nearest-neighbor model in which the binding of oligo-G_{M1} to one B-subunit enhances the affinity of adjacent B-subunits. The experiments yielded an intrinsic association constant of 1.05×10^6 M^{-1} at 37 °C and a cooperative free energy of -850 cal mol^{-1}. The magnitude of the cooperative free energy indicates a fourfold enhancement in the oligo-G_{M1} binding affinity of a B-subunit adjacent to a subunit to which oligo-G_{M1} is already bound. The intrinsic enthalpy change of binding was -22 kcal (mol oligo-G_{M1})$^{-1}$ and the cooperative interaction enthalpy was -11 kcal mol^{-1}.

The magnitude of the cooperative interaction enthalpy is consistent with a moderate structural "tightening" of the B-pentamer in agreement with spectroscopic data. Within the context of the cholera toxin–cell surface interaction, the cooperative enhancement has a twofold effect: It facilitates a complete (i.e., productive) attachment of the toxin to the membrane surface once the initial contact has occurred and it facilitates the release of the A-subunit into the interior of the mem-

brane through its associated conformational change.

Amino acid interactions with human plasminogen. A thermodynamic characterization by titration calorimetry of the binding of ϵ-amino caproic acid (EACA) to the isolated kringle 4 region (K4) of human plasminogen has recently been reported (*40*). Activation of human plasminogen is effected by the binding of α- and ω-amino acids. The K4 of human plasminogen is one of five highly homologous regions that are believed to be quite independent domains. These domains are believed to be the functionally significant structural components of plasmin(ogen) responsible for mediating interactions with substrates as well as with negative and positive effectors. Calorimetric titrations with EACA were consistent with a single-set-of-binding-sites model and produced model parameters of $n = 0.87$, $K_a = 3.82 \times 10^4$ M^{-1}, $\Delta H = -4.50$ kcal mol^{-1}, and $\Delta S = 6.01$ cal K^{-1} mol^{-1} (*40*). The lack of a significant pH dependence on the thermodynamics of EACA binding (in the range from 5.5 to 8.2) suggested that titratable groups on K4 do not affect this binding interaction.

Further experiments with a series of structural analogues of EACA (3-aminopropionic acid, 4-aminobutyric acid, 5-aminopentanoic acid, 7-aminoheptanoic acid, 8-aminooctanoic acid, *trans*-(4-aminomethyl)cyclohexanecarboxylic acid, and L-lysine) demonstrated that both the length of the hydrophobic region between the amino and ω-carboxyl groups of the ligand and ligand steric structural constraints are important factors in determining the affinity of interaction (*40*).

Calcium and magnesium binding to oncomodulin. The calcium- and magnesium-binding properties of oncomodulin, a calcium-binding protein found in a variety of tumor, transformed, and nonembryonic placental cells, have been thermodynamically characterized by direct binding studies and calorimetric titration experiments (*41*). Oncomodulin possesses two Ca^{2+} and/or Mg^{2+} binding sites. The first site binds either Ca^{2+} or Mg^{2+} ions and exhibits a much higher affinity for Ca^{2+} than Mg^{2+} ($K_a(Ca^{2+}) = 2.2 \times 10^7$ M^{-1}, $K_a(Mg^{2+}) = 4.0 \times 10^3$ M^{-1}). Calcium binding to this site is competitively inhibited by Mg^{2+}. The second site binds Ca^{2+} only, but with a lower intrinsic affinity than the first ($K_a = 1.7 \times 10^6$ M^{-1}). Despite these differences in Ca^{2+} binding affinity, the exothermic Ca^{2+} binding enthalpies were the same for each site ($\Delta H = -4.52$ kcal mol^{-1}) giving rise to different positive Ca^{2+} binding entropy changes for the two sites ($\Delta S = 18.4$ cal K^{-1} mol^{-1} for the high affinity site and $\Delta S = 13.4$ cal K^{-1} mol^{-1} for the low affinity site). Binding of M_b^{2+} is associated with an endothermic enthalpy change and an even more positive entropy change than that seen with Ca^{2+} binding to either site ($\Delta H = 3.1$ kcal mol^{-1} and $\Delta S = 26.5$ cal K^{-1} mol^{-1}).

The thermodynamics of ion binding to the Ca^{2+}–Mg^{2+} site are similar to those observed in parvalbumins, a family of structurally related Ca^{2+} and Mg^{2+} binding proteins that are believed to function simply as intracellular Ca^{2+} and Mg^{2+} buffers. The presence of a Ca^{2+}-specific site on proteins of this class, however, suggests that oncomodulin may function as a signal-transducing Ca^{2+} binding protein (*41*). The presence of such specific Ca^{2+} binding properties has been associated with other proteins of this class that are involved in signal transduction (e.g., calmodulin, troponin C, S100, calpains, squidulin, and Ca^{2+} vector protein) and is believed to provide a mechanism for inducing conformational changes that regulate interactions with target proteins in response to changes in intracellular Ca^{2+} (*41*). Comparison of the thermodynamics of Ca^{2+} binding to oncomodulin at its Ca^{2+}-specific site to that of calmodulin shows some interesting differences. Whereas modulation of the exposure of hydrophobic protein regions is suggested to be involved in the functional regulation of calmodulin by Ca^{2+} binding (because of the strong entropy-driven nature of the binding interaction), Ca^{2+} binding to oncomodulin may be primarily electrostatic in nature (because of the nearly equal favorable enthalpic and entropic contributions of Ca^{2+} binding) (*41*).

Conclusion

The ability to measure small heats of reaction on the order of 10^{-7}–10^{-6} cal (mL of solution^{-1}) has opened the door to a direct thermodynamic characterization of many biological systems. Current sensitivity levels of isothermal titration microcalorimeters allow direct examination of binding processes exhibiting K_as as high as 10^8–10^9 M^{-1}. High sensitivity is also important when considering structurally complex systems like biological membranes, intact cells, or other biological systems that are difficult to concentrate or obtain in relatively large amounts. The recent developments in ITC technology presented here together with parallel advancements in data analysis methods are permitting a direct calorimetric characterization of biological phenomena previously beyond the scope of this experimental technique.

References

(1) Biltonen, R.; Freire, E. *CRC Crit. Rev. Bioc.* **1978**, *5*, 85.
(2) Privalov, P. L. *Adv. Prot. Chem.* **1982**, *35*, 1.
(3) Freire, E. *Comments Mol. Cell. Biophys.* **1989**, *6*, 123.
(4) Privalov, P. L.; Tiktopulo, E. I.; Venyaminov, S., Yu.; Griko, Yu., V.; Makhatadze, G. I.; Khechinashvili, N. N. *J. Mol. Biol.* **1989**, *205*, 737.
(5) Spokane, R. B.; Gill, S. J. *Rev. Sci. Instrum.* **1981**, *52*, 1728.
(6) Donner, J.; Caruthers, M. H.; Gill, S. J. *J. Biol. Chem.* **1982**, *257*, 14826.
(7) McKinnon, I. R.; Fall, L.; Parody, A.; Gill, S. J. *Anal. Biochem.* **1984**, *139*, 134.
(8) Ramsay, G.; Prabhu, R.; Freire, E. *Biochemistry* **1986**, *25*, 2265.
(9) Myers, M.; Mayorga, O. L.; Emtage, J.; Freire, E. *Biochemistry* **1987**, *26*, 4309.
(10) Schon, A.; Freire, E. *Biochemistry* **1989**, *28*, 5019.
(11) Wiseman, T.; Williston, S.; Brandts, J. F.; Lin, L-N. *Anal. Biochem.* **1989**, *179*, 131.
(12) Mills, F. C.; Johnson, M. L.; Ackers, G. K. *Biochemistry* **1976**, *15*, 5350.
(13) Chu, A. H.; Turner, B. W.; Ackers, G. K. *Biochemistry* **1984**, *23*, 604.
(14) Doyle, M. L.; DiCera, E.; Gill, S. J. *Biochemistry* **1988**, *27*, 820.
(15) Straume, M.; Johnson, M. L. *Biochemistry* **1988**, *27*, 1302.
(16) Straume, M.; Johnson, M. L. *Biophys. J.* **1989**, *56*, 15.
(17) Goldberg, R. N. *Biophys. Chem.* **1975**, *3*, 192.
(18) Goldberg, R. N. *Biophys. Chem.* **1976**, *4*, 215.
(19) Johnson, R.; Biltonen, R. *J. Am. Chem. Soc.* **1975**, *97*, 2349.
(20) Bolen, D. W.; Flogel, M.; Biltonen, R. L. *Biochemistry* **1971**, *10*, 4136.
(21) Flogel, M.; Biltonen, R. L. *Biochemistry* **1975**, *14*, 2603.
(22) Atha, D. H.; Ackers, G. K. *Biochemistry* **1974**, *13*, 2376.
(23) Gaud, H. T.; Barisas, B. G.; Gill, S. J. *Biochem. Biophys. Res. Commun.* **1974**, *59*, 1389.
(24) Atha, D. H.; Ackers, G. K. *J. Biol. Chem.* **1971**, *246*, 5845.
(25) Eftink, M.; Biltonen, R. In *Biological Microcalorimetry*; Beezer, A. E., Ed.; Academic Press: New York, 1980; pp. 343–412.
(26) Barisas, B. G.; Gill, S. J. *Ann. Rev. Phys. Chem.* **1978**, *29*, 141.
(27) Langerman, N.; Biltonen, R. *Methods Enzymol.* **1979**, *61*, 261.
(28) Suurkuusk, J.; Wadso, I. *Chemica Scripta* **1982**, *20*, 155.
(29) van Holde, K. E. *Physical Biochemistry*, 2nd ed.; Prentice-Hall: Englewood Cliffs, NJ, 1985; Chapter 3.
(30) Cantor, C. R.; Schimmel, P. R. *Biophysical Chemistry, Part III: The Behavior of Biological Macromolecules*; W. H. Freeman: New York, 1980; Chapter 15.
(31) Flogel, M.; Biltonen, R. L. *Biochemistry* **1975**, *14*, 2610.
(32) Flogel, M.; Albert A.; Biltonen, R. L. *Biochemistry* **1975**, *14*, 2616.
(33) Rudolph, S. A.; Gill, S. J. *Biochemistry* **1974**, *13*, 2451.
(34) Gaud, H. T; Gill, S. J.; Barisas, B. G.; Gersonde, K. *Biochemistry* **1975**, *14*, 4584.
(35) Noll, L. A.; Gaud, H. T.; Gill, S. J.; Gersonde, K.; Barisas, B. G. *Biochem. Biophys. Res. Commun.* **1979**, *88*, 1288.
(36) Gill, S. J.; Gaud, H. T.; Barisas, B. G. *J. Biol. Chem.* **1980**, *255*, 7855.
(37) Gillespie, L. L.; Argan, C.; Taneja,

A. T.; Hodges, R. S.; Freeman, K. S.; Shore, G. C. *J. Biol. Chem.* **1985**, *260*, 16045.
(38) Sattler, J.; Schwartzmann, G.; Knack, I.; Rohm, K. H.; Wiegandt, H. *Hoppe-Seyler's Z. Physiol. Chem.* **1978**, *359*, 719.
(39) Goins, B.; Freire, E. *Biochemistry* **1988**, *27*, 2046.
(40) Sehl, L. C.; Castellino, F. J. *J. Biol. Chem.* **1990**, *265*, 5482.
(41) Cox, J. A.; Milos, M.; MacManus, J. P. *J. Biol. Chem.* **1990**, *265*, 6633.

Ernesto Freire is a professor in the Department of Biology and director of the Biocalorimetry Center at The Johns Hopkins University. He received B.S. and M.S. degrees in biochemistry from the University Cayetano Heredia, Lima, Peru, and a Ph.D. in biophysics from the University of Virginia. His research work has been in the area of molecular biophysics, particularly in the development of new methods for the study of the energetics and thermodynamic mechanisms of protein folding, conformational equilibrium, and self-assembly of complex macromolecular systems.

Obdulio L. Mayorga is a visiting scientist in the Biocalorimetry Center at The Johns Hopkins University. He is a professor of physical chemistry at the University of Granada, Spain. He received a Ph.D. in physical chemistry from the University of Granada. His research work is in the area of calorimetric instrumentation development and in the analysis of biological systems using calorimetric techniques.

Martin Straume is the director of operations of the Biocalorimetry Center in the Department of Biology at The Johns Hopkins University. He received a B.S. degree in biochemistry and an M.S. degree in chemistry from Lehigh University and a Ph.D. in biochemistry from the University of Virginia. His research work has involved biophysical characterizaion of lipid–lipid and lipid–rhodopsin interactions, thermodynamic analysis of ligand binding to human hemoglobin, and development of high-sensitivity titration calorimetric instrumentation.

THE JOURNAL OF BIOLOGICAL CHEMISTRY
© 1984 by The American Society of Biological Chemists, Inc.

Vol. 259, No. 15, Issue of August 10, pp. 9384-9389, 1984
Printed in U.S.A.

AMP and IMP Binding to Glycogen Phosphorylase *b*

A CALORIMETRIC AND EQUILIBRIUM DIALYSIS STUDY*

(Received for publication, November 29, 1983)

Pedro L. Mateo, Carmen Baron‡, Obdulio Lopez-Mayorga, Juan S. Jimenez, and Manuel Cortijo

From the Physical Chemistry Department, Faculty of Sciences, Granada University, Granada, Spain

Reaction microcalorimetry and equilibrium dialysis have been used to study the binding of AMP and IMP to glycogen phosphorylase *b* (EC 2.4.1.1) at 25 °C and pH 6.9. The combination of both techniques has enabled us to obtain some of the thermodynamic parameters for these binding processes.

Four binding sites were found to be present in the dimeric active enzyme for both AMP and IMP. The binding to two high-affinity sites, which, in our opinion, correspond to the activator sites, seems to be cooperative. The two low-affinity sites, which would then correspond to the inhibitor sites, appear to be independent when the nucleotides bind to the enzyme. The negative ΔG^0 of binding/site at 25 °C is the result in all cases of a balance between negative enthalpy and entropy changes. The large differences in ΔH and ΔS^0 for the binding of AMP to the activator sites (−27 and −70 kJ mol^{-1}; −22 and −150 J·K^{-1} mol^{-1}) suggest the existence of rather extensive conformational changes taking place in phosphorylase *b* on binding with the allosteric activator. Whereas the affinity of AMP for the activator sites is about 1 order of magnitude higher than that of IMP, the affinity of both nucleotides, including their ΔH and ΔS^0 values, seems to be the same for the inhibitor sites.

Glycogen phosphorylase *b* (EC 2.4.1.1) is a key enzyme in glycogen metabolism which undergoes a distinctive allosteric activation by AMP. Initial studies (1, 2) showed the existence of one AMP site/enzyme protomer. Recent evidence for two AMP-binding sites/monomeric unit of the enzyme has, nevertheless, been provided at 4 °C by equilibrium dialysis (3) and x-ray diffraction studies (4). Support for the presence of these two sites at 25 °C was also supplied by the biphasic thermal titration curves of the enzyme with AMP (5–8). We have shown, however, in a recent communication (9) that these biphasic calorimetric profiles were due, in our case, to the presence of an impurity, AMP aminohydrolase (EC 3.5.4.6), and that monophasic thermal curves are obtained when phosphorylase *b* is freed from this impurity (9, 10). This result cast doubts on previous experimental evidence for a second AMP site/monomer of phosphorylase *b* in solution at 25 °C.

In order to perform quantitative thermodynamic analysis of ligand binding to multisubunit proteins displaying site cooperativity, additional equilibrium techniques, besides calorimetry, are required. Even with several techniques, this energetic characterization can often become complicated due to the complexity of the process itself, and not much information of this kind is found in the literature (11–15).

In this context, we have undertaken the study of the binding of AMP, and also IMP, to phosphorylase *b* by equilibrium dialysis and microcalorimetry at 25 °C and pH 6.9. Under these conditions, four sites have been found per active dimer of the enzyme for both AMP and IMP, which have been assigned to the two nucleotide or activator sites, N, and to the two nucleoside or inhibitor sites, I (4, 16, 17). The binding is, in all cases, enthalpy-driven at 25 °C, overcoming a negative entropy barrier.

MATERIALS AND METHODS

Glycogen phosphorylase *b* was prepared from rabbit skeletal muscle by the method of Fisher *et al.* (18, 19) with the modifications described by Krebs *et al.* (20). The catalytic activity of the enzyme was determined by the assay of Hedrick and Fisher (21). The preparations used had specific activities of 80–90 units/mg. Protein concentration was determined from absorbance measurements at 280 nm using the absorbance coefficient $E^{1\%}_{1cm} = 13.2$ (22). The molecular weight of the monomer was taken as 97,400 (23). The enzyme was crystallized at least three times and used within 1 week of the final crystallization. Phosphorylase *b* preparations were freed from AMP by passing them through a Sephadex G-25 column equilibrated with 50 mM KCl, 0.1 mM β-mercaptoethanol, 0.1 mM EDTA, 50 mM buffer solution (glycylglycine, glycerophosphate, or Tris), adjusted to pH 6.9. The A_{260}:A_{280} ratio for the AMP-free phosphorylase *b* solutions was always less than 0.53. Traces of AMP aminohydrolase were eliminated by incubation with alumina Cγ, as has been described elsewhere (10).

[5′-^{14}C]AMP and [5′-^{14}C]IMP were obtained from the Radiochemical Center, Amersham, England. AMP, IMP, glycylglycine, alumina Cγ, Tris, and β-mercaptoethanol were purchased from Sigma; sodium glycerophosphate was from Merck, and EDTA was from Fluka. All chemicals used were of the highest available purity. Distilled, deionized water was used throughout.

An LKB flow microcalorimeter with a water bath at 25 °C was used for the calorimetric measurements. The temperature in the water bath was controlled by a proportional heater with adjustable precision based on a combination threshold detector and zero-crossing trigger (24). The control of the bath temperature was better than 0.01 °C. Electrical and chemical calibrations were made in the same range as that which we obtained in the calorimetric experiments themselves. The chemical calibration was accomplished by the neutralization of Tris with HCl (25). Enzyme and AMP (or IMP) solutions were allowed to flow into the calorimeter at rates of 7 ml h^{-1} in most experiments, with occasional changes in order to check the completeness of the reaction. The dilution gradient method of Mountcastle *et al.* (26) was also used in the phosphorylase *b*/IMP calorimetric titration (see Fig. 5). All appropriate corrections for heats of dilution and mixing were applied. The enzyme activity was routinely checked prior to and after the calorimetric and dialysis experiments. The pH values of the buffer, AMP, IMP, and enzyme solutions were controlled at 25 °C before initiating the binding reaction. The equilibrium dialysis experiments were carried out at 25 °C as described by Helmreich *et al.* (27).

* This research was supported by a grant from the Comision Asesora from the Spanish government. The costs of publication of this article were defrayed in part by the payment of page charges. This article must therefore be hereby marked "*advertisement*" in accordance with 18 U.S.C. Section 1734 solely to indicate this fact.

‡ Supported by a fellowship from the Formación de Personal Investigator.

RESULTS

Binding of AMP to Phosphorylase b—The binding of AMP to phosphorylase *b* was observed as a function of the activator concentration by equilibrium dialysis at 25°C and pH 6.9 (Fig. 1). The result of this binding is presented in a Scatchard plot in Fig. 2, where Y stands for the saturation fraction and $\nu = nY$ for n (number of sites) equal to 4. The shape of the curve which shows a maximum is of the form expected for a system exhibiting positive cooperativity. Extrapolation of the lower part of the plot leads to a value clearly higher than 2 mol of AMP bound per mol of enzyme at saturation. Morange *et al.* (3), using the same technique, found at 4 °C that there were two classes of AMP-binding sites/subunit of phosphorylase *b*, a low affinity and a high affinity site, *i.e.* four sites/dimer. Similar results were also obtained at 4 °C by Johnson *et al.* (4) in x-ray diffraction studies using an AMP concentration (100 mM).

The shape of the Scatchard plot suggests that AMP starts to bind to the lower-affinity sites when the high-affinity sites are practically saturated. Hence, most of the experimental points at low AMP concentration in Fig. 1 would mainly correspond to the binding of AMP to the high-affinity sites, these being for the most part responsible for the cooperativity shown in the Scatchard plot. Assuming then that the values with $\nu < 2$ correspond only to the binding to the two high-affinity sites, a straight Hill plot is obtained for these values with a Hill coefficient of 1.4 ± 0.1, which agrees well with those obtained by other authors (28–31) for these sites at similar AMP concentrations.

The reaction of AMP with phosphorylase *b* can be considered as the binding of AMP to two independent sets of sites. The high-affinity sites show positive cooperativity according to their Hill coefficient, while the low affinity sites can themselves be considered as independent of each other, an assumption that is justified below. On this basis, the saturation fraction, Y, as a function of the free AMP concentration is

$$Y = \frac{1}{2}\cdot\frac{K_{m_1}[\mathrm{AMP}] + K_{m_1}K_{m_2}[\mathrm{AMP}]^2}{1 + 2K_{m_1}[\mathrm{AMP}] + K_{m_1}K_{m_2}[\mathrm{AMP}]^2} + \frac{1}{2}\cdot\frac{K_{m_3}[\mathrm{AMP}]}{1 + K_{m_3}[\mathrm{AMP}]} \quad (1)$$

where K_{m_i} stands for the microscopic binding constants at the ith site, and $K_{m_3} = K_{m_4}$. K_{m_1} and K_{m_2} values can be initially calculated from the Hill coefficient, n_H, and the concentration of the free ligand at 50% saturation of the high-affinity sites, $S_{0.5}$, obtained from the previous Hill plot, according to the following relations (32).

$$n_H = \frac{2}{1 + (K_{m_1}/K_{m_2})^{1/2}} \quad \text{and} \quad S_{0.5} = \frac{1}{(K_{m_1}\cdot K_{m_2})^{1/2}} \quad (2)$$

The value of K_{m_3} can be obtained by subtracting the saturation curve corresponding to the two high-affinity sites, using the K_{m_1} and K_{m_2} values given by Equation 2 (first term in Equation 1), from the experimental points. The resulting difference represents the saturation data for the second class of sites. A Hill plot of these new values gives a straight line with a Hill coefficient equal to 0.97 ± 0.15, which can be taken as evidence of the non-cooperativity of the low-affinity sites. The binding constant calculated from this plot, K_{m_3}, and the K_{m_1} and K_{m_2} values obtained above were then used as input for the iterative Newton-Gauss method (see Ref. 33) to fit all the experimental data to the theoretical Equation 1. The optimum K_{m_1}, K_{m_2}, and K_{m_3} values thus obtained are shown in Table I. Curves in Figs. 1 and 2 are the theoretical ones using the calculated binding constants (Table I).

The results of the calorimetric titration of phosphorylase *b* with AMP in three different buffer solutions at 25 °C and pH 6.9 are shown in Fig. 3. The binding of AMP was exothermic in all cases, giving rise to a well-defined monophasic curve. This curve is the same regardless of the buffer system used, and since the heats of ionization of the three buffers are different (34), no proton uptake or release seems to occur in the activator binding to the enzyme, particularly to the high-affinity sites.

Fig. 3 shows the heat evolved per mol of phosphorylase *b* dimer as a function of free AMP concentration in equilibrium with the enzyme. This concentration was calculated by using the binding constants previously obtained in the dialysis experiments (Table I). As stated before, the AMP binding to phosphorylase *b* can be understood as the binding of a ligand, S, to a protein, P, with two sets of sites: the high-affinity sites, N, and the low-affinity sites, I. Thus, $[P_N]$ and $[P_I]$ are the protein concentration when the high- and low-affinity

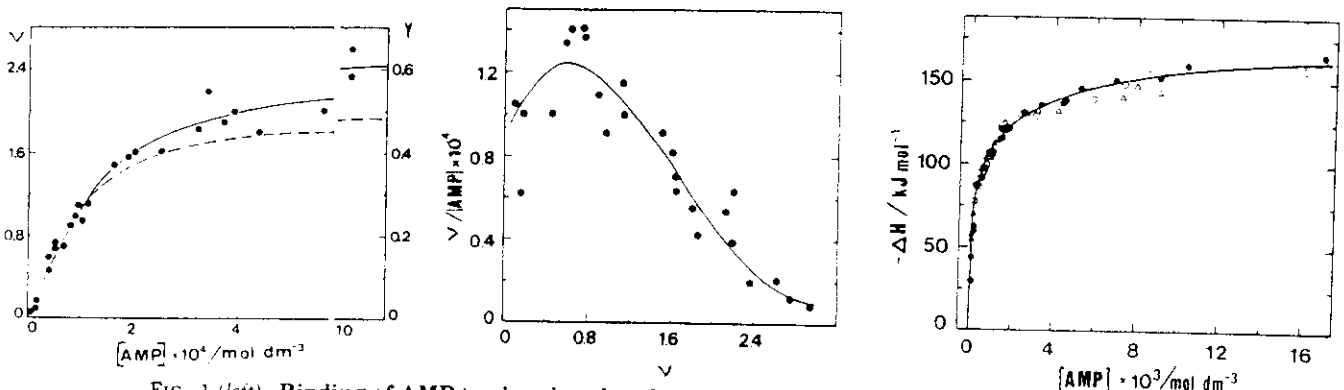

FIG. 1 (*left*). **Binding of AMP to phosphorylase *b* at pH 6.9.** Data were obtained by equilibrium dialysis at 25 °C. The saturation fraction, Y, and the moles of AMP bound per mol of enzyme, ν, are plotted *versus* the free AMP concentration. The enzyme concentration was 60 μM, and the buffer used was 50 mM Tris, 50 mM KCl, 0.1 mM EDTA and 1 mM β-mercaptoethanol. The *solid line* was drawn using Equation 1 and the values listed in Table I. The *dashed line* is the theoretical one corresponding to the binding of AMP to the high-affinity sites (see text).

FIG. 2 (*center*). **Scatchard plot of the data included in Fig. 1.** The theoretical curve was calculated using the values listed in Table I.

FIG. 3 (*right*). **Calorimetric titration of phosphorylase *b* with AMP at pH 6.9 and 25 °C.** The heat released per monomer of enzyme is plotted as a function of the free nucleotide concentration. Enzyme concentration was 5 mg/ml. Titration was in 50 mM glycylglycine (●), 50 mM glycerophosphate (○), and 50 mM Tris (△). All solutions contained 50 mM KCl, 0.1 mM EDTA, 0.1 mM β-mercaptoethanol. The *curve* corresponds to Equation 5 using the values shown in Table I.

TABLE I

Apparent thermodynamic parameters for the binding of AMP and IMP to phosphorylase b at 25 °C and pH 6.9

The uncertainties are standard errors in the fitting of the curves.

	Nucleotide	N sites	I sites	Total
$K_m \cdot 10^{-3}/M^{-1}$	AMP	4.0 ± 1	26.5 ± 9	0.32 ± 0.2
	IMP	0.74 ± 0.2	2.1 ± 2	0.6 ± 0.4
ΔG^0/kJ mol^{-1}	AMP	−20.5 ± 1	−25.2 ± 1	−14.3 ± 2	−74.3 ± 3
	IMP	−16.4 ± 1	−18.9 ± 3	−15.8 ± 2	−67.0 ± 4
ΔH/kJ mol^{-1}	AMP	−27 ± 7	−70 ± 9	−38 ± 2	−173 ± 12
	IMP	−18 ± 5	−33 ± 21	−37 ± 13	−125 ± 28
ΔS^0/J·K^{-1} mol^{-1}	AMP	−22 ± 23	−150 ± 30	−82 ± 10	−336 ± 40
	IMP	−6 ± 12	−47 ± 71	−71 ± 44	−195 ± 95

sites, respectively, are empty; $[P_NS]$ is the protein concentration with only one high-affinity site empty regardless of the state of the low-affinity sites; $[P_NS_2]$ is the concentration of protein with AMP bound to both high-affinity sites regardless of whether the low-affinity sites are empty or not. The protein states P_IS and P_IS_2 are defined similarly. The binding can then be represented by the following equilibria

$$\begin{aligned} P_N + S &\rightleftharpoons P_NS; \quad K_1 = 2K_{m_1}; \quad \Delta H_1 \\ P_NS + S &\rightleftharpoons P_NS_2; \quad K_2 = K_{m_2}/2; \quad \Delta H_2 \\ P_I + S &\rightleftharpoons P_IS; \quad K_3 = 2K_{m_3}; \quad \Delta H_3 \\ P_IS + S &\rightleftharpoons P_IS_2; \quad K_4 = K_{m_4}/2; \quad \Delta H_4 \end{aligned} \tag{3}$$

where K_i and K_{m_i} are the macroscopic and microscopic binding constants, respectively, ΔH_i stands for the enthalpy values/mol of AMP bound to each site, and $K_{m_3} = K_{m_4}$ and $\Delta H_3 = \Delta H_4$ since the two low-affinity sites are considered as being independent.

From the above Equation 3, the enthalpy change/mol of enzyme (dimer), ΔH, is given by

$$\Delta H = \frac{\Delta H_1[P_NS] + (\Delta H_1 + \Delta H_2)[P_NS_2]}{[P_N] + [P_NS] + [P_NS_2]} + \frac{\Delta H_3[P_IS] + 2\Delta H_3[P_IS_2]}{[P_I] + [P_IS] + [P_IS_2]} \tag{4}$$

which can be expressed as the following.

$$\Delta H = \frac{2\Delta H_1 K_{m_1}[S] + (\Delta H_1 + \Delta H_2)K_{m_1}K_{m_2}[S]^2}{1 + 2K_{m_1}[S] + K_{m_1}K_{m_2}[S]^2} + \frac{2\Delta H_3 K_{m_3}[S]}{1 + K_{m_3}[S]} \tag{5}$$

The experimental data in Fig. 3 were fitted by trial and error to Equation 5 giving the values for ΔH_i that minimize the deviations of the observed values of ΔH from the calculated ones. These ΔH_i values were later optimized by the Newton-Gauss method (see Ref. 33) using the K_{m_i} values previously obtained. The curve in Fig. 3 is that corresponding to Equation 5 for the calculated K_{m_i} and ΔH_i values. Thermodynamic parameters for the binding of AMP to phosphorylase *b* at 25 °C and pH 6.9 obtained from the ΔH_i values and the microscopic binding constants are included in Table I.

Binding of IMP to Phosphorylase b—The binding of IMP to phosphorylase *b* was also achieved by equilibrium dialysis and calorimetry at 25 °C and pH 6.9 in the same way as described above for the AMP binding. The enzyme concentration for the equilibrium dialysis experiments was 15 mg/ml, higher than that used for the AMP binding, since phosphorylase *b* displays a lower affinity for IMP than for AMP. The experimental results for Y and ν *versus* free IMP concentration are shown in Fig. 4. A Scatchard plot of these values clearly extrapolates to $\nu = 4$ (data not shown).

Thermal titration data of the protein by IMP are displayed in Fig. 5 for two different buffer systems, Tris and glycylglycine. Experiments using the latter buffer were carried out following the exponential gradient method described by Mountcastle *et al.* (26). There is no apparent difference between the results for the two buffers and the methods used for the thermal titrations.

The dialysis data of the IMP binding give rise to a practically straight Scatchard plot, which might be taken as evidence for the existence of four identical and independent binding sites. It has been established from x-ray diffraction studies (4), however, that there are two types of IMP sites, namely, the two N and two I sites/dimer. This being the case, the simplest analysis of the data would be to consider that the IMP is binding to two independent sets of sites without any cooperativity. Thus, the saturation fraction is given as

$$Y = \frac{1}{2}\cdot\frac{K_{m_N}[IMP]}{1 + K_{m_N}[IMP]} + \frac{1}{2}\cdot\frac{K_{m_I}[IMP]}{1 + K_{m_I}[IMP]} \tag{6}$$

taking K_{m_N} and K_{m_I} as the binding constants for the high (N)- and low (I)-affinity sites, respectively. The fitting of the dialysis data to this equation gives the optimum values $K_{m_N} = 1250 \pm 360\ M^{-1}$ and $K_{m_I} = 600 \pm 200\ M^{-1}$.

On the other hand, the fact of having different sites should give rise to a Scatchard plot showing convexity towards the X axis (47), while we have indicated that our plot is practically straight. This means that some factor is counteracting the curvature towards the axis, and this could be explained if there were some positive cooperativity during the binding process (47). In this respect, the binding of IMP to the N sites has been reported by several authors (35–37) as cooperative, as is the case for the AMP binding to those sites. In addition, the binding of several ligands (nucleosides, nitrogen bases, FMN) to the I sites has been shown to be non-cooperative (3, 38), which, as we saw before, seems also to be the case for AMP.

Therefore, the nature of the IMP binding to phosphorylase *b* seems to be qualitatively comparable to that of AMP. In other words, the overall IMP binding process could be described similarly to that of AMP and, consequently, with the same equation for the saturation fraction as Equation 1. In order to fit the experimental data to this equation, an initial value of $K_{m_3} = K_{m_4} = K_{m_I} = 600\ M^{-1}$ and different couples of K_{m_1} and K_{m_2} values which fulfilled the relation $(K_{m_1} \cdot K_{m_2})^{1/2} = K_{m_N} = 1250\ M^{-1}$ were used. The optimum values obtained for K_{m_1}, K_{m_2}, and K_{m_3} by a later application of the Newton-Gauss iterative method (see Ref. 33) are included in Table I.

The enthalpy change/mol of dimer would also be described by an equation such as Equation 5, and the corresponding enthalpies/site were obtained as described before for the AMP binding to the enzyme. The thermodynamic parameters for the binding of IMP to phosphorylase *b* at 25 °C and pH 6.9 are also included in Table I.

The different shape of the Scatchard plot for the AMP binding compared to that of IMP could be explained by the

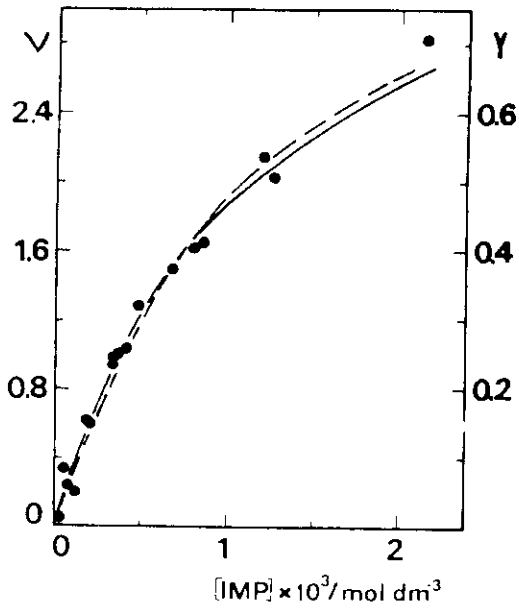

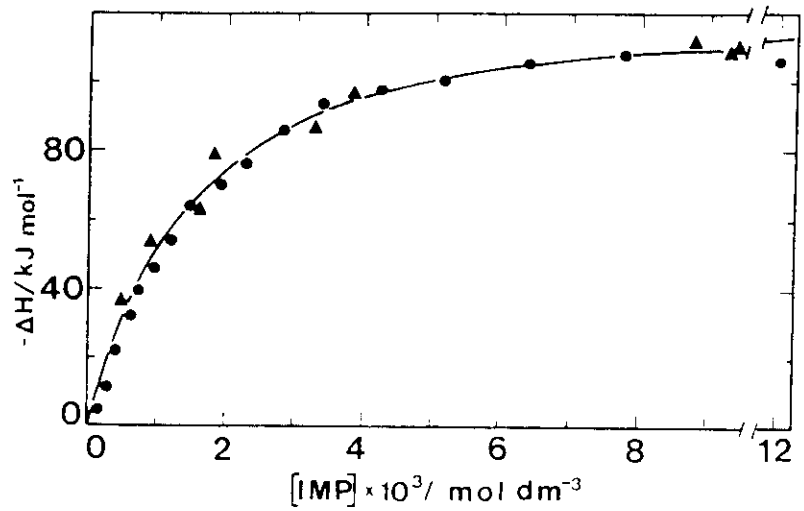

FIG. 4 (*left*). **Binding of IMP to phosphorylase *b* at pH 6.9 and 25 °C as measured by equilibrium dialysis.** The enzyme concentration was 75 μM, and the buffer used was the same as in Fig. 1. The *solid line* is the one corresponding to Equation 6 for the values $K_1 = 600\ M^{-1}$ and $K_N = 1250\ M^{-1}$. The *dashed line* was drawn using an equation similar to Equation 1 for IMP binding and the values included in Table I.

FIG. 5 (*right*). **Thermal titration of phosphorylase *b* with IMP at pH 6.9 and 25 °C.** The heat evolved per mol of enzyme is plotted *versus* the total IMP concentration. The enzyme concentration was 6.3 mg/ml in 50 mM KCl, 0.1 mM EDTA, and 0.1 mM β-mercaptoethanol. ▲, 50 mM glycylglycine; ●, 50 mM Tris and following the exponential gradient method (see text). The *solid curve* gives values of enthalpy calculated according to an equation similar to Equation 5 using the data listed in Table I.

fact that the binding of AMP to the N sites shows higher cooperativity than that of IMP to those sites and also because of the very close affinity of IMP for both the N and I sites, while the AMP affinity for the N sites is more than 1 order of magnitude higher than the AMP affinity for the I sites (Table I).

It should be stressed at this point that it is not possible, when working within a limited range of accuracy, to obtain a unique valid fit of experimental binding data when several different binding sites are involved. It is only through given certain assumptions and accepting certain restrictions that a given set of binding parameters can be arrived at. Furthermore, their physical meaning is not only limited by their standard uncertainties (particularly high in our case for the IMP binding to phosphorylase *b*) but also by the assumptions and, to some extent, the behavior that these parameters are forced to follow.

DISCUSSION

In addition to the x-ray studies of Johnson *et al.* (4) on crystals of phosphorylase *b* and those of dialysis by Morange *et al.* (3) and Buc *et al.* (48), the main evidence for a second AMP-binding site/monomer at 25 °C was the biphasic calorimetric profiles of Wang *et al.* (5), Ho and Wang (6), and Merino *et al.* (7, 8). The results of these latter groups showed clear divergences concerning both the AMP saturation range for the second site, I, and the ΔH value for this site. We initially obtained biphasic curves for this thermal titration, but, as was shown, it was due to the presence of an enzymic impurity in our phosphorylase preparations, which, once eliminated (10), gave rise to monophasic calorimetric curves (9). It is not possible, however, to obtain information about the number of sites from calorimetric experiments alone when dealing with allosteric enzymes, as it is in the case of phosphorylase *b*. The combination of equilibrium dialysis and calorimetric studies enables us now to actually obtain the number of binding sites for AMP and IMP in solution at 25 °C, as well as to characterize the thermodynamic parameters associated on binding both nucleotides. The main difference between the binding of these two activators appears to be in the much closer affinity of IMP for the two types of sites, N and I, in the dimer than in the case of AMP.

Ho and Wang (6) gave an average ΔH value, −13.2 kcal (mol site)$^{-1}$, for AMP binding to the two N sites of the phosphorylase *b* dimer at 25 °C. Twice this value compares well with ΔH_1 and ΔH_2 obtained in our study for this site (Table I). These authors detected an association of the enzyme to the tetrameric state upon AMP binding at 18 °C, while no association seemed to occur at 25 °C (6). We did calorimetric experiments at different phosphorylase concentrations (Fig. 6), and there was no detectable change in the heat evolved for the concentration range investigated. Thus, no protein association effects seemed to occur in our experiments.

To our knowledge, only Steiner *et al.* (39) have tried to identify the contribution of each N site to the enthalpy change on the binding of AMP, although they did not investigate the other binding sites because they only used low AMP concentrations (≤1 mM). While their values at 23 °C are somewhat different from ours, the total ΔH for the N sites coincides with ours within experimental uncertainty. This difference also correlates with the comparison between our K_{m_1} and K_{m_2} values and theirs, in the sense that we obtain a higher homotropic cooperativity as indicated by the Hill coefficient (1.4 in our case, 1.2 in their case). This variation could be attributed to small differences in temperature, pH, and buffer used, although Dreyfus *et al.* (29) also obtained a Hill coefficient of 1.4 at 20 °C for this binding. An equal value of 1.4 had previously been obtained by Avramovic and Madsen (28) and other authors (30, 31).

The binding of AMP and IMP to the N sites shows positive

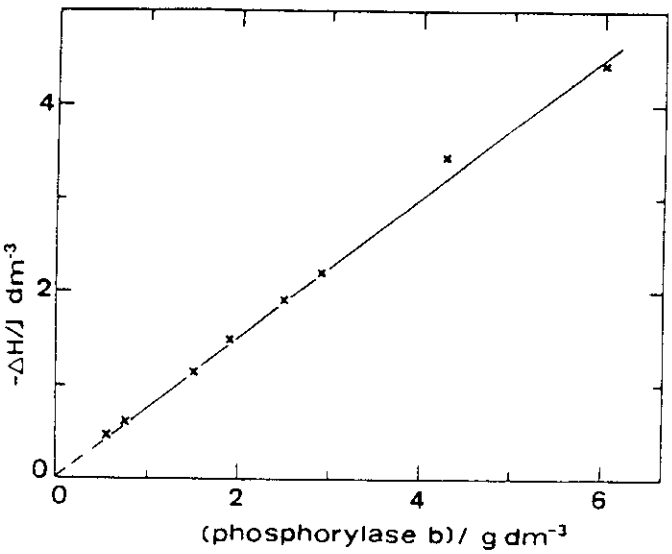

FIG. 6. **Dependence of the heat of binding of AMP to phosphorylase *b* with the enzyme concentration at pH 25 °C.** The heat evolved per unit volume of solution is plotted *versus* the enzyme concentration. The AMP concentration was 8.7 mM in a 50 mM Tris buffer solution containing 50 mM KCl, 0.1 mM EDTA, and 0.1 mM β-mercaptoethanol.

homotropic cooperativity. This effect is more pronounced in the AMP binding (n_H = 1.4) than that of IMP (n_H = 1.2). The difference in cooperativity is also seen in the ΔH values. Thus, in the case of AMP, the ΔH values are very different, −27 and −70 kJ mol^{-1}, favoring the entrance of a second AMP molecule into the dimer. The corresponding ΔS^0 values go in an opposite direction, balancing to some extent the enthalpic influence. The binding at 25 °C is clearly of an enthalpic character. The same qualitative situation applies to the IMP binding, although here the ΔH and ΔS^0 values are comparatively lower than in the AMP binding. The differences in ΔH and ΔS^0 values between the two N sites for both nucleotides make for a higher affinity and cooperativity in the binding of AMP than in IMP binding to those sites.

A structural interpretation of these thermodynamic parameters is not possible at this point since these values are the joint product of those of the so-called intrinsic binding (40) and those of the conformational change produced in the macromolecule, which is structurally responsible for the cooperative effect. We are currently working out a method to evaluate both contributions to the overall binding process (41).

The corresponding thermodynamic parameters for the binding of AMP and IMP to the I sites are very close for the two nucleotides within experimental uncertainty (Table I). This implies that the I site (nucleoside or inhibitor site) does not apparently discriminate between the two nucleotides. This site seems to be more specific for the inhibitors of the enzyme, such as adenine or adenosine, although their binding to the I site is also non-cooperative (3, 38). It has been suggested that any ligand bound to this site would produce some enzyme inhibition (17), and we have detected in this case a decrease in the enzymic activity at high AMP concentrations (results not shown). In this context, it has also been suggested that the low activation produced by IMP in comparison to that produced by AMP could be assigned to the close affinity of IMP for both the N (activator) and I (inhibitor) sites (17). Besides this possibility, however, we have seen that the thermodynamic parameters for binding AMP and IMP to the activator sites are different enough to expect different conformational changes and, therefore, different final conformations. The differences in these AMP- and IMP-induced conformational changes have been reported by several researchers using various techniques, such as ESR (42), fluorescence (43), and SH reactivity (3).

The binding of these nucleotides to the I site is enthalpy-driven at 25 °C, overcoming the negative entropy barrier (Table I). It seems that the enthalpic contribution would mainly come from the interaction between Tyr-612 and/or Phe-285 with the nitrogen bases in the nucleotides (44). The ΔS^0 values cannot be easily accounted for since the site structure is not well defined at present. The binding of FMN to this site in phosphorylase *a* shows a negative ΔC_p value which is itself a function of temperature (38). If it were also the case for our nucleotides, one would expect a change in the sign of ΔS^0 at temperatures somewhat lower than 25 °C. This FMN binding shows the same enthalpy value as AMP and IMP, −37 kJ mol^{-1}, but a positive change in the entropy is responsible for the higher affinity of this compound for the I site at 25 °C (38).

Finally, the binding of AMP to the I site (which, it has been suggested, may play a possible role *in vivo* in controlling the enzyme activity (7)) does not seem to have much physiological role in muscle given the levels of free AMP in either resting muscle or under extreme fatigue (45, 46) and the affinity of AMP for this site, although our affinity values were obtained *in vitro*, in the absence of any other physiological effectors and/or substrates.

REFERENCES

1. Fisher, E. H., Pocker, A., and Saari, J. C. (1970) in *Essays in Biochemistry* (Campbell, P. W., and Dickens, F., eds) Vol. 6, pp. 23–68, Academic Press Inc., Ltd., London
2. Graves, D. J., and Wang, J. H. (1972) in *The Enzymes* (Boyer, P. D., ed) 3rd Ed., Vol. 7, pp. 435–482, Academic Press, New York
3. Morange, M., Garcia-Blanco, F., Vandenbunder, B., and Buc, H. (1976) *Eur. J. Biochem.* **65**, 553–563
4. Johnson, L. N., Sture, E. A., Wilson, K. S., Sansom, M. S. P., and Weber, I. T. (1979) *J. Mol. Biol.* **134**, 639–652
5. Wang, J. H., Kwok, S.-C., Wirch, E., and Suzuki, I. (1970) *Biochem. Biophys. Res. Commun.* **40**, 1340–1347
6. Ho, H. C., and Wang, J. H. (1973) *Biochemistry* **12**, 4750–4755
7. Merino, C. G., Garcia-Blanco, F., and Laynez, J. (1977) *FEBS Lett.* **73**, 97–100
8. Merino, C. G., Garcia-Blanco, F., Pocovi, M., Menendez, M., and Laynez, J. (1980) *J. Biochem. (Tokyo)* **87**, 1483–1490
9. Cortijo, M., Baron, C., Jiménez, J. S., and Mateo, P. L. (1982) *J. Biol. Chem.* **257**, 1121–1124
10. Baron, C., Mateo, P. L., Cortijo, M., and Jimenez, J. S. (1982) *Anal. Biochem.* **124**, 84–87
11. Velick, S. F., Baggott, J. P., and Sturtevant, J. M. (1971) *Biochemistry* **10**, 779–786
12. Allewell, N. M., Friedland, J., and Niekamp, K. (1975) *Biochemistry* **14**, 224–230
13. Niekamp, C. W., Sturtevant, J. M., and Velick, S. F. (1977) *Biochemistry* **16**, 436–445
14. Atha, D. H., and Ackers, G. K. (1974) *Biochemistry* **13**, 2376–2382
15. Gaud, H. T., Barisas, B. G., and Gill, S. J. (1974) *Biochem. Biophys. Res. Commun.* **59**, 1389–1394
16. Fletterick, R. J., and Madsen, N. B. (1980) *Annu. Rev. Biochem.* **49**, 31–61
17. Dombradi, V. (1981) *Int. J. Biochem.* **11**, 125–139
18. Fisher, E. H., Krebs, E. G., and Kent, A. B. (1958) *Biochem. Prep.* **6**, 68–72
19. Fisher, E. H., and Krebs, E. G. (1962) *Methods Enzymol.* **5**, 369–373
20. Krebs, E. G., Love, D. S., Bratvold, G. E., Trayser, K. A., Meyer, W. L., and Fischer, E. H. (1964) *Biochemistry* **3**, 1022–1033
21. Hedrick, J. L., and Fischer, E. H. (1965) *Biochemistry* **4**, 1337–1343
22. Buc, M. H., and Buc, H. (1968) in *FEBS Symposium: Regulation*

of Enzyme Activity and Allosteric Interactions, Oslo, July 1967, pp. 109–130, Academic Press, New York
23. Titani, K., Koide, A., Hermann, J., Ericsson, L. H., Kumar, S., Wade, R. D., Walsh, K. A., Neurath, H., and Fisher, E. H. (1977) *Proc. Natl. Acad. Sci. U. S. A.* **74**, 4762–4766
24. Mira, J., Cortijo, M., and López, O. (1980) *Inf. Automática* **46**, 44–50
25. Sturtevant, J. M. (1972) *Methods Enzymol.* **26**, 227–253
26. Mountcastle, D., Freire, E., and Biltonen, R. L. (1976) *Biopolymers* **15**, 355–371
27. Helmreich, E., Michaelides, M. C., and Cori, C. F. (1967) *Biochemistry* **6**, 3695–3710
28. Avramovic, O., and Madsen, N. B. (1968) *J. Biol. Chem.* **243**, 1656–1662
29. Dreyfus, M., Vandenbunder, B., and Buc, H. (1980) *Biochemistry* **19**, 3634–3642
30. Campbell, I. D., Dwek, R. A., Price, N. C., and Radda, G. K. (1972) *Eur. J. Biochem.* **30**, 339–347
31. Danforth, W. H., Helmreich, E., and Cori, C. F. (1962) *Proc. Natl. Acad. Sci. U. S. A.* **48**, 1191–1199
32. Levitzki, A. (1975) in *Enzymology* (Ebner, K. E., ed) Vol. 2, pp. 1–41, Marcel Dekker Inc., New York
33. Fraser, R. D. B., and Suzuki, E. (1973) in *Physical Principles and Techniques of Protein Chemistry* (Leach, S. J., ed) Part C, pp. 301–357, Academic Press, New York
34. Christensen, J. J., Hansen, L. D., and Izatt, R. M. (eds) (1976) *Handbook of Proton Ionization Heats and Related Thermodynamic Quantities*, John Wiley & Sons, New York
35. Buc, H. C., Buc, M. H., Garcia-Blanco, F., Morange, M., and Winkler, H. (1973) *Metabolic Interconversion of Enzymes*, pp. 21–31, Springer-Verlag, New York
36. Black, W. J., and Wang, J. H. (1968) *J. Biol. Chem.* **243**, 5892–5898
37. Bennick, A., Dwek, R. A., Griffiths, J. R., and Radda, G. K. (1973) *Ann. N. Y. Acad. Sci.* **222**, 175–191
38. Sprang, S., Fletterick, R., Stern, M., Yang, D., Madsen, N., and Sturtevant, J. (1982) *Biochemistry* **21**, 2036–2048
39. Steiner, R. F., Greer, L., Gunther, C., and Horan, C. (1976) *Biochim. Biophys. Acta* **445**, 610–621
40. Eftink, M., and Biltonen, R. (1980) in *Biological Microcalorimetry* (Beezer, A. E., ed) pp. 343–412, Academic Press Inc., Ltd., London
41. Mateo, P. L. (1983) *International Symposium on Thermodynamic of Proteins and Biological Membranes*, Abstr. S-VI-2, Granada, Spain
42. Busby, S. J. W., and Radda, G. K. (1976) *Curr. Top. Cell. Regul.* **10**, 89–160
43. Vandenbunder, B., Morange, M., and Buc, H. C. (1976) *Proc. Natl. Acad. Sci. U. S. A.* **73**, 2696–2700
44. Sprang, S., and Fletterick, R. J. (1979) *J. Mol. Biol.* **131**, 523–551
45. Aragon, J. J., Tornheim, K., and Lowenstein, J. M. (1980) *FEBS Lett.* **117**, K56–K64
46. Jenkins, J. A., Johnson, L. N., Stuart, D. I., Stura, E. A., Wilson, K. S., and Zanotti, G. (1981) *Philos. Trans. R. Soc. Lond. B Biol. Sci.* **293**, 23–41
47. Dahlquist, F. W. (1978) *Methods Enzymol.* **48**, 270–299
48. Buc, H., Buc, M. H., Morange, M., Ondin, L. C., and Winkler, H. (1973) in *Dynamic Aspects of Conformation Changes in Biological Macromolecules* (Sadron, C., ed) pp. 225–245, D. Reidel, Holland

Thermodynamics of the Binding of AMP to Glycogen Phosphorylase *a**

(Received for publication, June 16, 1986)

Pedro L. Mateo, Juan F. González‡, Carmen Barón, Obdulio López-Mayorga, and Manuel Cortijo

From the Departmento de Química Física, Facultad de Ciencias, Universidad de Granada, 18071 Granada, Spain

The binding of AMP to rabbit muscle glycogen phosphorylase *a* (EC 2.4.1.1.) has been studied by equilibrium dialysis and isothermal microcalorimetry at pH 6.9 over a temperature range of 25 °C to 35 °C. Thermal titration experiments were carried out in various buffer systems. We have found by these methods that a certain number of protons are released when the protein binds to the ligand and are taken up by the buffer.

The tetramer of phosphorylase *a* has been shown to have four equal and independent, non-cooperative binding sites for AMP at 25 °C, 30 °C, and 35 °C; these sites can be assigned to the so-called nucleotide or, activator, sites in the protein. The binding constants together with the changes in Gibbs energy, enthalpy, and entropy per site for the AMP binding were calculated at each temperature. A negative $\Delta C'_p$ value of -2.3 ± 0.2 J K^{-1} (AMP bound)$^{-1}$ was obtained for this binding process.

The hydrophobic and vibrational contributions of the heat capacity and entropy changes have been resolved by the method described by Sturtevant (Sturtevant, J. M. (1977) *Proc. Natl. Acad. Sci. U. S. A.* 74, 2236–2240). From this analysis, it appears that the binding is, in all cases, enthalpy-driven, the two entropic contributions, hydrophobic and vibrational, having opposing effects.

Highly temperature-dependent ΔH and ΔS values have been found in many protein-ligand binding processes. This must be due to the existence of a rather large $\Delta C'_p$ for these processes. The structural interpretation of the changes in the thermodynamic functions is usually complicated, particularly when the process is accompanied by extensive conformational changes in the macromolecule. This appears to occur whenever the binding turns out to be very cooperative, for example, in the binding of O_2 to hemoglobin, or AMP to glycogen phosphorylase *b*. The large heat capacity and entropy changes are considered to originate largely from hydrophobic effects, although there are several other contributing factors (1).

We studied the cooperative binding of AMP to the phosphorylase *b* dimer and found the thermodynamic parameters at 25 °C (2). The difference between this protein and its interconvertible active form, phosphorylase *a*, lies in the phosphorylation of the Ser-14 residue in the *a* form, which is also known to be a tetramer at concentrations of a few milligrams per ml (3). The Fourier difference analysis by x-ray diffraction studies in both forms has shown that minor differences exist between them, mainly in the ordering of the 19 N-terminal residues (4, 5). We have now studied, by equilibrium dialysis and isothermal calorimetry, the binding of AMP to phosphorylase *a*. The binding has been found to be non-cooperative, as had previously been reported (6, 7), and we have calculated its thermodynamic functions over a range of temperatures. The vibrational and hydrophobic contributions to these functions have been obtained as described elsewhere (8). To our knowledge, this is the first time that a calorimetric study has been carried out with this system. We have made some observations about the possible specific interactions and molecular events responsible for the thermodynamic parameters, which we also compare with those of the *b* form of the enzyme.

MATERIALS AND METHODS

Proteins and Chemicals—Phosphorylase *b* was prepared from rabbit skeletal muscle according to the method of Fisher *et al.* (9, 10) with the modifications described by Krebs *et al.* (11). The catalytic activity of the enzyme was determined by the assay of Hedrick and Fisher (12). The preparations used had specific activities of 80–90 units/mg. The protein concentration was calculated from absorbance measurements at 280 nm using the absorbance coefficient $E^{1\%}_{1cm} = 13.2$ (13). The molecular weight of the monomer was taken as 97,400 from its known sequence (14). The enzyme was crystallized at least three times and used within 1 week of the final crystallization. Enzyme preparations were freed of AMP by passing them through a column equilibrated with 50 mM KCl, 0.1 mM β-mercaptoethanol, 0.1 mM EDTA, 50 mM buffer solution adjusted to pH 6.9. The A_{260}:A_{280} ratio for the AMP-free phosphorylase *b* solutions was always less than 0.53. Possible traces of AMP aminohydrolase (EC 3.5.4.6) were eliminated by incubation with alumina Cγ as we have described elsewhere (15).

Phosphorylase *b* kinase (EC 2.7.1.38) was also prepared from rabbit skeletal muscle by the method of Krebs (16) with the modifications proposed by Cohen (17). Glycogen phosphorylase *a* was obtained from the phosphorylation of the *b* form of the enzyme by using ATP, Ca^{2+}, and Mg^{2+} in the presence of phosphorylase *b* kinase (10). The phosphorylase *a* was also recrystallized at least three times and obtained no more than 1 day prior to use. Solutions of phosphorylase *a* were prepared by dialysis of the crystal suspensions against the required buffer solution for 24 h at 4 °C. The suspension was then centrifuged at 15,000 × *g* for 20 min at 4 °C, and the crystals were redissolved at 30 °C in the same buffer. The ratio A_{260}:A_{280} was in all cases less than 0.55.

The protein concentration was determined in the same way as that of phosphorylase *b*. The specific activity of the enzyme in the absence of AMP was always in the range of 50–60 units/mg, while this value increased to about 80–90 in the presence of AMP.

[5′-^{14}C]AMP was obtained from the Radiochemical Center, Amersham, England. The AMP, alumina Cγ, Tris, Hepes,[1] and β-mercaptoethanol were purchased from Sigma; the sodium glycerophosphate was bought from Merck, and the EDTA and ATP were from Fluka, while the Sephadex G-25 and Sepharose 4B were manufactured by Pharmacia. All the chemicals used were of the highest available

* This research was supported in part by a grant from the "Comisión Asesora" of the Spanish government. The costs of publication of this article were defrayed in part by the payment of page charges. This article must therefore be hereby marked "*advertisement*" in accordance with 18 U.S.C. Section 1734 solely to indicate this fact.

‡ Supported by a fellowship from the "Formación del Personal Investigador." Present address: Laboratorio y Control Ambiental, CTLA, ENDESA.

[1] The abbreviations used are: Hepes, 4-(2-hydroxyethyl)-1-piperazineethanesulfonic acid; l, liter.

Techniques—The equilibrium dialysis experiments were carried out at 25 °C, as described elsewhere (2), according to the method of Helmreich *et al.* (18). An LS 7500 Beckman scintillation counter was used in the dialysis experiments to calculate the enzyme saturation fraction by AMP. The fluorescence intensity of the protein, as a function of the enzyme concentration, both in the presence and the absence of AMP, was measured with an LS-5 Perkin-Elmer luminescence spectrometer with a thermostat. The protein concentration and enzymatic assays were undertaken with a Cary-210 spectrophotometer with the cells maintained at 25 °C.

Isothermal calorimetry experiments were carried out at 25, 30, and 35 °C using an LKB 2277 BioActivity Monitor equipped with a flow unit. Electrical and chemical calibrations were made in the same range as that which we obtained in the calorimetric experiments themselves. The chemical calibration was accomplished by the neutralization of Tris with HCl (19). Phosphorylase *a* and AMP solutions were allowed to flow into the calorimeter cells at rates of about 15 and 5 ml h^{-1}, respectively, in most experiments. The completeness of the reaction was checked by occasional changes in the flow rate of the reactants. All appropriate corrections for heats of dilution and mixing were applied. The heat effect of the enzyme dilution was negligible in all cases. The phosphorylase *a* activity was routinely checked prior to and after the calorimetric and dialysis experiments. The pH values of the several buffers, AMP, and enzyme solutions were controlled at each temperature before starting the binding reaction. Calorimetric experiments initially planned at 20 °C could not be carried out due to the spontaneous, fast crystallization and consequent precipitation of the enzyme within the calorimetric tubing, thus precluding calorimetric measurements at this and lower temperatures. This fact was checked and confirmed by parallel experiments undertaken outside the calorimeter at 20 °C.

RESULTS

Fluorescence Determinations—Glycogen phosphorylase *b* shows two fluorescence transitions (20): one is caused by the protein moiety (excitation and emission maxima at 280 nm and 335 nm, respectively, and a quantum yield of 0.12), and the other is associated with its cofactor, pyridoxal 5′-phosphate (excitation maxima at 335 and 425 nm, emission maximum at 535 nm, and a quantum yield of 0.012). Muñoz *et al.* (21) have recently shown that this pyridoxal 5′-phosphate fluorescence is quenched by the addition of Mg^{2+}-AMP to the dimeric *b* form, which promotes the tetramerization of the enzyme. We have in fact determined the quantum yield of the pyridoxal phosphate fluorescence of the *a* form at 9 mg/ml, where the enzyme is a tetramer, and found that it is half of the value described for the *b* form (results not shown). Thus, we have used this fluorescence of the cofactor to determine any change taking place in the quaternary structure of the protein under the conditions in which we have conducted the dialysis and calorimetric experiments (see below). The quantum yield is independent of the excitation wavelength, within the range of 330 nm to 440 nm (as occurs with the *b* form). The enzyme was excited at 425 nm in our experiments in order to keep the absorption of the samples below 0.1. We then carried out measurements of the pyridoxal phosphate fluorescence intensity, both in the presence and the absence of 1 and also 10 mM AMP, as a function of the enzyme concentration within the range 2–12 mg/ml at 25 and 35 °C. In all cases, straight lines were obtained when plotting the fluorescence intensity *versus* the protein concentration (results not shown) for the whole range investigated. Thus, there was no evidence for intermolecular effects, *i.e.* detectable association-dissociation phenomena, dependent on the enzyme concentration for the above range.

Equilibrium Dialysis Measurements—The binding of AMP to the phosphorylase *a* tetramer was observed by equilibrium dialysis as a function of the nucleotide concentration at 25 °C and pH 6.9 in 50 mM Hepes buffer (Fig. 1). If the curve in Fig. 1 is compared to that of the binding of AMP to phosphorylase *b* at 25 °C (2), it is evident that the *a* form of the enzyme has a higher affinity for AMP than the *b* form. The Scatchard plot of this binding data is practically straight and clearly extrapolates to 4 mol of AMP bound per mol of enzyme at saturation. A Hill plot of these experimental values leads to a Hill coefficient, n_H, of 1.1 ± 0.1. This indicates a very low or indeed nil cooperativity, within experimental error, for the AMP binding to the tetramer. As expected, this result agrees with the straight line of the Scatchard plot and also with similar conclusions reported in the literature (6, 7, 22). There is a dramatic difference in cooperativity when AMP binds to the nucleotide sites of phosphorylase *a* and *b*, the latter in its dimeric form showing an n_H value of 1.4 ± 0.1 (2).

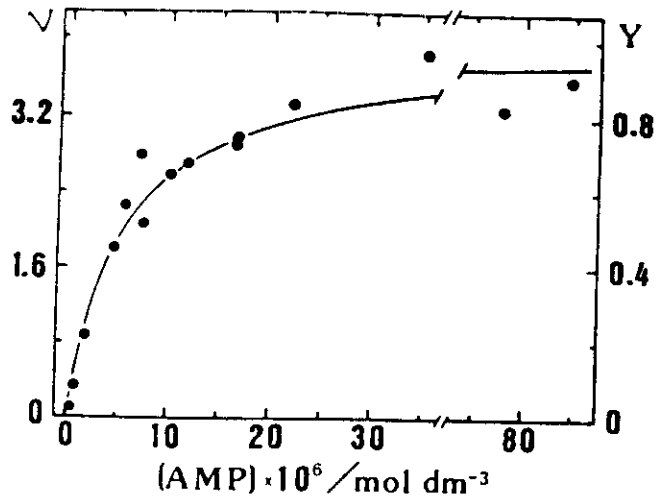

FIG. 1. **Binding of AMP to phosphorylase *a* at pH 6.9.** The data were obtained by equilibrium dialysis at 25 °C. The saturation fraction, *Y*, and the mol of AMP bound per mol of enzyme, ν, are plotted *versus* the free AMP concentration. The enzyme concentration was 3 mg cm^{-3} and the buffer used was 50 mM Hepes, 50 mM KCl, 0.1 mM EDTA, and 1 mM mercaptoacetic acid. The *solid line* was drawn using Equation 1 and the *K* value listed in Table I.

If we take into account the negligible cooperativity during the binding of AMP to phosphorylase *a*, it is completely reasonable to consider the four AMP sites in the enzyme as being independent. Then, the calculation from the Hill plot of the value of the microscopic binding constant, *K*, for any site is straightforward. This value was used as the initial input value for the iterative Newton-Gauss method (23) to fit all the experimental data in Fig. 1 to the equation

$$Y = \frac{K[\mathrm{AMP}]}{1 + K[\mathrm{AMP}]} \qquad (1)$$

The optimum *K* value thus obtained was $(1.8 \pm 0.2)10^5$ M^{-1}, practically equal to that calculated from the Hill plot. The theoretical curve in Fig. 1 results from this estimated binding constant.

Calorimetric Experiments—The enthalpy change during the binding of AMP to phosphorylase *a* was measured as a function of the nucleotide concentration at several different temperatures and with various buffers. The buffer systems employed were 50 mM Hepes, 50 mM Tris, and 50 mM β-glycerophosphate, all adjusted to pH 6.9 and containing 50 mM KCl, 0.1 mM EDTA, and 0.1 mM β-mercaptoethanol. The temperatures used were 25, 30, and 35 °C.

The heat evolved during the AMP binding, at each temperature and ligand concentration, changes with the buffer system used and, therefore, on the binding of AMP, the protein's state of protonation changes and the extent of this change depends on temperature. The interpretation of the experi-

mental enthalpy data, ΔH, thus requires that the heat of ionization of the buffers used, ΔH_i, should be known at each temperature; these values have been reported in the literature (24). Thermal titration curves for the binding of AMP to phosphorylase *a* have been carried out with different buffers. The binding of AMP was exothermic and gave rise to well-defined monophasic curves in all the cases investigated (results not shown).

The analysis of the calorimetric results at 25 °C is quite straightforward since we are dealing with a binding process of AMP to four equal and independent sites, where the association constant, K, is known. Hence, the individual calorimetric data, ΔH, should be proportional to the saturation fraction, Y, according to the equation

$$\Delta H = m\ Y\ \Delta H_t \tag{2}$$

where m stands for the number of binding sites, 4, and ΔH_t for the corresponding total heat effect, which can itself be expressed as

$$\Delta H_t = \Delta H_b + n\ \Delta H_i \tag{3}$$

with n being the number of protons exchanged between the protein and the buffer during the binding, ΔH_i the heat of buffer ionization, and ΔH_b the enthalpy change per mol of AMP bound. The slope of ΔH *versus* Y leads to the ΔH_t value for each buffer, and a second fitting of ΔH_t *versus* ΔH_i provides the values of ΔH_b and n (Fig. 2). The ΔH_t values can be alternatively obtained by fitting $1/\Delta H$ *versus* $1/[AMP]$ according to the following equation (25)

$$\frac{1}{\Delta H} = \frac{1}{mK\Delta H_t} \times \frac{1}{[AMP]} + \frac{1}{m\ \Delta H_t} \tag{4}$$

where the free AMP concentration, [AMP], is calculated from the known K value. The intercept provides the ΔH_t value, while the K value, obtained from the slope, coincides with that previously arrived at through the dialysis experiments. The good fitting of this equation confirms the non-cooperativity of the AMP binding at 25 °C. The ΔH_t values, as well as the ΔH_b and n values thus obtained (Equation 4), are the same as those found before (Equation 2).

The thermodynamic binding parameters at 30 °C and 35 °C have been obtained in the following manner: at each temperature, 30 °C or 35 °C, Equation 4 can be fitted according to the iterative process proposed by Bolen *et al.* (26). Thus, final ΔH_t and K values are obtained for each buffer at the temperature in question. An average K value results from the K values calculated for each buffer, while ΔH_b and n are arrived at by using Equation 3 with the ΔH_t values for each buffer (Fig. 2).

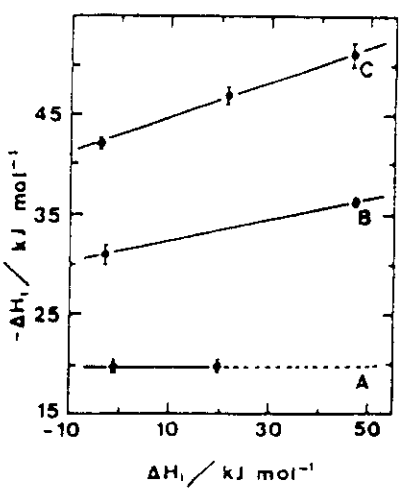

FIG. 2. **The variation of the enthalpy change per site of phosphorylase *a* with AMP (ΔH_t) with the heat of ionization of the buffer (ΔH_i).** *Lines A, B,* and *C* correspond to experiments carried out at 25, 30, and 35 °C, respectively.

The equilibrium constants at 25, 30, and 35 °C should be initially consistent in terms of the van't Hoff equation. Thus, the K values at 30 °C and 35 °C can be recalculated from the K value at 25 °C using the binding enthalpies and assuming ΔC_p to be independent of temperature. The integrated form of the van't Hoff equation is then

$$\ln \frac{K_2}{K_1} = \frac{1}{R}\left(\frac{\Delta H_1}{T_1} - \frac{\Delta H_2}{T_2}\right) + \frac{\Delta C_p}{R} \ln \frac{T_2}{T_1} \tag{5}$$

where the heat capacity change, $\Delta C_p = (\partial \Delta H/\partial T)_p$, can be obtained from the temperature dependence of the ΔH_b values. Minor variations arose in the K values thus obtained from Equation 5 at 30 °C and 35 °C.

Finally, the thermal data at 25, 30, and 35 °C were fitted to the general equation

$$\Delta H = \frac{m\ K[AMP]}{1 + K[AMP]}\left|\Delta H_b + n\ \Delta H_i\right| \tag{6}$$

by means of the Newton-Gauss method, using the binding constants as fixed parameters and the values of ΔH_b and n, already obtained, as inputs in the iteration. Once more, the optimum values found in this way for these two parameters were practically the same, within experimental error, as those used as the input values in the Newton-Gauss method (23).

Once the influence of the extent of protonation during the binding was taken into account and the appropriate corrections to the experimental titration data were made (Equation 7), three single sets of thermal values, $\Delta H(c)$, were obtained, one for each temperature.

$$\Delta H(c) = \Delta H - \frac{mK[AMP]}{1 + K[AMP]}\ n\ \Delta H_i \tag{7}$$

The *solid lines* in Fig. 3 result from the application of Equation 8 to these corrected values.

$$\Delta H(c) = \frac{mK[AMP]}{1 + K[AMP]}\ \Delta H_b \tag{8}$$

The variation of ΔH_b *versus* T, which leads to a ΔC_p value of -2.3 ± 0.2 kJ K^{-1} (mol of AMP bound)$^{-1}$, is shown in Fig. 4. Gibbs energy and entropy changes for the binding of AMP were obtained from the K and ΔH_b values, and these functions are displayed at each temperature in Table I. The standard state is that of 1 mol l^{-1}. The calculation of thermodynamic functions implies the usual approximation of setting standard enthalpies equal to the observed ones.

DISCUSSION

The thermodynamic parameters which characterize a given binding process may include structural contributions arising from different molecular events. One such contribution might be a change in the aggregation state of either reactant. Our thermal dilution experiments (see "Materials and Methods") appear to rule out this element. The fluorescence results also confirm that no AMP-induced protein association/dissociation effects occurred in our binding experiments.

The dialysis measurements at 25 °C point to the AMP binding to the phosphorylase *a* tetramer taking place at the four equal and independent nucleotide sites, a conclusion which agrees with previous publications (6, 7, 22). At 30 °C and 35 °C, the number and the non-cooperative character of

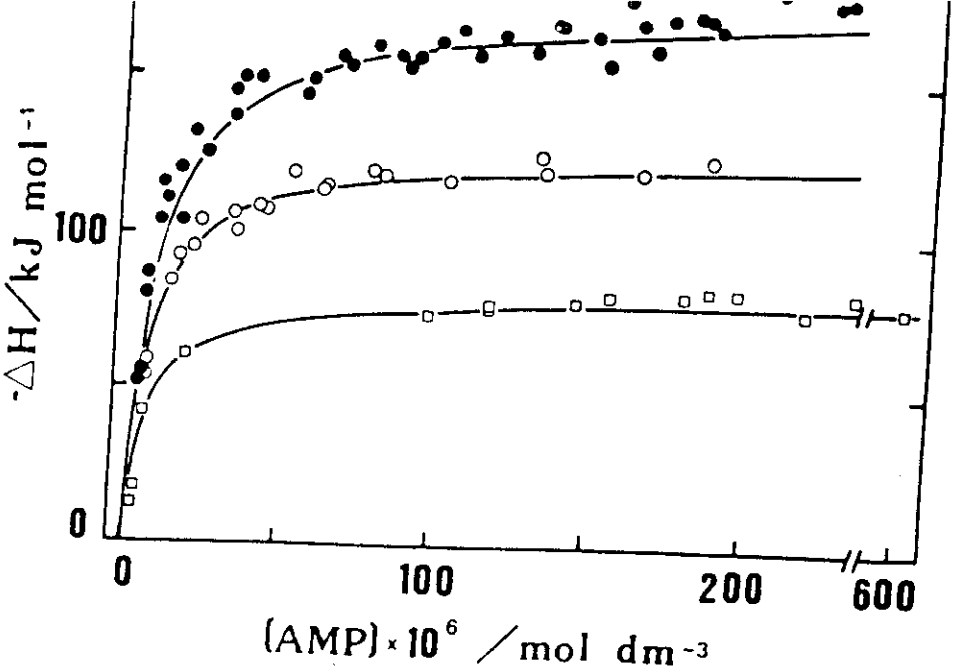

FIG. 3. **Calorimetric titration curves of the phosphorylase *a* tetramer with AMP at pH 6.9.** Experimental values are corrected for the thermal effect of the buffer protonation due to the release of protons by the enzyme-ligand system during the binding (Equation 7). The *solid lines* are the theoretical ones corresponding to Equation 8 and obtained from the values shown in Table I. □, 25 °C; ○, 30 °C; ●, 35 °C.

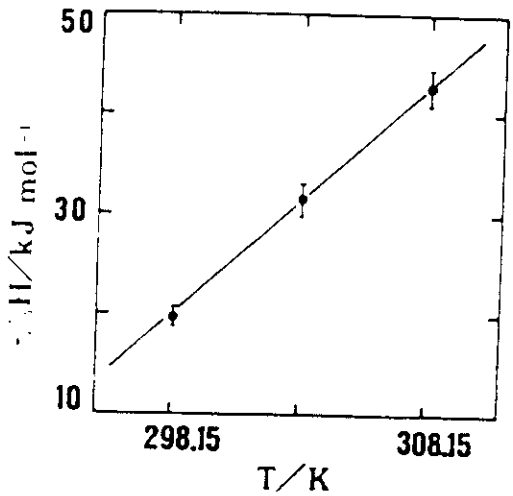

FIG. 4. **The variation with temperature of the binding enthalpy per mol of AMP bound to phosphorylase *a* at pH 6.9.** The ΔH values (Table I) come from the intercepts of the lines in Fig. 2 for $\Delta H_i = 0$. The slope of the line leads to a ΔC_p equal to -2.3 ± 0.2 kJ K^{-1} (mol of AMP bound)$^{-1}$.

TABLE I

Thermodynamic parameters for the binding of one molecule of AMP to glycogen phosphorylase a at pH 6.9

The uncertainties are standard errors in the fitting of the curves.

Temperature	$K \times 10^{-6}$ M^{-1}	ΔG°	ΔH	ΔS°
°C		kJ mol^{-1}	kJ mol^{-1}	J K^{-1} mol^{-1}
25	1.8 ± 0.2	−30.0 ± 1.0	−19.9 ± 1.0	34 ± 4
30	1.6 ± 1.1	−30.2 ± 1.7	−31.4 ± 1.8	−4 ± 12
35	1.2 ± 0.7	−30.0 ± 1.5	−42.6 ± 1.9	−41 ± 11

the binding sites seem to be the same as at 25 °C. Thus, the extrapolations of both the initial slopes and the plateau regions in the calorimetric curves at 25, 30, and 35 °C give intercepts which correspond to 4.0 ± 0.1 independent sites per tetramer. In addition, the straight plots obtained from Equation 4 at 30 °C and 35 °C (results not shown) support the idea that the binding is non-cooperative. Furthermore, Hill plots, using the thermal data at 30 °C and 35 °C and assuming four sites, resulted in straight lines with the following Hill coefficients: $n_H(30\ °C) = 0.93 \pm 0.1$; $n_H(35\ °C) = 0.95 \pm 0.1$.

Another contribution to the thermodynamic functions is the exchange of protons during the binding. In our case, the number of protons taken up by the protein-ligand system, n, depends on temperature, and their values are (see "Results"): $n(25\ °C) = 0.0 \pm 0.1$; $n(30\ °C) = -0.10 \pm 0.02$; $n(35\ °C) = -0.17 \pm 0.05$. From the relation (24)

$$\left(\frac{\partial \Delta H'}{\partial \mathrm{pH}}\right)_T = -2.3\ RT^2 \left(\frac{\partial n}{\partial T}\right)_{pH} \qquad (9)$$

it follows that, at about pH 6.9, within the temperature range studied here, an increase or decrease in pH will give rise to a corresponding increase or decrease in the ΔH of binding.

The affinity of AMP for phosphorylase *a* seems to be practically the same throughout the 25–35 °C range (Table I) in spite of the evident differences in the ΔH and ΔS binding values. This enthalpy-entropy compensation appears to be more the rule than the exception in these binding processes, as well as in the stability of proteins and other biopolymers in their native conformations (27). The binding constant at 25 °C (Table I) is 1–2 orders of magnitude higher than that of the cooperative binding of AMP to the N sites of the phosphorylase *b* dimer (2). This known higher affinity of AMP for the *a* form of the enzyme may be related to the role of the 19 N-terminal residues of the protein, which are close to the dimer interface and to the N site, the structure of which is the main difference in the crystallographic studies of both forms of the enzyme (5).

The temperature derivatives of the Gibbs energy function, such as enthalpy, entropy, and heat capacity values, permit a more detailed molecular interpretation than the Gibbs function itself. It should be stressed here that the determination of these parameters without model assumptions of the reaction mechanism is only possible by direct calorimetric measurements. A rather high negative ΔC_p value is normal in

Techniques of Protein Chemistry (Leach, S. J., ed) Part C, pp. 301–357, Academic Press, New York
24. Hinz, H. J., Shiao, D. D. F., and Sturtevant, J. M. (1971) *Biochemistry* **10**, 1347–1352
25. Bjurulf, C., Laynez, J., and Wadso, I. (1970) *Eur. J. Biochem.* **14**, 47–52
26. Bolen, D. W., Flogel, M., and Biltonen, R. (1971) *Biochemistry* **10**, 4136–4140
27. Privalov, P. L. (1979) *Adv. Protein Chem.* **33**, 167–241
28. Mateo, P. L., and Sturtevant, J. M. (1977) *Biosystems* **8**, 247–253
29. Nickamp, C. W., Sturtevant, J. M., and Velick, S. F. (1977) *Biochemistry* **16**, 436–445
30. Schmid, F., Hinz, H. J., and Jaenicke, R. (1976) *Biochemistry* **15**, 3052–3059
Sturtevant, J. M. (1982) *Biochemistry* **21**, 2036–2048
33. Kauzmann, W. (1959) *Adv. Protein Chem* **14**, 1–63
34. Gurney, R. W. (1953) in *Ionic Processes in Solution*, McGraw-Hill Publications, Minneapolis, MN
35. Hoerl, M., Feldmann, K., Schnackers, K. D., and Helmreich, E. J. M. (1979) *Biochemistry* **18**, 2457–2464
36. Anderson, R. A., and Graves, D. J. (1973) *Biochemistry* **12**, 1895–1900
37. Suurkuusk, J. (1974) *Acta Chem. Scand. Ser. B Org. Chem. Biochem.* **28**, 409–417
38. Fletterick, R. J., Sprang, S., and Madsen, N. B. (1979) *Can. J. Biochem.* **57**, 789–797
39. Stura, E. A., Zanotti, G., Babu, Y. S., Sansom, M. S. P., Stuart, D. I., Wilson, K. S., and Johnson, L. N. (1983) *J. Mol. Biol.* **170**, 529–565
40. Fletterick, R. J. (1983) in *The Robert A. Welch Foundation Conferences on Chemical Research, Houston, TX*, pp. 170–220

THE JOURNAL OF BIOLOGICAL CHEMISTRY

Vol. 264, No. 22, Issue of August 5, pp. 12872-12878, 1989
Printed in U.S.A.

Thermodynamic Analysis of the Activation of Glycogen Phosphorylase *b* Over a Range of Temperatures*

(Received for publication, January 24, 1989)

Carmen Barón, Juan F. González‡, Pedro L. Mateo§, and Manuel Cortijo¶

From the Departamento de Química Física, Facultad de Ciencias, Universidad de Granada, 18071 Granada, Spain

Equilibrium dialysis and isothermal microcalorimetry experiments have been carried out to characterize the thermodynamics of the binding of AMP to glycogen phosphorylase *b* (EC 2.4.1.1) at pH 6.9 over the temperature range of 25–35 °C. Thermal titrations were performed at each temperature in various buffer systems, which have afforded the calculation of the number of protons exchanged when the AMP binds to each site in the protein. Thermodynamic parameters were obtained for the binding of AMP to the two nucleotide and the two inhibitor sites of the dimeric enzyme. The former show positive cooperativity while the latter behave as independent binding sites. A positive ΔC_p value was obtained for the AMP binding to the two N sites (1.3 and 1.4 kJ K^{-1} mol^{-1}), while the ΔC_p was negative for the binding to the I sites (−1.9 kJ K^{-1} mol^{-1}). The application of Sturtevant's method to our data (Sturtevant, J. M. (1977) *Proc. Natl. Acad. Sci. U. S. A.* 74, 2236–2240) and their comparison with a similar analysis undertaken with phosphorylase *a* (Mateo, P. L., González, J. F., Barón, C., Lopez-Mayorga, O., and Cortijo, M. (1986) *J. Biol. Chem.* 261, 17067–17072) has opened the way to some understanding of the thermodynamics of the allosteric transition in the protein.

Glycogen phosphorylase (EC 2.4.1.1) is one of the most complex macromolecules for which a high resolution atomic structure is available. The enzyme has two interconvertible forms, in which the difference between the inactive phosphorylase *b* and the active form, phosphorylase *a*, lies in the phosphorylation of the Ser-14 residue in the *a* form. Among the many effectors of the protein, AMP is the main allosteric activator for phosphorylase *b* and its interactions with the protein are therefore of importance. It is known from x-ray studies (1, 2) as well as from studies in solution (3–5) that the nucleotide binds to two distinct sites in the protomer, the allosteric activator site N and the inhibitor site I. Phosphorylase *a* also binds AMP in a non-cooperative manner (6–8) and increases its activity by 20–30%, reaching similar levels to those of the phosphorylase *b*-AMP complex (9). Several review articles on the biochemical and structural properties of phosphorylase have been published in recent years (10–13).

The binding of a ligand to a protein is usually accompanied by a rather large negative ΔC_p, which implies characteristic temperature-dependent ΔH and ΔS values for the binding. In the case of allosteric, cooperative binding processes, the energetics of the binding is difficult to analyze due to the conformational transitions, which are responsible for the cooperative binding. The molecular interpretation of such an analysis is also complicated because one rarely has detailed structural information about the nature of those transitions. The most direct and effective technique for a thermodynamic investigation is that of isothermal microcalorimetry, although for these complex cooperative processes additional experimental methods are also required.

We have previously reported on the thermodynamic study of the binding of AMP to phosphorylase *b* at 25 °C (5), as well as that of AMP to phosphorylase *a* between 25 and 35 °C (8). We have now extended the temperature range of the former study to 30 and 35 °C by additional equilibrium dialysis measurements at 25 °C and by calorimetry at 30 and 35 °C using various buffers of different protonation heats at pH 6.9. The present work throws light on the thermodynamics of the binding of AMP to both the N and I sites, including the ΔC_p values for each site, which have different signs. The data have been further analyzed by the method outlined by Sturtevant (14), and a comparison with the similar results for phosphorylase *a* (8) leads us to certain conclusions about the energetics of the conformational change in the protein and also to comment on the particular interactions and structural features responsible for the calculated thermodynamic functions of the binding.

MATERIALS AND METHODS

Enzymes and Chemicals—Glycogen phosphorylase *b* was prepared from rabbit skeletal muscle by the method of Fischer *et al.* (15, 16) with the modifications described by Krebs *et al.* (17). The catalytic activity of the enzyme was determined by Hedrick and Fischer's assay (18). The preparations used had specific activities of 80–90 units/mg. Protein concentration was determined from absorbance measurements at 280 nm, using the absorbance coefficient $E^{1\%}_{1cm} = 13.2$ (19). The molecular weight of the monomer was taken as 97,400 (20). The enzyme was crystallized at least three times. Phosphorylase *b* preparations were freed from AMP by chromatography on a Sephadex G-25 column equilibrated with 50 mM KCl, 0.1 mM 2-mercaptoethanol, 0.1 mM EDTA, 50 mM buffer solution (2-glycerophosphate, Hepes,[1] Pipes, or Tris), adjusted to pH 6.9. The A_{260}-A_{280} ratio for the AMP-free phosphorylase *b* solutions was always below 0.53. Possible traces of AMP aminohydrolase (EC 3.5.4.6.) (21) were eliminated by incubation with alumina C_γ, as has been described elsewhere (22).

[5′-^{14}C]AMP was obtained from the Radiochemical Center, Amersham, United Kingdom. AMP, alumina C_γ, Hepes, Pipes, and 2-mercaptoethanol were bought from Sigma, Tris and sodium 2-glycer-

* This work has been supported by Grant PR84-1233 from the CAICYT, Ministerio de Educación y Ciencia (Spain). The costs of publication of this article were defrayed in part by the payment of page charges. This article must therefore be hereby marked "*advertisement*" in accordance with 18 U.S.C. Section 1734 solely to indicate this fact.

‡ Present address: Servicio de Química y Radioquímica, Central Nuclear Vandellos, Endesa, Spain.

§ To whom correspondence should be addressed. Tel.: 58-272879. Fax: 58-270095.

¶ Present address: Departamento de Química Física II, Facultad de Farmacia, Universidad Complutense, 28040 Madrid, Spain.

[1] The abbreviations used are: Hepes, 4-(2-hydroxyethyl)-1-piperazineethanesulfonic acid; Pipes, 1,4-piperazinediethanesulfonic acid.

ophosphate from Merck, and EDTA from Fluka, while Sephadex G-25 was manufactured by Pharmacia LKB Biotechnology Inc. All chemicals used were of the highest available purity. Distilled, deionized water was used throughout.

Techniques—The equilibrium dialysis experiments were carried out at 25 °C using a Dianorm equilibrium dialysis system, according to the method of Helmreich *et al.* (23). An LS 7500 Beckman scintillation counter was used in the dialysis experiments to calculate the saturation fraction of the enzyme with AMP. The fluorescence intensity of the protein, as a function of the enzyme concentration, both in the presence and the absence of AMP, was measured with an LS-5 Perkin-Elmer luminescence spectrometer with a thermostat. The protein concentration and enzymatic assays were measured with a Cary-210 spectrophotometer with the cells maintained at 25 °C.

Isothermal calorimetry experiments were carried out at 30 and 35 °C using an LKB 2277 BioActivity monitor equipped with two flow units. Electrical and chemical calibrations were made in the same range as that which we obtained in the calorimetric experiments themselves. The chemical calibrations were made by neutralizing Tris with HCl (24). Enzyme and AMP solutions were allowed to flow into the calorimeter at equal rates of 7 $cm^3\ h^{-1}$ in the majority of experiments, with the occasional change to check the completeness of the reaction.

All appropriate corrections for heats of dilution and mixing were applied. The heat effect of the enzyme dilution was negligible in all cases. The phosphorylase *b* activity was routinely checked prior to and after the calorimetric and dialysis experiments. The pH values of the several buffers, AMP, and enzyme solutions were controlled at each temperature before and after the binding reaction.

RESULTS

Fluorescence Determinations—Glycogen phosphorylase *b* shows two fluorescence transitions (25): one is caused by the protein moiety (excitation and emission maxima at 280 and 335 nm, respectively, and a quantum yield of 0.12), and the other is associated with its cofactor, pyridoxal 5′-phosphate (excitation maxima at 335 and 425 nm, emission maximum at 535 nm, and a quantum yield of 0.012). The fluorescence intensity in the emission maximum at 535 nm is quenched by the addition of Mg^{2+}-AMP to the dimeric phosphorylase *b* (26), which promotes the tetramerization of the enzyme (27). We have used this fluorescence of the cofactor to determine any change taking place in the quaternary structure of the protein under conditions in which we have conducted the dialysis and calorimetric experiments.

The enzyme was excited at 425 nm to keep the absorbance of the samples below 0.1. We then carried out intensity measurements of the pyridoxal phosphate fluorescence, both in the absence and in the presence of either 1 or 10 mM AMP, as a function of the enzyme concentration within the range 0.5–14 mg cm^{-3} at 25 and 35 °C. In all cases we obtained a good linear dependence between the fluorescence intensity and the protein concentration for the whole range investigated (linear regression coefficient higher than 0.998). Thus, there was no evidence for any intermolecular effects, *i.e.* detectable association-dissociation phenomena, dependent on the enzyme concentration for the above range.

Equilibrium Dialysis Measurements—The binding of AMP to phosphorylase *b* has been previously studied as a function of the activator concentration by equilibrium dialysis at 25 °C and pH 6.9 in Tris buffer, using 25 different experimental data (5). Since the present calorimetric analysis relies critically on the precision and accuracy of the binding constants obtained from the dialysis study, we have carried out many more additional experiments to obtain more than 60 independent equilibrium dialysis data (compare, for example Fig. 1 here with Fig. 2 of Ref. 5) in order to calculate association equilibrium constant values with lower standard deviations. In a system as complex as the present one, the analysis of the calorimetric data requires the use of the binding constants obtained with other techniques (*i.e.* equilibrium dialysis). Thus, the information that it is possible to obtain from the calorimetric study largely depends on the precision of the association constants used. All equilibrium dialysis data are given in a Scatchard plot in Fig. 1. As we have previously shown (5), the reaction of AMP with the phosphorylase *b* dimer can be considered as being the binding of AMP to two independent sets of sites. The high affinity sites show positive cooperativity according to their Hill coefficient ($n_H = 1.4 \pm 0.04$), while the low affinity sites can themselves be considered as independent of each other ($n_H = 0.96 \pm 0.11$). On this basis, the saturation fraction, Y, as a function of the free AMP concentration, is

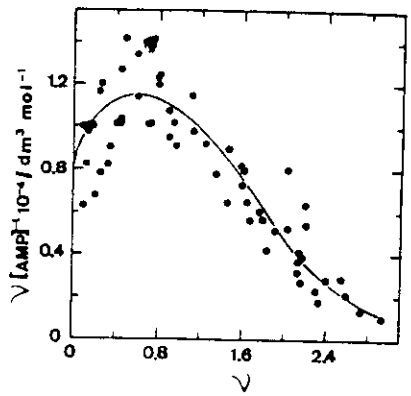

FIG. 1. **Scatchard plot for the binding of AMP to phosphorylase *b* at pH 6.9.** The data are obtained by equilibrium dialysis at 25 °C. The enzyme concentration was 8 mg cm^{-3} and the buffer solution used was 50 mM Tris, 50 mM KCl, 0.1 mM EDTA, and 1 mM 2-mercaptoethanol. The *solid line* is the theoretical one using the values given in Table I.

$$Y = \frac{1}{2}\frac{K_{m_1}[\mathrm{AMP}] + K_{m_1}K_{m_2}[\mathrm{AMP}]^2}{2K_{m_1}[\mathrm{AMP}] + 1 + K_{m_1}K_{m_2}[\mathrm{AMP}]^2} + \frac{1}{2}\frac{K_{m_3}[\mathrm{AMP}]}{K_{m_3}[\mathrm{AMP}] + 1} \quad (1)$$

where K_{m_i} stands for the microscopic binding constants at the ith site, and $K_{m_3} = K_{m_4}$.

The microscopic binding constant values given in Ref. 5 were used as the initial input values for the iterative Newton-Gauss method (28) to fit the total experimental data to the Equation 1. The optimum K_{m_1}, K_{m_2}, and K_{m_3} values thus obtained are shown in Table I. These new constant values are approximately equal to those obtained previously, within their standard deviations. Nevertheless, they have minor standard deviations. The curve in Fig. 1 is the theoretical one using the Scatchard equation for the calculated binding constants (Table I).

Calorimetric Experiments—The enthalpy change during the binding of AMP to phosphorylase *b* was measured as a function of the activator concentration at two new different temperatures and with various buffers at pH 6.9. The buffer systems employed were 50 mM Tris and 50 mM 2-glycerophosphate at 30 °C and 50 mM Hepes, 50 mM Pipes, 50 mM Tris, and 50 mM 2-glycerophosphate at 35 °C. In all cases the buffer solutions were 50 mM KCl, 0.1 mM EDTA, and 0.1 mM 2-mercaptoethanol. The thermal experimental data determined at 30 and 35 °C are shown in Fig. 2, where the enthalpy change per mol of the phosphorylase *b* dimer is plotted as a function of the total concentration of AMP. The binding of AMP is exothermic at 30 and 35 °C, as it also is at 25 °C (5), giving rise to well defined monophasic curves (Fig. 2). The titration curve at 25 °C was the same regardless of the buffer system (5), and since the ionization heats of the buffers are different (29) no proton uptake or release seemed to occur throughout the binding at that temperature. At both 30 and

TABLE I

Apparent thermodynamic parameters for the binding of AMP to phosphorylase b at 25 °C and pH 6.9

The uncertainties are standard errors in the fitting of the curves.

	N sites		I sites	Total N sites	Total I sites
$K_m \times 10^{-3}$ (M^{-1})	4.0 ± 0.7	23.7 ± 5.5	0.37 ± 0.05		
ΔG^0 (kJ mol^{-1})	−20.6 ± 0.5	−25.0 ± 0.6	−14.6 ± 0.3	−45.6 ± 0.6	−29.2 ± 0.6
ΔH (kJ mol^{-1})	−19 ± 6	−74 ± 7	−39 ± 2	−93 ± 2	−78 ± 3
ΔS^0 (J K^{-1} mol^{-1})	6 ± 20	−163 ± 25	−83 ± 6	−157 ± 7	−166 ± 11
ΔC_p (kJ K^{-1} mol^{-1})	1.3 ± 1.3	1.4 ± 1.7	−1.9 ± 0.5	2.7 ± 0.5	−3.8 ± 0.9

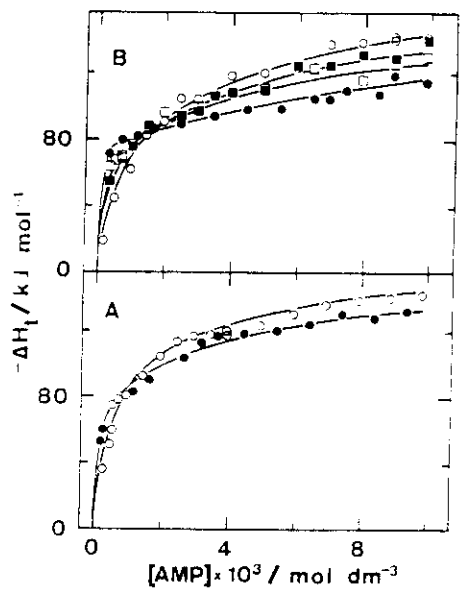

FIG. 2. **Calorimetric titration of phosphorylase *b* with AMP at pH 6.9 and at 30 °C (*A*) and 35 °C (*B*).** The heat envolved per dimer of enzyme is plotted *versus* the total AMP concentration. The enzyme concentration was 4 mg cm^{-3} in 50 mM KCl, 0.1 mM EDTA, and 0.1 mM 2-mercaptoethanol. ●, 50 mM Tris; □, Hepes; ■, Pipes; ○, 2-glycerophosphate. The *solid curves* are the theoretical ones obtained from the values listed in Table I and using the values for the number of protons calculated as described in the text.

35 °C, however, the heat evolved during the AMP binding depends upon the buffer system, due to a change in the protein's state of protonation, and we have found the extent of this change to be temperature-dependent. The analysis of the present experimental enthalpy data, ΔH_t, thus requires that the heat of ionization of the various buffers used should be known at each temperature (8); these values have been reported in the literature (29).

As mentioned before, the AMP binding to phosphorylase *b* can be understood as the binding of a ligand, S, to a protein, P, with two sets of sites: the high affinity sites, N, and the low affinity sites, I. The binding at each temperature can then be represented by the following equilibria:

$$\begin{aligned} P_N + S &\rightleftarrows P_NS \quad K_1 = 2K_{m_1}; \quad \Delta H_1 \\ P_NS + S &\rightleftarrows P_NS_2 \quad K_2 = K_{m_2}/2; \quad \Delta H_2 \\ P_I + S &\rightleftarrows P_IS \quad K_3 = 2K_{m_3}; \quad \Delta H_3 \\ P_IS + S &\rightleftarrows P_IS_2 \quad K_4 = K_{m_4}/2; \quad \Delta H_4 \end{aligned} \tag{2}$$

where K_i and K_{m_i} are the macroscopic and microscopic binding constants, respectively, and ΔH_i stands for the enthalpy change per mol of AMP bound to each site. P_N and P_I stand for the protein states when the high and low affinity sites are empty; P_NS corresponds to the protein state with only one high affinity site empty, regardless of whether the low affinity sites are empty or not. The protein states P_IS and P_IS_2 are defined similarly. In the binding of AMP to phosphorylase *b*, $K_{m_3} = K_{m_4}$ and $\Delta H_3 = \Delta H_4$, since the two equal low affinity sites are considered as being independent, as was shown to be the case at 25 °C (5).

From equation 2, the enthalpy change per mol of enzyme (dimer), ΔH_b, in a hypothetical buffer with zero ionization heat is given by

$$\Delta H_b = \frac{\Delta H_1[P_NS] + (\Delta H_1 + \Delta H_2)[P_NS_2]}{[P_N] + [P_NS] + [P_NS_2]} + \frac{\Delta H_3[P_IS] + 2\Delta H_3[P_IS_2]}{[P_I] + [P_IS] + [P_IS_2]} \tag{3}$$

which can be expressed as the following:

$$\Delta H_b = \frac{2\Delta H_1 K_{m_1}[S] + (\Delta H_1 + \Delta H_2)K_{m_1}K_{m_2}[S]^2}{1 + 2K_{m_1}[S] + K_{m_1}K_{m_2}[S]^2} + \frac{2\Delta H_3 K_{m_3}[S]}{1 + K_{m_3}[S]} \tag{4}$$

As pointed out before, there is a net proton exchange, n, when the AMP binds to the enzyme (dimer). Let n_1, n_2, and n_3 stand for the number of protons exchanged by the system when AMP binds to the first and second high affinity sites and one of the two low affinity sites, respectively. Then the n value, which is itself a function of the saturation of the enzyme by AMP, can be expressed similarly to Equation 3 as

$$n = \frac{n_1[P_NS] + (n_1 + n_2)[P_NS_2]}{[P_N] + [P_NS] + [P_NS_2]} + \frac{n_3[P_IS] + 2n_3[P_IS_2]}{[P_I] + [P_IS] + [P_IS_2]} \tag{5}$$

or

$$n = \frac{2n_1 K_{m_1}[S] + (n_1 + n_2)K_{m_1}K_{m_2}[S]^2}{1 + 2K_{m_1}[S] + K_{m_1}K_{m_2}[S]^2} + \frac{2n_3 K_{m_3}[S]}{1 + K_{m_3}[S]} \tag{6}$$

At each temperature the number of protons exchanged by the protein-ligand system, n, will be released or taken up by the buffer present in the medium. In our case the situation is particularly complicated since, in addition to the buffer used in each case, the free ligand itself, AMP, has also buffering capacity at pH 6.9 (pK = 6.427 at 25 °C (29)). Moreover, the buffering effect of the free AMP will depend on its concentration, and it is clear that this effect cannot be neglected due to the AMP concentration range used compared to that of the buffer itself. Therefore the number of protons, n, will be equal to the sum of those exchanged by the buffer, n_B, and the free ligand, n_S:

$$n = n_B + n_S \tag{7}$$

The values of n_B and n_S are obviously not independent, and it can be shown that they follow an equation of the following form:

$$n_S = \frac{an_B}{b + cn_B} \tag{8}$$

where a, b, and c are functions of the protein concentration, the pH, and the pK values and concentrations of both the buffer and the free AMP (see "Appendix").

Hence, the experimental calorimetric data, ΔH_t, is given by

$$\Delta H_t = \Delta H_b + n_B \Delta H_B + n_S \Delta H_S \quad (9)$$

where the new symbols, ΔH_B and ΔH_S, stand for the ionization heats of the buffer and free ligand, respectively.

From Equations 7 and 8 the value of n_B results as

$$n_B = \frac{1}{2c}\left[cn - b - a + ((a + b - cn)^2 + 4bcn)^{1/2}\right] \quad (10)$$

with a similar equation for n_S as a function of n. These two expressions for n_S and n_B can replace the corresponding values in Equation 9, leading to a ΔH_t which would depend on n and ΔH_b. Since these two latter values are given by Equations 6 and 4, we would finally obtain the experimental ΔH_t value at each temperature as a function of K_{m_i}, ΔH_i, and n_i, for the three sites, $i = 1, 2, 3$.

At this point we would have three equations for ΔH_t, corresponding to one for 25, 30, and 35 °C. Fitting all the experimental data to these three equations would involve dealing with a large number of unknowns. This analysis, however, can be simplified by taking into account some restrictions these values have to abide by and also by making some reasonable assumptions about the behavior of the system.

Thus, the three K_m values at 25 °C are known from the dialysis experiments. In addition the enthalpy changes and the constant values for each site have to be consistent in terms of the Kirchhoff and the van't Hoff equations, respectively. The integrated forms of these equations for a constant ΔC_p value are

$$\Delta H(T_2) = \Delta H(T_1) + \Delta C_p(T_2 - T_1) \quad (11)$$

and

$$\ln \frac{K(T_2)}{K(T_1)} = \frac{1}{R}\left(\frac{\Delta H(T_1)}{T_1} - \frac{\Delta H(T_2)}{T_2}\right) + \frac{\Delta C_p}{R} \ln \frac{T_2}{T_1} \quad (12)$$

The number of protons for the three sites, n_1, n_2, and n_3, have been shown to be zero at 25 °C within experimental error (5). These values, however, are not zero at 30 and 35 °C, as seen in Fig. 2, where an increasing proton-exchange effect from 30 to 35 °C can be clearly observed. Given the short temperature range investigated, we have assumed the n_i values to have a linear dependence with temperature, *i.e.* $n_i(T_2) = n_i(T_1) + m_i(T_2 - T_1)$. This behavior is similar to that found for the binding of AMP to phosphorylase *a* (8). With this assumption and the above restrictions we can arrive at a general equation for the experimental ΔH_t values, including all the buffers and the three temperatures used, where the values to fit would be ΔH_i (at 25 °C), ΔC_{p_i} and m_i, for the three sites, $i = 1$, 2, and 3. The experimental thermal data, which correspond to more than 150 independent calorimetric measurements, were fitted to the general equation by trial and error using the ΔH_i values at 25 °C previously reported (5). The ΔH_i (25 °C), ΔC_{p_i}, and m_i were optimized by the Newton-Gauss method (28). The curves in Fig. 2 are the theoretical ones using the calculated values. Thermodynamic parameters for the binding of AMP to phosphorylase *b* at 25 °C and pH 6.9, obtained from the ΔH_i and K_{m_i} values, and including the ΔC_{p_i} values, are included in Table I. The three enthalpy values at 25 °C compare well with those previously reported (5), which vindicate the general data analysis carried out simultaneously for the three temperatures. Fig. 3 shows the variations of ΔH and $T\Delta S°$ *versus* temperature and, as has been reported in the literature for many binding studies (14), the $\Delta G°$ values remain practically constant for each site within the temperature range of 25–35 °C. The m_i values

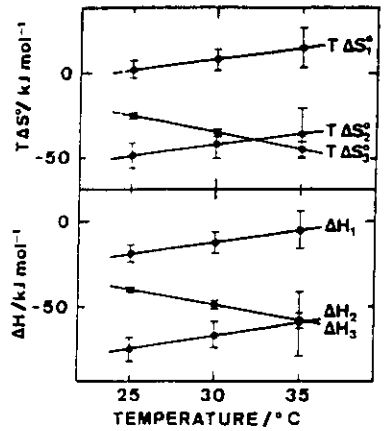

FIG. 3. **Temperature dependence of the enthalpy and entropy changes for the binding of AMP to phosphorylase *b* at pH 6.9.** The ΔH and $T\Delta S°$ values are calculated using the data shown in Table I.

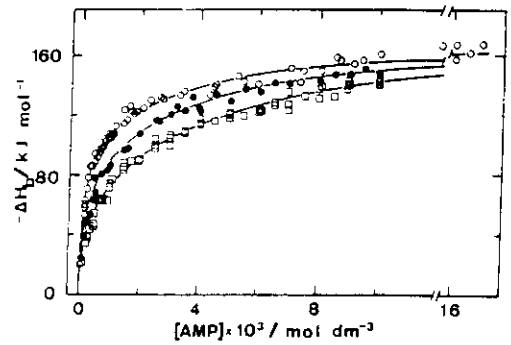

FIG. 4. **Thermal titration of phosphorylase *b* with AMP at pH 6.9.** Experimental values are corrected for the thermal effect of the protons exchanged with the buffer systems. The corrected heat data are plotted as a function of the free AMP concentration at 25 °C (○), 30 °C (●), and 35 °C (□). The *solid curves* are the theoretical ones corresponding to Equation 4 for the enthalpy and constant values obtained using Equations 11 and 12, respectively, and the data listed in Table I (see text for details).

obtained are $m_1 = -0.25 \pm 0.04$, $m_2 = 0.26 \pm 0.06$, and $m_3 = 0.05 \pm 0.02$, which lead to a negative n_1 value and positive n_2 and n_3 values for temperatures between 25 and 35 °C. Fig. 4 includes the three sets of data at 25, 30, and 35 °C after correction for the proton exchange thermal effects, together with the theoretical calorimetric binding curves also corrected for the proton effects, *i.e.* the ΔH_b values *versus* the free AMP concentration.

We should mention at this point that when dealing with ligand binding to multisite complex proteins the experimental data analysis is only possible if certain assumptions are accepted, *i.e.* the restrictions the system is supposed to obey. Only in this way can a set of individual binding parameters such as the one shown in Table I be arrived at. In our case the assumptions made were to consider the ΔC_{p_i} values as being constant (the norm for this type of study) and also the m_i values, within the 25 to 35 °C range. Nevertheless, it should be pointed out, that when performing our data analysis, using the three K_{m_i} values at 25 °C with either plus or minus one-half of their standard deviations (Table I), the optimal fitting practically leads to the same values for the rest of the thermodynamic parameters as those obtained here within their uncertainties (Table I).

DISCUSSION

The association of the phosphorylase *b* dimer into a tetramer caused by AMP in the presence of Mg^{2+} has been reported

at 25 °C (26). Other authors (31, 32) have also detected aggregation of the enzyme when AMP binds at low temperatures, although not at 25 °C. If this were to be the case, an enthalpic contribution arising from the change in the association state (the extent of which would depend on temperature, AMP, and protein concentrations) would show up in the calorimetric data. We have already demonstrated (5), by carrying out thermal AMP titrations at different protein concentrations, that no phosphorylase association effects occur on the binding of AMP at 25 °C. Here we have also made use of the co-factor fluorescence intensity, in the absence of AMP and in the presence of 1 and 10 mM AMP, to confirm the nonexistence of intermolecular interactions at 25 and 35 °C, since this intensity is a very sensitive indicator of the association state of the protein (8, 26). In this way, we found a linear dependence between the fluorescence intensity and protein concentration within the range 0.5–14 mg cm^{-3} at both temperatures. Our thermal dilution experiments at 30 and 35 °C also agree with this conclusion. Therefore, it is apparent that no AMP-induced phosphorylase association/dissociation effects took place in our equilibrium dialysis and calorimetric binding experiments.

In order to analyze the calorimetric data correctly the first question that needs answering is whether there is any proton exchange during the binding. The usual way to do this is to carry out the thermal titration in various buffers of sufficiently different protonation heats. We have already shown, within experimental uncertainty, that there is no such exchange at 25 °C (5). This does not hold true, however, at 30 and 35 °C (Fig. 2), where two and four different buffers, respectively, were used; a similar behavior has been reported for the binding of AMP to phosphorylase *a* (8). It is worth noting that at both 30 and 35 °C at the AMP concentrations at which the different buffer titration curves intersect (Fig. 2) the net proton exchange, n, is zero. This situation obviously implies a different proton behavior during the binding of AMP to the four sites, *i.e.* there should be simultaneous release and take up of protons depending upon each AMP bound.

In fact, for temperatures between 25 and 35 °C, the protein-ligand system releases protons when AMP binds to the first site and takes them up on binding to the three other sites. This means that one or several pK values, corresponding to some proton accepting groups of the enzyme-ligand system, decreases (*i.e.* become more acidic) upon binding of AMP to the first site, while these pK values increase when the effector binds to the other three sites. There are various reasons which may explain these changes in the pK values. Among these, a variation in the micropolarity of the chemical groups appears to us to be the most plausible explanation, given the high effect of the medium polarity (or water availability) on the pK values observed in analogous systems (30).

Once the protonation effect has been corrected, the thermodynamic parameters for the binding can be obtained, as explained under "Results." Table I shows these values at 25 °C, including the ΔC_p values, from which the calculation of any other parameter within the range 25–35 °C is straight forward. Fig. 3 illustrates the significant temperature dependence of the binding enthalpy and entropy, as might be expected from the ΔC_p values. Despite the clear differences in the ΔH and $\Delta S°$ binding values/site, the affinity of AMP for each site, *i.e.* the corresponding $\Delta G°$ value, appears to be practically the same from 25 to 35 °C. This is another example of the so-called enthalpy-entropy compensation, common to many binding processes and, in fact, to practically any type of process dealing with biopolymers in an aqueous solution (14, 33).

The cooperative nature of the binding of AMP to the two N sites can also be seen in their ΔH and $\Delta S°$ values (see Fig. 3 and Table I). The most striking difference between the binding to the N and I sites resides in the fact that ΔC_p is positive for both N sites and negative for the I sites. Negative ΔC_p values are normal in binding studies (14), as is, for instance, the noncooperative binding of AMP to phosphorylase *a* (8). The positive ΔC_p values for the N sites are, however, quite exceptional, and they are undoubtedly related to AMP's highly cooperative binding to these sites and the AMP-induced structural change responsible for this cooperativity.

It is not possible to attempt any structural interpretation of the thermodynamic parameters for the binding of AMP to each N site, since the parameters for each site contain different contributions arising from the cooperative structural change (Table I). The total ΔH values for the AMP binding to the N sites at 30 and 35 °C are -79 ± 10 and -60 ± 14 kJ (mol of dimer)$^{-1}$ respectively, while the corresponding $\Delta S°$ values are -112 ± 8 and -68 ± 15 J K^{-1} (mol of dimer)$^{-1}$. The variation in these parameters with temperature is just the opposite to that found for the binding of AMP to the N sites of phosphorylase *a* (8), due to the negative ΔC_p value in the *a* form of enzyme (-2.3 ± 0.2 kJ K^{-1} (mol of AMP)$^{-1}$).

Sturtevant's approach (14), which has recently been commented upon by Baldwin (36), throws more light on the interpretation of our thermodynamic functions. The application of Sturtevant's method to our values leads to the hydrophobic (h) and vibrational (v) contributions to ΔS_u and ΔC_p shown in Table II, where ΔS_u stands for the standard unitary entropy units (37, 38). It is worth comparing similar results for the AMP binding to the N sites of phosphorylase *a* (8) (obtained at the same temperatures, 25, 30, and 35 °C) with the corresponding ones in Table II, where it is noteworthy that the four parameters have opposite signs for the *a* and *b* forms of the enzyme. It is clear from the x-ray diffraction (39) and solution studies (40) that the remarkable differences between the AMP binding to the N sites in both enzymes cannot derive from the minor differences in the AMP interactions at both N sites and, therefore, must be put down to the conformational transition that takes place in phosphorylase *b* on the binding of AMP. Thus, a comparison of the data in our Table II and that of Table II in Ref. 8 should lead one to expect positive values for ΔC_p(h), ΔC_p(v), and ΔS_u(v) and negative ones for ΔS_u(h) for this transition, *i.e.* the activation process of the enzyme. From the sign in these parameters it seems that there should be a "loosening" of the structure with a concomitant increase in ΔC_p(v) and ΔS_u(v) on activation, from which the enzyme goes from the inactive to the fully active conformation. The positive ΔC_p(h) and negative ΔS_u(h) can reasonably be interpreted in terms of hydrophobic interactions; thus, the number of contacts between the apolar residues of the protein and the solvent should increase on enzyme activation. This conclusion agrees with the structural

TABLE II

Hydrophobic (h) and vibrational (v) contributions to the entropy and heat capacity for the binding of AMP to glycogen phosphorylase b at pH 6.9

T	N sites				I sites			
	ΔC_p (h)	ΔC_p (v)	ΔS_u (h)	ΔS_u (v)	ΔC_p (h)	ΔC_p (v)	ΔS_u (h)	ΔS_u (v)
°C	J K^{-1} (mol dimer)$^{-1}$							
25	2257	471	−587	495	−2948	−826	766	−868
30	2245	483	−554	508	−2928	−848	726	−890
35	2238	491	−518	516	−2914	−860	678	−904

information provided by Sprang and Fletterick (41), according to which there is a 2000-Å^3 island of solvent at the center of the subunit contact region; this central cavity, which can accommodate some 150–180 water molecules, which are inaccessible to the bulk of the solution in the inactive conformation, becomes deeper and narrower and opens up to the external solvent on activation, thus making for a more extended water-protein interaction, particularly for the first 75 N-terminal residues in both subunits (41).

The contribution of the allosteric conformational change would be the dominant one in the values of Table II for the AMP binding to the N sites. From these values it would be possible to conclude that for the dimeric enzyme some 60 internal vibrational modes would be activated as a result of the "intrinsic" binding (35) of 2 mol of AMP plus the concomitant conformational change (14), while there would be an increase of about 24 mol of "hydrophobic water" in the overall process (14). These numbers should be considered as a net balanced change in those water molecules since, on the other hand, there should be a loss of some hydrophobic water molecules due to the binding of AMP to the N sites, which Anderson and Graves (42) have described as being hydrophobic. An additional interaction expected from the ΔC_p and $\Delta S°$ values would be the possible net formation or the strengthening of hydrogen bonds, which would also agree with the negative ΔH values. The overall binding of AMP to the N sites is thus favored by the enthalpy and vibrational entropy, which surmount the high hydrophobic entropy barrier, a barrier that results mainly from the above-mentioned conformational change.

The binding of AMP to the I sites has been shown to be noncooperative between 25 and 35 °C, and therefore its thermodynamic parameters might be attributed to those of an intrinsic binding (35). The affinity of the nucleotide for these sites is between 1 and 2 orders of magnitude lower than that for the N sites, while we have again an example of the enthalpy-entropy compensation giving rise to a practically constant affinity throughout the above temperature range (Fig. 3). The ΔC_p for this binding has the usual negative value for this type of process (14) and compares well with that reported for the binding of FMN to the I site of phosphorylase *a*, -1.7 ± 0.5 kJ K^{-1} mol^{-1} at 30 °C (43), although in this case the ΔC_p was found to be a function of the temperature.

The negative ΔC_p can be interpreted, in terms of hydrophobic interactions, as being mainly due to a decrease in contacts between apolar protein groups and the solvent on the binding of AMP to the I sites. This interpretation, however, would also suggest a positive entropy change, but, in fact, $\Delta S°$ is negative for this binding (Fig. 3). The application of Sturtevant's method (Table II) once again clarifies this point, given the positive value of $\Delta S_u(h)$. Here there seems to be a tightening of the structure with a loss of about 50 internal vibrational modes, with a liberation of approximately 15 mol of water that were previously in contact with apolar regions when 1 mol of AMP binds the I sites. From Table II it is now clear that the binding of the nucleotide to the I sites is both enthalpy- and hydrophobic entropy-driven between 25 and 35 °C, overcoming the opposite vibrational entropy contribution. The negative ΔH should mainly come from the net formation of hydrogen bonds and of electrostatic pairs and, to a minor extent, from van der Waals' interactions.

Since the possible net formation of hydrogen bonds would make for a positive ΔC_p contribution, our estimation of the contribution of the hydrophobic effect to the binding might be a minimal evaluation of its relative importance.

Finally, it is interesting to note that in the overall binding of the four AMP molecules to the two N and two I sites of the dimer the net change in the water molecules in contact with the protein is very small, while there are also opposite effects to the rigidity or flexibility of the global protein conformation due to AMP's binding to both types of sites. This overall cancellation effect might be related to the enzyme activation on the binding of AMP to the N sites and to the inhibitory characteristics of the I sites.

Acknowledgments—We are grateful for the excellent technical assistance of Dr. O. López-Mayorga and we thank Dr. J. M. Sánchez-Ruiz for helpful suggestions.

APPENDIX

In a solution with two systems with buffering capacity, B and S, the following equilibria exist:

$$\begin{aligned} HB &\rightleftharpoons H^+ + B^- \quad K_B \\ HS &\rightleftharpoons H^+ + S^- \quad K_S \end{aligned} \tag{A1}$$

where K_B and K_S are equilibrium constants, defined as

$$K_B = \frac{[H^+][B^-]}{[HB]} \quad \text{and} \quad K_S = \frac{[H^+][S^-]}{[HS]} \tag{A2}$$

The concentration of the components at equilibrium are given by

$$\begin{aligned} [B^-] &= \frac{K_B C_B}{[H^+] + K_B}; \qquad [HB] = \frac{[H^+]C_B}{[H^+] + K_B} \\ [S^-] &= \frac{K_S C_S}{[H^+] + K_S}; \qquad [HS] = \frac{[H^+]C_S}{[H^+] + K_S} \end{aligned} \tag{A3}$$

where C_B and C_S are the total concentrations of B and S, respectively.

If a concentration of protons ($[H^+]_i$) is generated in the solution the concentration of all the components will change and a new equilibrium will be arrived at. The new concentration of all the components will then be given by

$$\begin{aligned} [B^-]_e &= \frac{K_B C_B}{[H^+] + K_B} - [H^+]_B; \quad [HB]_e = \frac{[H^+]C_B}{[H^+] + K_B} + [H^+]_B \\ [S^-]_e &= \frac{K_S C_S}{[H^+] + K_S} - [H^+]_S; \quad [HS]_e = \frac{[H^+]C_S}{[H^+] + K_S} + [H^+]_S \end{aligned} \tag{A4}$$

where $[H^+]_B$ and $[H^-]_S$ stand for the proton concentrations taken up by the B and S systems, respectively, and $[H^+]$ for the initial free proton concentration.

The proton concentration in the new equilibrium will be given by

$$[H^+]_e = [H^+] + [H^+]_i - [H^+]_B - [H^+]_S \tag{A5}$$

Substituting Equations A4 and A5 into Equations A2 applied to this new equilibrium, the ratio of K_S to K_B results

$$\frac{K_S}{K_B} = \frac{(K_S C_S - [H^+]_S[H^+] - [H^+]_S K_S)}{(C_B[H^+] + [H^+]_B[H^+] + [H^+]_B K_B)} \cdot \frac{(K_B C_B - [H^+]_B[H^+] - [H^+]_B K_B)}{(C_S[H^+] + [H^+]_S[H^+] + [H^+]_S K_S)} \tag{A6}$$

Rearranging Equation A6, we have

$$[H^+]_S = \frac{a[H^+]_B}{b + c_1[H^+]_B} \tag{A7}$$

with a, b, and c_1 being the values given by

$$\begin{aligned} a &= K_S C_S([H^+] + K_B)^2; \quad b = K_B C_B([H^+] + K_S)^2 \\ c_1 &= (K_B - K_S)([H^+] + K_S)([H^+] + K_B) \end{aligned} \tag{A8}$$

In our particular case, 1 mol of the protein-ligand dimer

exchanges n protons with the two buffers present in the medium, and the proton concentration exchanged will be nC_e, where C_e is the enzyme concentration.

Thus, n_B and n_S being now the number of protons released by B and S, respectively, we have

$$[H^+]_B = -n_B C_e \quad \text{and} \quad [H^+]_S = -n_S C_e. \tag{A9}$$

Finally, by substituting Equations A9 into A7 and rearranging, we obtain Equation 8 given in the text:

$$n_S = \frac{a n_B}{b + c n_B}$$

where $c = -c_1 C_e$.

REFERENCES

1. Kasvinsky, P. J., Madsen, N. B., Sygusch, J., and Fletterick, R. J. (1978) *J. Biol. Chem.* **253**, 3343–3351
2. Johnson, L. N., Stura, E. A., Wilson, K. S., Sansom, M. S. P., and Weber, I. T. (1979) *J. Mol. Biol.* **134**, 639–653
3. Morange, M., Garcia Blanco, F., Vandenbunder, B., and Buc, H. (1976) *Eur. J. Biochem.* **65**, 553–563
4. Uhing, R. J., Janski, A. M., and Graves, D. J. (1979) *J. Biol. Chem.* **254**, 3166–3169
5. Mateo, P. L., Barón, C., López-Mayorga, O., Jiménez, J. S., and Cortijo, M. (1984) *J. Biol. Chem.* **259**, 9384–9389
6. Avramovic, O., and Madsen, N. B. (1968) *J. Biol. Chem.* **243**, 1656–1662
7. Dreyfus, M., Vandenbunder, B., and Buc, H. (1980) *Biochemistry* **19**, 3634–3642
8. Mateo, P. L., González, J. F., Barón, C., López-Mayorga, O., and Cortijo, M. (1986) *J. Biol. Chem.* **261**, 17067–17072
9. Busby, S. J. W., and Radda, G. K. (1976) *Curr. Top. Cell. Regul.* **10**, 89–161
10. Fletterick, R. J., and Madsen, N. B. (1980) *Annu. Rev. Biochem.* **49**, 31–61
11. Dombradi, V. (1981) *Int. J. Biochem.* **13**, 125–139
12. Cohen, P. (1982) *Nature* **296**, 613–620
13. Sansom, M. S. P., Stuart, D. I., Acharya, K. R., Hajdu, J., McLaughlin, P. J., and Johnson, L. N. (1985) *J. Mol. Struct.* **123**, 3–25
14. Sturtevant, J. M. (1977) *Proc. Natl. Acad. Sci. U. S. A.* **74**, 2236–2240
15. Fischer, E. H., Krebs, E. G., and Kent, A. D. (1958) *Biochem. Prep.* **6**, 68–73
16. Fischer, E. H., and Krebs, E. G. (1962) *Methods Enzymol.* **5**, 369–373
17. Krebs, E. G., Love, D. S., Bratvold, G. E., Trayser, K. A., Meyer, W. L., and Fischer, E. H. (1964) *Biochemistry* **3**, 1022–1033
18. Hedrick, J. L., and Fischer, E. H. (1965) *Biochemistry* **4**, 1337–1343
19. Buc, M. H., and Buc, H. (1968) *FEBS Symposium: Regulation of Enzyme Activity and Allosteric Interactions*, Oslo, Norway, July 1967, pp. 109–130, Academic Press, New York
20. Titani, K., Koide, A., Hermann, J., Ericsson, L. H., Kumar, S., Wade, R. D., Walsh, K. A., Neurath, H., and Fischer, E. H. (1977) *Proc. Natl. Acad. Sci. U. S. A.* **74**, 4762–4766
21. Cortijo, M., Barón, C., Jiménez, J. S., and Mateo, P. L. (1982) *J. Biol. Chem.* **257**, 1121–1124
22. Barón, C., Mateo, P. L., Cortijo, M., and Jiménez, J. S. (1982) *Anal. Biochem.* **124**, 84–87
23. Helmreich, E., Michaelides, M. C., and Cori, C. F. (1967) *Biochemistry* **6**, 3695–3710
24. Sturtevant, J. M. (1972) *Methods Enzymol.* **26**, 227–253
25. Cortijo, M., Steinberg, I. Z., and Shaltiel, S. (1971) *J. Biol. Chem.* **246**, 933–938
26. Muñoz, F., Sánchez, C., Echevarria, G., and Garcia-Blanco, F. (1984) *An. Quim.* **80A**, 553–557
27. Muñoz, F., Valles, M. A., Pocovi, M., Echevarria, G., and Garcia Blanco, F. (1983) *Biophys. Chem.* **18**, 249–256
28. Froser, R. D. B., and Suzuki, E. (1973) in *Physical Principles and Techniques of Protein Chemistry* (Leach, S. J., ed) Part C, pp. 301–357, Academic Press, New York
29. Christensen, J. J., Hansen, L. D., and Izatt, R. M. (eds) (1976) *Handbook of Proton Ionization Heats and Related Thermodynamic Quantities*, pp. 93, 152, 159, John Wiley & Sons, New York
30. Cortijo, M., Llor, J., and Sanchez-Ruiz, J. M. (1988) *J. Biol. Chem.* **263**, 17960–17969
31. Kastenschmidt, L. L., Kastenschmidt, J., and Helmreich, E. (1968) *Biochemistry* **7**, 4543–4556
32. Ho, H. C., and Wang, J. H. (1973) *Biochemistry* **12**, 4750–4755
33. Lumry, R., and Gregory, R. B. (1986) in *The Fluctuating Enzyme* (Welch, G. R., ed) pp. 58–133, John Wiley & Sons, New York
34. Levitzki, A. (1975) in *Enzymology* (Ebner, K. E., ed) Vol. 2, pp. 1–41, Marcel Dekker Inc., New York
35. Eftink, M., and Biltonen, R. (1980) in *Biological Microcalorimetry* (Beezer, A. E., ed) pp. 343–412, Academic Press, New York
36. Baldwin, R. L. (1986) *Proc. Natl. Acad. Sci. U. S. A.* **83**, 8069–8072
37. Kauzmann, W. (1959) *Adv. Protein Chem.* **14**, 1–63
38. Gurney, R. W. (1953) *Ionic Processes in Solution* (Hammett, L. P., ed) pp. 96–98, McGraw-Hill Publications, Minneapolis, MN
39. Stura, E. A., Zanotti, G., Babu, Y. S., Sansom, M. S. P., Stuart, D. I., Wilson, K. S., and Johnson, L. N. (1983) *J. Mol. Biol.* **170**, 529–565
40. Harris, W. R., Miller, J. F., and Graves, D. J. (1986) *Arch. Biochem. Biophys.* **250**, 446–455
41. Sprang, S., and Fletterick, R. J. (1980) *Biophys. J.* **18**, 175–192
42. Anderson, R. A., and Graves, D. J. (1973) *Biochemistry* **12**, 1895–1900
43. Sprang, S., Fletterick, R., Stern, M., Yeng, D., Madsen, N., and Sturtevant, J. M. (1982) *Biochemistry* **21**, 2036–2048